LUND UNIVERSITY

Always on the wing - Fluid dynamics, flight performance and flight behavior of common swifts

Henningsson, Per

2010

Always on the wing

Fluid dynamics, flight performance

and flight behavior of common swifts

To Teresa

Always on the wing

Fluid dynamics, flight performance

and flight behavior of common swifts

Per Henningsson

Dissertation 2010

A doctoral thesis at a university in Sweden is produced either as a monograph or as a collection of papers. In the latter case, the introductory part constitutes the formal thesis, which summarizes the accompanying papers. These have either already been published or are manuscripts at various stages (in press, submitted or in ms).

Contents

This thesis is based on the following papers:

Paper I and IV are reprinted with permission from the publishers.

Always on the wing

Fluid dynamics, flight performance
and flight behavior of common swifts

Included papers are referred to by roman numerals (I-VI).

Introduction

Flight fascinates us as humans. We have all at some point wondered at the graceful flight of the gulls after the ferry, the precision in the flight of a bat as it captures an insect in the summer night, or the extraordinary stability of a small hoverfly as it appears frozen in the air when it hovers in front of a flower. Our fascination and admiration for these flying creatures largely comes from the fact that we, ourselves, are bound to the ground of the Earth. For all ages people have looked at flying birds, bats and insects and wondered how the things they are doing are possible. We find flight to be a very complex thing, much because we cannot relate directly to it. Walking, for example, is a very complex way of locomotion too. Just taking a single step involves a complicated sequence of muscle, tendon and skeleton interactions, not to mention the neural system necessary to control this and keep the body balanced. But, because this is a locomotion we posses ourselves, we usually do not find it nearly as fascinating. We are not overly impressed by our own ability to walk through the grocery store without knocking every shelf over along our way, but we may find it remarkable when we see a sparrowhawk fly through a dense forest without touching any of the branches. Flight still is, to a large extent, a mystery to us. The study of flight goes far back in the history of science. The famous works of Leonardo da Vinci (1452-1519) show us that he studied in great detail the wing morphology and flight apparatus of both birds and bats. Also, already at that early stage, one of the objectives, apart from sheer curiosity, was to try to build flying machines that could take us humans up into the air, granting us the freedom of flight that we for so long had yearned for. At the time of da Vinci the knowledge about how airflow regimes change with the scale of the flying object (as nowadays described by the Reynolds' number, which we will return to later) had not yet been acquired, so the most obvious thing then was to mimic the birds or bats as closely as possible (see e.g. Lindhe Norberg, 2002 for a nice historical overview). We now know that it is a bad idea to design a Boeing airliner in the shape of a bat. Thus, the early attempts to take to the skies were often catastrophic. It was not until the Wright brothers in 1903, 400 years after da Vinci, constructed their first powered aircraft that we can say that the attempts were finally successful. A lot has happened to aircraft design since the Wright brothers. Aircrafts get bigger, faster, more maneuverable and more efficient all the time. Yet, our designs pale in comparison

with any of nature's flyers. None of our aircrafts can perform a landing similar to that of an eagle, can pull out of a dive like a falcon, can hover with the precision of a hummingbird or can fly for as long as a godwit without refueling. Fantastically advanced as a modern aircraft may be, it is still a bulky, noisy, heavy, inefficient creation compared to any flying animal and we still have a lot to learn from them.

Studying animal flight is not only of interest for the purpose of building flying machines, but is of great importance if the ambition is to understand the lives of the animals, their biology and ecology. The ability to fly is one of the key features of birds and is obviously under strong selection during evolution, resulting in specialized adaptations. By investigating the mechanisms of bird flight, we learn about the costs and constraints experienced by the birds. From this we can draw conclusions about which factors underlie their behaviors, such as, for example, choice of flight speeds, strategies during migration, or foraging flight. Since the flight ability plays this central role in the biology of birds, the knowledge of the mechanisms underlying the aerodynamics of birds is potentially a key to understanding the biological building blocks of avian life.

The focus of this dissertation is on this second part, flight in relation to ecology. It represents an attempt to describe and understand the flight of one of the most advanced flyers of the natural world, the common swift (*Apus apus* L.). Common swifts, or swifts for short, are aerial insectivores that spend almost their entire lifetime on the wing. They forage in the air, roost in the air, collect nest materials in the air and they even sometimes mates in the air. The only time these birds ever land for a long period of time is during breeding. When the chicks are big enough to fledge, they will leap out of the nest and after this point they will remain airborne for up to three years before they make their first breeding attempt (Lack, 1956). Such an extremely aerial lifestyle is naturally linked to special adaptations. The reason for studying such birds is that they, in a way, represent the essence of a bird. Swift are very accomplished flyers and by understanding their aerodynamics

we will obtain further knowledge of both the possibilities and constraints of animal flights. The studies presented in this dissertation have involved investigations of the aerodynamics and kinematics of the swifts by the use of a wind tunnel, the flight behavior of the birds in the wild during migration and roosting flights using radar and the peak performance in terms of flight speeds in display flight using stereo high-speed filming. In this dissertation I will take you on a journey through the wonders of these amazing birds. We will examine the innermost complexity of the wake of these birds, visit the mechanisms of their kinematics, study their flight behavior on migration and marvel at their high speed flights during display. But first, we need to know some basics of aerodynamics to be able to appreciate the results presented.

Basic aerodynamic theory

We may want to start with the concept of the Reynolds' number. This number is the ratio between inertial forces and viscous forces and it quantifies the relative importance of these two forces for a particular flow condition. It depends on the speed of the flow, the size of the object in the flow and the properties of the fluid and is defined as:

$$Re = \frac{Ul}{\nu},\qquad(1)$$

where U is the airspeed (speed relative to the surrounding air), l is the characteristic length of the object in the fluid (e.g. wing chord or frontal area) and ν is the kinematic viscosity. At low Reynolds' numbers the viscous forces are dominating, while at high Reynolds' numbers inertial forces dominate. Furthermore, the flow regime at low Reynolds' numbers is characterized by laminar flow (smooth, parallel), whereas the flow at high Reynolds' number is characterized by turbulent flow. Birds often operate in an intermediate range of Reynolds' numbers ($Re \approx 3 \times 10^4$), which is inconvenient for analysis. These numbers lie well below what is typically considered to be the value where viscous forces

are negligible, but they are well above the value considered as the upper limit for where the flow is laminar and well-organized (see e.g. Spedding et al., 2003b). There is nothing we can do about this, but it is important to acknowledge it since it will be a potential problem in all flow analysis of birds.

When a bird flies level and at a constant speed it has to counteract two forces acting on it: weight and drag. The weight is pulling the bird downwards and the drag tends to decelerate the bird. To balance these two forces the bird has to generate lift and thrust. Lift is a force that is generated perpendicular to the airflow that meets the wing. In the case of a flying bird, both weight and drag are counteracted by the aerodynamic force generated by the wing. To be correct, therefore, lift in the case of the bird involves both the force counteracting drag, i.e. thrust, and the force counteracting weight, i.e. the effective lift. Lift is a consequence of the pressure difference above and below the wing created when the air flows over the wing. When the air meets the wing it is separated at the leading edge and depending on the shape of the wing and the orientation of it in relation to the airflow, i.e. the wing's angle of attack, it will move more or less faster on the upper part of the wing than it does across the lower part. This is what causes the pressure difference and subsequently lift. This is one way to describe the generation of lift, but it can be explained in an alternative way as well. A wing, or airfoil, can be defined as a device that can produce circulation in its vicinity without itself rotating (e.g. Vogel, 1994). The circulation that the airfoil creates is called the 'bound circulation'. This circulation is, however, fictive; the air does not actually circle around the wing. The strength of this fictitious vortex surrounding the wing is proportional to the 'translational velocity' of the wing, which is the velocity component originating from the oncoming airflow. The circulation and the translational velocity together create the overall lifting flow. The spanwise lift force, L', is proportional to the circulation according to the Kutta-Joukowski theorem

$$L' = \rho U \Gamma, \tag{2}$$

where L' is the spanwise lift force, ρ is the air density and Γ is the circulation in the bound vortex.

The power requirement for level steady flight is equal to the drag of the bird times the flight speed:

$$P = DU, \tag{3}$$

where D is the total drag.

Until now we have treated drag as one force, but it is often decomposed into several parts. Here we will consider three that are commonly considered to be the most important for animal flight:

Parasite drag, which in turn consists of friction and form drag, is caused by moving the bird's body (excluding the wings) through the air and can be calculated as

$$D_{\text{par}} = \tfrac{1}{2} \rho S_b C_{\text{D,par}} U^2, \tag{4}$$

where S_b is the body frontal area and $C_{\text{D,par}}$ is the parasite drag coefficient. *Profile drag* is the drag generated when moving the wings through the air and is calculated as

$$D_{\text{pro}} = \tfrac{1}{2} \rho S_w C_{\text{D,pro}} U^2, \tag{5}$$

where S_w is the wing area and $C_{\text{D,pro}}$ is the profile drag coefficient.

Induced drag is a consequence of generating lift. It is introduced by the downwash induced by the wings and tail of the bird when creating lift. It can be calculated as

$$D_{\text{ind}} = \frac{2kL^2}{\rho \pi b^2 U^2}, \tag{6}$$

where k is the induced drag factor (by which the drag deviates from that of a wing with an elliptical lift distribution) and b is the wingspan.

Thus, total power required for a bird in level steady flight is

$$P = U(D_{par} + D_{pro} + D_{ind}). \qquad (7)$$

We will return to these drag components later on, since they were all estimated in paper III based on the gliding flight of a swift.

In order to make the lift and drag of a particular bird comparable to those of others, the forces may be converted into dimensionless coefficients. These coefficients control for the size of the bird, the flight speed and the air density. The lift coefficient is calculated as

$$C_L = \frac{2L}{\rho S_w U^2} \qquad (8)$$

and the drag coefficient is calculated as

$$C_D = \frac{2D}{\rho S_w U^2}. \qquad (9)$$

Methods

Study species, the common swift

The study species throughout this dissertation has been the common swift. It is a migratory species that breeds in Eurasia between approximately latitudes 35° to 65° and winters in tropical Africa. As mentioned earlier, these birds spend the majority of their lifetime on the wing. Adult birds basically do not land for any other reason than breeding, which happens once a year, although extreme weather conditions may force some birds to seek shelter by clinging on to tree foliage as described in Holmgren (2004). The rest of the time, these birds are airborne. In fact, they have evolved towards this completely aerial lifestyle to such an extent that they no longer are able to perch like other birds or take off from the ground (an adult in good condition may sometimes be able to do so, but it is rare). Swifts are renowned for being advanced flyers (e.g. del Hoyo et al., 1999). This reputation probably comes largely from the display flights the birds perform during summer evenings.

During these 'social events', the birds fly around close to a breeding colony, often at low altitude at high speeds emitting their characteristic high pitched call. The phenomenon is often called 'screaming parties' due to these calls. The flights during this behavior are indeed impressive and in paper V these flights were studied by the use of stereo high-speed filming in the field close to a breeding colony. This spectacular flight behavior may be the most well-known behavior of the swifts, but swifts are also advanced flyers when it comes to aerodynamically efficient flight. This is presented in paper I, II and III, so we will return to it later.

Using wild birds in experiments

The birds used in the experiments in this dissertation were all wild birds. In papers I, II and III the birds were juveniles that were captured in their nests as close to their natural fledging time as possible. By doing so, the time the birds were kept in captivity was minimized, which in turn minimized the risk to the birds. Also, by taking the birds as late as possible, they were fed by the adults for as long as possible and had time to do their natural flight muscle training in the nest (see Lack, 1956) before they were captured for their premier flight in the wind tunnel. All birds used in the wind tunnel experiments, eight of them, all flew very well, although each time only one of two birds that were captured for experiments would fly in a favorable manner for the purpose of the studies. The swifts were in general very good birds to work with in the tunnel, they flew steadily for long periods of time, were easy to handle and were quite calm. They also required very simple housing (Fig. 1). However, they are hard to keep in captivity for long times; they do not feed by themselves but need to be hand fed every other hour throughout the day. Furthermore, the birds do not spontaneously open their beak when presented with food. Instead the beak has to be opened by hand and the food inserted in the mouth by the use of a syringe. The food consisted of a mixture of crickets, dried insects, a few maggots, vitamins, calcium and a few

Figure 1. The housing for the swifts is very simple. The birds are kept in a plastic box with nest bowls. To the birds, this environment is probably similar to that of the nest, because they seem very relaxed whenever they are in the box.

drops of water. None of the birds were kept longer than 12 days in captivity. After this time, for some reason, maintaining the weight of the birds started to become difficult. In order to secure the safety of the birds, experiments were always aborted when these signs appeared. At this point the birds were kept for half a day more without performing any experiments in order to feed them to a good weight before they were released into the wild.

Wind tunnel

The study of animal flight by the use of a wind tunnel is a relatively recent method. Greenwalt, in 1961, was the first to use the wind tunnel principle with a live animal when he studied the flight of a hummingbird (Greenwalt, 1961). The wind tunnel he used had a very simple design: basically just a feeder put downstream from a fan, but the technique opened up a whole new set of possibilities in the study of animal flight. The biggest advantage of a wind tunnel is that the airspeed that the animal is subjected to can be controlled. Relative to the wind tunnel, the animal will be flying stationary in the airflow,

but aerodynamically the situation is exactly the same as if the bird was flying through still air at the same airspeed. By the use of a wind tunnel, details in the kinematics and aerodynamics of the flying animal can be studied that would never be possible in the wild. Since Greenwalt's brilliant development of the methods for the study of animal flight, many different aspects have been studied, such as aerodynamics, kinematics and energetics (*birds*: e.g. Pennycuick, 1968a; Torre-Bueno and Larochelle, 1978; Tucker and Heine, 1990; Pennycuick et al., 1996; Rosén et al., 2004; Spedding et al., 2003a, b; Rosén et al., 2004; Warrick et al., 2005; Tobalske et al., 2007. *Bats*: e.g. Hedenström et al., 2007; Muijres et al., 2008; Riskin et al., 2008; Hubel et al., 2009. *Insects*: e.g. Ellington et al., 1996; Bomphrey et al., 2005; Bomphrey, 2006).

In engineering it is common to use wind tunnels when designing, for example, airplanes and cars, but still today there are only a few wind tunnels designed, built and dedicated to the study of animal flight. The wind tunnel at Lund University, which was used for all wind tunnel studies in this dissertation (papers I, II, III), is one of these. It is a closed circuit wind tunnel, which means that the air is circulated through

the tunnel. This property is very convenient when doing flow visualization, as we will see later. The wind tunnel has an octagonal test section, 1.22 m wide and 1.08 m high. The 1.2 m upstream part of the test section, where the actual measurements are taken, has Plexiglas walls and the 0.5 m downstream part is open, providing quick and easy access to the flying animal during experiments. It is in this aspect this tunnel differs the most from the ones commonly used in engineering, which have closed test sections. The background turbulence of the tunnel is low (Pennycuick, et al., 1997; Spedding et al., 2009). The airspeed of the tunnel can be varied continuously from 0 to 38 ms^{-1} (although none of the swifts could ever fly faster than 11 ms^{-1}) and it can be tilted to simulate both descending and ascending flight, which was used for the gliding flight study presented in paper III.

High-speed filming

A flying bird moves its wings, tail and body along complex trajectories and the movements happen in very rapid succession. To be able to study these motions in detail, they have to be slowed down in some way and this is where the use of high-speed cameras comes in handy. The cameras that have been used for the wind tunnel studies in this dissertation have been filming the bird at either 60 or 250 frames per second (fps). In paper I the basic kinematics of the swift was studied using a single camera setup filming at 60 fps. Points on the bird were digitized manually for each frame of each sequence. In paper III the bird was filmed from above at 250 fps also with a single camera and the films were used to measure area and span of wings and tail of the bird in flight.

High-speed cameras have been used in all studies of flow visualization (papers I, II and III) to record the overall flight behavior (e.g. stability) and the location of the bird with respect to the measuring location for the flow visualization (see below). In these cases the bird has been filmed with a single camera, either from behind or from above. In paper I this 'position camera' was the

same as the one used to derive basic kinematic parameters and in paper III the camera was the same as the one used to measure the wing and tail morphology of the gliding bird.

Flow visualization

When an animal flies through the air it causes disturbances in the air, which is left behind it as an aerodynamic 'footprint'. This footprint, or wake, reflects the magnitude and time history of the aerodynamic forces generated by the wings, tail and body. Newton's third law dictates that the forces exerted by the animal on the fluid are equal and opposite to the forces exerted by the fluid on the animal. Studying the wake of a flying animal to estimate the forces generated by it is an elegant method that causes minimal disturbance to the animal. In all studies of the wake of swifts presented in this dissertation (papers I, II and III) the birds were flying freely in the tunnel without any restrictions (Fig. 2). The technique for wake visualization used in this dissertation has been digital particle image velocimetry (DPIV), which is a relatively recent technique as applied to animal flight.

The technique works like this: a thin fog (□1 μm particle size) is continuously inserted into the wind tunnel downstream of the test section. Since the Lund wind tunnel has circulatory flow, the smoke is recycled in the tunnel until it is evenly distributed. During a wake measurement the fog particles are illuminated by a pulsed laser generating a very intense light. The light from the laser is spread by lenses into a thin light sheet. The smoke particles that are illuminated within this light sheet are photographed by one or two cameras (depending on whether the setup is mono or stereo DPIV) that are synchronized with the laser flashes. Since the laser light is so intense, the exposure time of the cameras is short, resulting in sharp images. The laser light is emitted in pulse pairs with a short time interval in between, so that the fog images that are recorded by the cameras show a slight pattern-shift between them. This shift is afterward analyzed by software that correlates the fog patterns in the first image with those in

Figure 2. A swift flying freely in the Lund wind tunnel. Doing experiments on birds that are not restricted or guided in the tunnel by any means is time-consuming and sometimes even almost frustrating. At this particular moment the experimenter seems quite happy, though. Photo by Anders Hedenström.

the second. From this procedure, a vector field can be calculated for the measured area. Since the fog particles are small and buoyant they are assumed to follow the airflow nearly perfectly, thus, the motion of the air is visualized. For the studies in this dissertation two different DPIV systems were used: for paper I a single camera system with 10 Hz repetition rate was used and for papers II and III a two camera (stereo) system with a 200 Hz repetition rate was used. A low repetition rate means that the resulting wake images will have to be compiled from several separated wing beats to represent the wake over time, whereas a high repetition rate results in higher time resolution, i.e. consecutive frames within wing beats are sampled and thereby represent a true time series. Furthermore, the stereo setup also gives the out-of-plane velocity in each frame, which allows for e. g. analysis of

the wake defect due to drag or thrust generated by the flying animal (see paper III).

Field stereo high-speed filming

A common way to study kinematics in a wind tunnel is to use calibrated cameras to calculate three-dimensional (3D) motions of the bird. In the study presented in paper V, the principle of this technique was taken outdoors with the aim of studying the natural flight of swifts in the wild. Two cameras were set at different angles towards a volume of interest, in this case close to a breeding swift colony located in the gable of a house that swifts frequently flew past, together resulting in a stereo view of the volume. The difference in angles between the cameras results in slightly different images of the same

view and this difference is used to calculate 3D coordinates within the measured volume. The cameras were calibrated in the field by filming a calibration cube of a size of $2\times2\times2$ meters. It is the volume of the calibration cube that dictates the measuring volume, since it is only within this volume that the cameras are calibrated. Just outside the volume it is still likely that the coordinates are reasonably accurate, but how fast the quality of such extrapolations drops when moving outside the calibrated volume depend on the optics in the lenses of the cameras.

The technique of stereo high-speed filming in the field brings some obvious opportunities: it is possible to study the birds while they are flying in the open air, completely unaffected by the experiment. On the other hand, there are a couple of drawbacks as well. First of all, the measuring volume is bound to be rather small. In the study in this dissertation (paper V) the volume was, as mentioned, 8 m³, which is at first glance much bigger than the volume often used in the wind tunnel, which is often roughly one m³. However, since the birds in the field fly in nearly still air, the volume measured also dictates the longest possible flight trajectory, whereas in the tunnel where the bird is stationary and instead the air is moving, the effective flight trajectory can be much longer. Secondly, the procedure of calibration in the field is not done in a heartbeat. The calibration object (in paper V this consisted of nine poles put into the ground over a 2×2 m grid with 36 markers in total) has to be measured carefully in the field. The coordinates of each of the markers on this object needs to be measured and the accuracy of these measurements will directly dictate the quality of the calibration of the cameras and ultimately the accuracy of the measured trajectories.

The technique of stereo high-speed filming used in this dissertation is not new; it is similar to that used by e.g. Buchanan and Evans (2000) with the difference that high-speed cameras were used here and that the cameras were calibrated to generate the 3D trajectories. Buchanan and Evans (2000) calculated the 3D coordinates based on the distance between the cameras and the focal length of the lenses. The advantage of performing a calibration such as the one explained here is that the error in the final coordinates becomes smaller. In the study in this dissertation the estimated error was 2%, compared with 6% error estimated by Buchanan and Evans (2000) for their data.

Tracking radar

The radar technique is an elegant way of studying flying animals without any interference. The Lund University Radar used in this dissertation (papers IV and VI) is a tracking radar, i.e. it tracks individual birds and the resulting data consist of 3D trajectories of each of the tracked birds. This, former military radar, originally designed and used for completely different purposes, is sensitive enough to track a small bird, which opens up a fantastic opportunity for studying animal movement. Here follows a short description of how a radar in principle operates: Electromagnetic waves are transmitted in pulses from the radar antenna and are scattered if they encounter an object. A small part of the scattered waves are reflected back to the radar and the distance to the object is calculated based on the delay in the echo. The position of the antenna directly provides the angular coordinates of the object. Combined with the distance, polar coordinates are obtained. A tracking radar transmits beams with a slight offset around the axis in the direction of the antenna. When the tracked object is moving out of the centre of the overlap of these beams, the radar compensates by moving the antenna. Recording fluctuations in the echo provides the 'echo signature' of the object, which in the case of birds corresponds to the wing beat frequency or bounding-flight frequency (e.g. Bruderer, 1997). Swifts are especially well suited for being studied with tracking radar, since their echo signature is characteristic, which means that the birds can be recognized from the radar signal (Bruderer and Weitnauer, 1972; Bäckman & Alerstam, 2001, 2002) as opposed to most other birds.

The resulting directions and speeds that are calculated for the trajectories of the birds correspond to their direction relative to the ground, called 'track', and speed relative to the

ground, called 'ground speed'. This direction and speed is relevant for estimating the true direction and speed for the bird, for example on migration, since it is the actual progress it is making on its journey towards is destination. From an aerodynamic point of view, speed of the bird relative to the surrounding air (airspeed) is more relevant. Flight direction relative to the air, called 'heading', is the direction the bird is actually flying towards. The heading/airspeed vector, in combination with the wind, results in the bird's track. In order to calculate the heading and airspeed of the bird tracked by the radar, a measurement of the wind is required. For the studies in this dissertation this was done by releasing weather balloons carrying a reflector approximately every third hour. The reflector is carried upwards by the balloon and is tracked by the radar, providing a wind profile from the ground up. Heading and airspeed for each bird track were calculated using wind measurements from the altitude at which the particular bird was flying.

Results and discussion

Aerodynamics of flapping flight

A flying animal, unlike an aircraft, produces both lift and thrust with the wings. As mentioned in the introduction, the lift force is directed perpendicular to the flow that meets the wings. In gliding flight, the direction of the flow only depends on the direction of flight. In flapping flight the wings are moving up and down and this added velocity will change the resultant direction of the oncoming flow. During the downstroke, when the wing is moving downwards, the direction from where the flow is coming will be shifted downwards and therefore the lift generated by the wings will be rotated forward, thus creating a component of thrust. During the upstroke, when the wings are moving upwards, lift will be tilted backwards, which means that negative thrust will be created. To achieve a net forward thrust over the wingbeat the animal needs to adjust the wings in some

way during the upstroke, e.g. by sweeping the wings to reduce the effective wing span or by changing angle of attack of the wing.

Wake topology

The idea of visualizing the wake of a flying animal was introduced by Magnan et al. (1938) when they used tobacco smoke to visualize the wake of a flying pigeon. It was a very simple experiment and the result showed a wake of some sort, but the speed was not known. However, the method of visualizing wakes by the use of smoke particles was a great step forward for the study of animal flight and the principle of the method is even still used today (e.g. a recent one is Bomphrey et al., 2009 on bumblebees), although under more controlled circumstances. From the time of the experiments by Magnan and coworkers up to rather recently, the study of wakes of flying animals was not a very big research field. Between 1938 and 2003 only six papers were published on wakes of animals in active, flapping flight (Kokshaysky, 1979; Spedding et al., 1984; Rayner et al., 1986; Spedding et al., 1986; 1987b; Spedding et al., 2003b). Only a few of these studies involved quantitative measurements of the wake and only the last one was performed in a wind tunnel. In the last few years the research field of animal flight has been growing rapidly, with studies on birds, bats and insects.

Before the study by Spedding et al. (2003b) the wake topologies that had been found led to the interpretation that the birds generated distinctly different wakes during slow and fast flight and that the animal switched between these abruptly, similar to the way animals behave in terrestrial locomotion, e.g. a horse changing from trot to gallop. The different wake structures were called 'gaits' as an analogy to this. At slow speeds a wake was found that consisted of a single vortex loop shed during each downstroke while the upstroke was inactive (Kokshaysky, 1979; Spedding et al., 1984; Spedding, 1986). This wake was called the 'vortex ring wake'. At higher speeds a different wake was found, consisting of a pair of trailing wingtip vortices

of nearly constant circulation (Rayner et al., 1986 ; Spedding, 1987). This wake was named the 'constant circulation wake'. When Spedding et al. (2003b) studied the wake of a thrush nightingale flying in a wind tunnel over a range of flight speeds they found that the wake did not change abruptly like in the case of 'gaits', but rather changed gradually from one to the next. This study was the first to show this and it was also the first one to apply the technique of digital particle image velocimetry (DPIV; see above) to the study of a flying animal.

A third wake model, called 'ladder wake', has been proposed for animals that fly with rigid, relatively inflexible wings, such as hummingbirds (Pennycuick, 1988) or swifts. As described above, for animals that flex the wings during the upstroke, the net forward thrust can be achieved by an asymmetry in the effective span of the downstroke and upstroke. If the wings are not flexed during the upstroke the net positive thrust must be achieved in some other way. In the ladder wake model the asymmetry comes from changes in circulation instead of in wake width. The wings leave a pair of continuous trailing wingtip vortices, but in addition, spanwise vortices are shed between them at both turning points in the wingbeat. A distinct vortex with positive circulation is shed from the wings at the beginning of the downstroke, as the circulation of the bound vortex (see introduction) on the wings increases. At the transition from downstroke to upstroke a corresponding vortex with negative circulation is shed, as the circulation in the bound vortex decreases. Since the ladder wake had never been observed it was one of the objectives for paper I.

In paper I a juvenile swift was flown at cruising speed in the wind tunnel and the wake was sampled with DPIV. Basic kinematics, such as wingbeat frequency, wingbeat amplitude and wingspan ratio between upstroke and downstroke, was recorded by a single high-speed camera filming the bird from behind. The wake was sampled in the far wake (0.4-0.5 m downstream the bird) in the longitudinal plane, i.e. from the side of the bird, thereby potentially

Figure 3. Three-dimensional wake topology of the swift in cruising flight. The image frame is as if the bird flew obliquely from right to left and slightly into the paper, leaving the trace of one wingbeat in still air, starting at upper turning point. Green tubes show the wingtip vortices. Cylinders in shades of red are spanwise vortices with positive circulation and cylinders in shades of blue have negative circulation. The color intensity and tube diameter are proportional to the strengths of each component. The geometry is deduced from a combination of wingbeat kinematics and streamwise plane section data.

revealing the ladder shaped wake if the predictions about the ladder wake were correct. However, the wake that was found did not fit the ladder wake model. The wake consisted of a pair of trailing wingtip vortices, but instead of the distinct shedding of spanwise vortices at the turning points, as the model predicted, an almost continuous shedding of spanwise vortices was found over the complete wingbeat (Fig. 3). During the downstroke, vortices with positive circulation were shed and the strength of the shed vortices gradually increased as the downstroke progressed. This reflects a gradual increase in the circulation of the bound vortex. At mid-downstroke the circulation in the shed vortices reached a peak, suggesting that the rate of increase in the bound vortex circulation was the highest at that point. By the end of the downstroke the strength of the vortices was again weaker and around the transition from downstroke to upstroke the shed vortices gradually switched to negative circulation. Then during the upstroke the vortices shed showed a similar pattern as during the downstroke, only with opposite sign. This suggests a gradual decrease of the circulation in the bound vortex. This new wake topology was named 'continuous change wake', due to this smooth change of the circulation in the bound vortex without any abrupt changes throughout the wingbeat. Just as predicted, the swift did not flex the wings to a large extent during the upstroke. The asymmetry in thrust between downstroke and upstroke needed for a net positive thrust was achieved, as the principle of the ladder wake states, by changes in circulation in the bound vortex, but also to some degree by flexion of the wings. The model was tested by reconstructing the wake topology based on wingbeat kinematics and circulation measures and lift was calculated. The lift calculated matched the lift required for weight support well.

In paper II the flapping flight of the swift was revisited. This time the goal was to investigate a range of flight speeds and to examine the transverse plane behind the bird, i.e. looking from behind. From the time of paper I to paper II a new DPIV system had been installed, that allowed for 200 frames per second, so the objective was also to make a time-resolved wake reconstruction (see e.g. Hedenström et al., 2009). The swift was this time flown at 5.7, 7.7 and 9.9 ms^{-1}, which spanned the range where it was possible to get the bird to fly steadily. Since the view was now perpendicular to the flow, some new features of the wake became visible. Apart from the wingtip vortices that had been seen already in paper I, a pair of 'wing root vortices' and a pair of tail vortices were discovered. Wing root vortices have recently been found in the wakes of bats (Hedenström et al., 2007; 2009; Hubel et al., 2009), birds (Johansson and Hedenström, 2009) and insects (Bomphrey et al., 2009). We can already from these few studies conclude that this structure is present in rather different animals, suggesting that it is a fundamental structure, possibly originating as a consequence of having to incorporate a low-lifting body into a wing design (cf. Bomphrey et al. 2009). A probable reason for this wake structure is that, when considering the lift distribution over the wings from tip to tip, there is a drop in the lift generated at the location of the body. This drop in the lift distribution has to result in some kind of wake disturbance, which in the case of the animals studied so far, including the swift, appears to be the wing root vortex. However, even if this structure is a consequence of a constraint, it may still be an advantage. The root vortex, together with the wingtip vortex, form wake structures for each wing that are more or less detached from each other. This means that each wing can operate more independently, which may give rise to higher maneuverability and refined control of flight (cf. Bomphrey et al., 2009). The wake found in paper II also involved tail vortices. These structures reflect the forces generated by the tail and were present at all speeds, at least for certain parts of the wingbeat. The circulation in the tail vortices was relatively low in comparison with the wingtip vortices (roughly 3-5 times smaller). However, if examining the time history of circulation of the two structures over the wingbeat, the timing of the peak in tail vortex circulation was inversely matched with that of the wingtip vortex, i.e. when the wingtip vortices had high circulation the tail

vortices had low circulation and vice versa. This suggests that the bird used the tail either as an extra lifting surface in parts of the wingbeat where lift from the wings was low, or that the tail was used to stabilize some perturbation introduced during the periods of high wing lift. Consistent with the results from paper I, the change in the circulation found in the wake varied smoothly over the wingbeat without any abrupt changes. Since the time resolution of the wake time series was much higher in paper II than in paper I, it was possible to generate a 3D wake representation based on consecutive frames within wingbeats. These plots show the

constant streamwise vorticity trailing the swift during a little over one wingbeat for each of the three speeds examined (Fig. 4). These 3D-wake representations showed a slightly different wake compared to what was described in paper I. Bear in mind, though, that the two models come from two different views of the wake, literally, one from the side and one from behind. None of the wake representations are necessarily wrong, but rather the two together represent the more complete picture. The structures found in the longitudinal wake images, i.e. the spanwise vortices interconnecting the two wingtip vortices are still there, but their topology is most likely

Figure 4. Iso-surfaces showing 1.5 wingbeats for each speed. a) 5.7 ms^{-1}. b) 7.7 ms^{-1}. c) 9.9 ms^{-1}. The view is oriented so as if the bird was flying obliquely towards the observer from left to right. Red colored patches represent positive circulation (clockwise rotation as seen in direction of flight) and blue colored patches represent negative circulation (counter-clockwise rotation as seen in direction of flight).

more complex than the cartoon model implies (Fig. 3; the intention of the cartoon was to begin with to illustrate a simplified view of the wake). The wingtip vortices, the wing root vortices and the tail vortices are probably connected with these structures in some manner (cf. Hedenström et al., 2007), but exactly how this looks is not possibly to derive from the present data.

Force production

Both in paper I and II the models that were formulated were used to estimate the forces produced by the flying swift. In paper I the model assumed that all of the circulation that was shed into the wake reflected the change in the circulation of the bound vortex. Therefore, the approach was to integrate the circulation over the wingbeat in order to get a cumulative measure of the circulation in a 'bookkeeping' manner. It was assumed that the circulation in the bound vortex was zero at the beginning of the downstroke based on measurements of frames captured at this point. Thus, any change, increase or decrease, in the bound vortex would then exactly correspond to a shed vortex of the same strength, but with opposite sign. This estimate of the bound vortex circulation was then used to calculate the vertical impulse created over the wingbeat. Impulse is force over a time period and therefore, by dividing impulse by the time duration of the wingbeat, the average lift could be calculated. This force should ideally match the weight of the bird, since it is known that the bird is flying levelly, neither descending nor ascending. Indeed, the force calculated in this manner matched the weight of the bird within the range of experimental uncertainties. Therefore, the model was considered adequate to describe the wake and it was used to estimate the drag of the bird in order to estimate the effective lift-to-drag ratio (*L:D*). This quantity is a measure of the bird's overall flight efficiency: a high *L:D* implies that the bird uses an energy efficient flight style and vice versa, which is naturally of relevance for a bird like the swift that spends nearly all its time on the wing. The effective *L:D* for the swift flying in the tunnel

was estimated to be 13.3, which was the highest estimated yet for birds in flapping flight.

In paper II, the corresponding model was again used to estimate the forces generated by the swift. Since the measurements this time was taken in the transverse plane, the circulation measures were assumed to directly reflect the circulation in the bound vortex rather than its change, as described for the longitudinal case. The model included wingtip vortices, wing root vortices and tail vortices, since these structures were the main features of the wake and were therefore assumed to reflect most of the consequences of force production. In this analysis the calculated force was not sufficient to account for the weight of the bird, but rather 50-60% thereof. This is a concern, since such a result implies that the wake representation is incorrect in some way. A similar problem has been addressed by Hubel et al. (2009) about a wake study of a bat in flapping flight. In that study the lift calculated was also roughly half of that required to support the weight of the animal even though it was flying levelly. Hubel et al. (2009) gave two potential explanations of this deficit. Firstly, that the vortex structure was partly destroyed by background turbulence or other unsteady phenomena and secondly, that a portion of the vortex sheet was lost due to diffusion before it converged in the wingtip vortex. Both of these explanations are possibly applicable to the case of the swift, but there is potentially an additional explanation: the wingtip vortex and the wing root vortex may interact in a way that distorts the wake as it travels downstream. In aeronautics, there is a well-known phenomenon, often called Crow-instability after its discoverer (Crow, 1970), in which vortex pairs interact in an increasingly complex way as the wake evolves downstream of the wing. This phenomenon has been empirically tested and the results have shown that counter-rotating vortex pairs interact by initially contracting together and subsequently the weaker (in this case root) vortex moves around the stronger (in this case wingtip) vortex and finally wraps around it into a complex structure (e.g. Bristol et al. 2004). For the analysis of the wake of the swift (and potentially for the analysis of the bat in Hubel et

al., 2009), this would result in an underestimate of the wake width of the wingtip vortices and an overestimate of the wake width of the wing root vortices. If the lift is calculated according to eq. 2 and multiplied by the span, which it was in paper II, this could potentially result in an underestimate of the true force, since the positive contribution to lift reflected in the wingtip vortices are underestimated while the negative contribution to lift reflected in the root vortices are overestimated. This is potentially a general problem when measuring far wakes (which is often required when working with freely flying animals due to safety issues) in the transverse plane.

Aerodynamics of gliding flight

In gliding flight the bird does not produce any self-powered forces but instead produces the aerodynamic forces by converting potential energy into kinetic energy. By doing so, the bird loses altitude. The ratio between the rate of gain in distance (forward speed) and the rate of loss in altitude (sink speed) is a measure of the birds' gliding efficiency. This measure is the *L:D* ratio, which we discussed earlier regarding flapping flight, although here it is the actual *L:D* ratio of the wing/body configuration, whereas in flapping it was the resulting effective *L:D* ratio when the flapping motion was taken into account. Unlike most aircrafts the birds are able to adjust their wing shape dynamically during flight (there are some aircrafts that have a simplified version of this feature, e.g. Grumman F-14). By reducing the wingspan and wing area as flight speed increases, the birds can minimize drag (Tucker, 1987). This behavior has been seen in several studies of different birds (e.g. Pennycuick, 1968a; Tucker and Heine, 1990; Rosén and Hedenström, 2001).

Fixed swift wings and bodies

To investigate the aerodynamic effect of changing the wing shape in flight, Lentink et al. (2007) examined the aerodynamic properties of the wings of swifts in a wind tunnel. Parts of the measurements were performed in the Lund wind tunnel and it was the initiation of the project that led to this dissertation. Swifts are capable of alternating their wing area and wingspan to a large extent by flexing the wing in the wrist joint, 'sweeping' the wing backwards. Lentink at al. (2007) took wings from dead swifts and freeze-dried them in different wing sweep configurations. Lift and drag were measured on these preserved wings in a wind tunnel over a range of flight speeds and angles of attack. The results showed that the performance of the swift wings was greatly affected by the sweep angles of the wings. Choosing the most suitable sweep could halve the sink rate or triple the turning rate (Lentink et al., 2007). Extended wings were best when considering slow glides and turns, whereas swept wings were best when considering fast glides.

Gliding flight of a real swift

From an aerodynamic point of view, gliding flight is less complex than flapping flight. Firstly, in steady gliding flight, per definition, there is no kinematics since the bird does not perform any internal movement. This naturally generates a much simpler wake than that of flapping flight. Secondly, one aerodynamic force component that is present in flapping flight, the thrust, is taken out of the picture, since the bird does not generate any self-powered forward force, but extract the forward force needed to balance drag from its potential energy. This means that the total force generated is always directed perpendicular to the glide path angle, which in turn does not vary over time as in flapping flight. The wake is also convenient in terms of analysis, since most aerodynamic theories come from steady state aerodynamics.

The gliding flight of birds has been studied before by various approaches: by flying along with the birds in a light weight motor-glider (Pennycuick 1971a; 1971b), by the use of range finders (e.g. Tucker, 1988; Tucker et al., 1998; Rosén and Hedenström, 2002), by tracking radar (e.g. Spaar and Bruderer, 1996; Spaar and
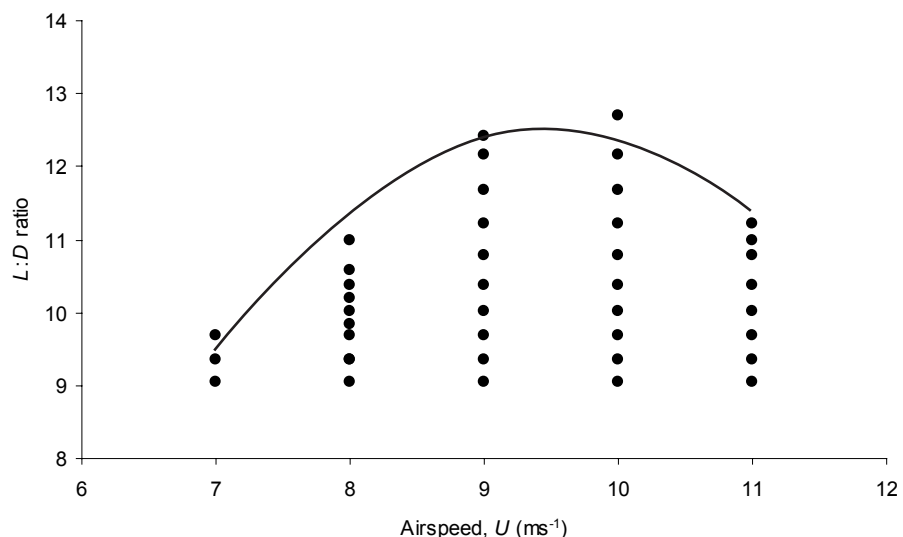
Bruderer, 1997) and in tiltable wind tunnels (e.g. Pennycuick, 1968a; Tucker and Parrott, 1970; Spedding, 1987a; Tucker, 1987; Tucker and Heine 1990; Rosén and Hedenström, 2001). However, very few studies of the wake of gliding birds have been performed and no recent efforts have been made using modern techniques that allow for quantitative wake measurements.

The swift is, to a large extent, a gliding bird. It constantly alternates between flapping and gliding (in paper IV the proportion of gliding in freely flying swifts was found to be around 40%). In paper III the objective was to examine the performance of these birds in gliding flight. The swift was flown at flight speeds from 7 to 11 ms^{-1} in the wind tunnel. For each speed the minimum tilt angle at which the swift could glide at was found. This angle corresponded to the minimum glide angle for the bird at that speed. When all speeds were examined the result was the glide super-polar, which describes the minimum sink rate with respect to forward speed. Since the bird was gliding at equilibrium, the lift and drag of the bird could be calculated based on the speed and tilt angle of the tunnel. Lift-to-drag ratio of the swift was calculated for the different speeds and the overall maximum was 12.7, found at a flight speed of 10 ms^{-1} (Fig. 5).

The wake of the gliding swift was sampled using stereo-DPIV at the minimum tilt angle for each speed. Compared with the wake found for the flapping flight it was, as predicted, simpler, consisting of a pair of trailing wingtip vortices and a pair of trailing tail vortices. No root vortex was found (Fig. 6). Based on this wake structure a simple model was formulated. The model was tested by using it to calculate the lift produced by the bird and the result showed that it matched well with the lift required to support the weight of the bird.

A second objective of paper III was to examine how the swift changed its wing shape with different speeds and sink rates. As described above, the bird may benefit from adjusting its wingspan and wing area with speed. The wing and tail posture of the gliding bird was recorded by a high-speed camera filming the bird from above at each speed and tilt angle. The wingspan, wing area and tailspan were measured from the recorded film sequences. Wingspan varied linearly with flight speed, decreasing with increasing flight speed, which suggests that the swift was trying to minimize profile drag as speed increased (cf. Tucker, 1987). The relationship between wingspan and wing area was also examined and a linear relationship was found: when span increased so did wing area and vice versa.

Figure 5. Lift to drag ratio (*L:D*) of every speed and angle combination measured. The curve represents the maximum *L:D* over the range of airspeeds. The curve has a maximum of 12.5 at a flight speed of 9.5 ms^{-1}. The highest *L:D* measured was 12.7, which was found at 10 ms^{-1}.
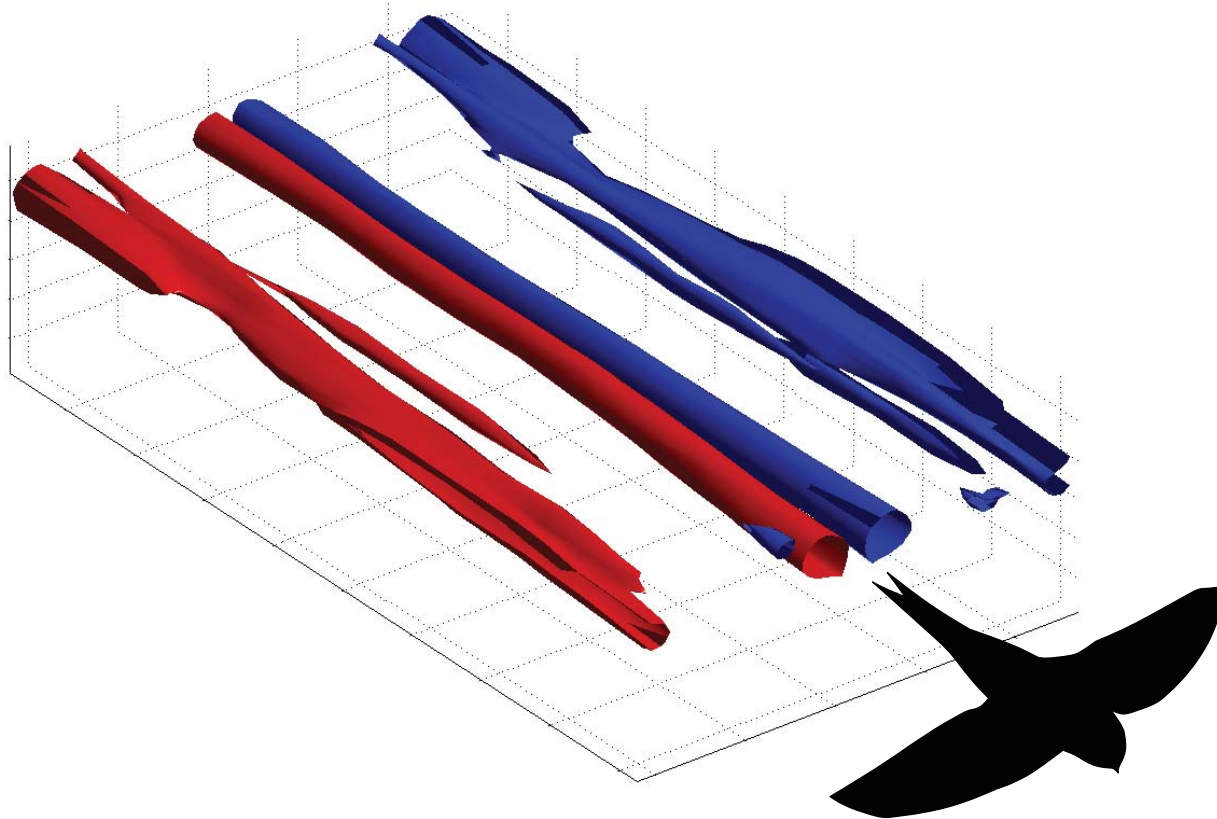
Figure 6. Vorticity iso-surface plot of a gliding swift at 9 ms⁻¹. The view is obliquely from above and from in front of the bird's flight path, as illustrated by the bird-silhouette. The plot is based on data from one side of the bird, wing and tail, which has been mirrored in the plot to illustrate the full wake. Tail vortices and wingtip vortices are the major structures in the wake of the gliding swift and appear clearly in this plot. Red colored patches represent positive circulation and blue colored patches negative circulation.

Drag components

As mentioned earlier, the wake in paper III was sampled using stereo-DPIV at the minimum tilt angle for each speed. The stereo setup allowed for an estimate of the out-of-plane velocity in addition to the in-plane 2D flow measured with a single camera setup. This feature was used to estimate the wake defect behind the body. When a body is pushed through the air its drag will reduce the momentum in the air behind it. Therefore, if it is possible to measure this momentum loss behind the body, it is possible to estimate the drag of it (see e.g. Pennycuick et al., 1992). This was done by measuring the deceleration of the air in the stereo-DPIV images in the wake area behind the body excluding the wake structures of the wings and tail. Attempts have been previously made to measure parasite drag on stuffed birds in wind tunnels (e.g.

Pennycuick et al., 1988; Tucker, 1990), but indications were found that suggested that the measured drag of a dead bird was an overestimate of what a live bird of the same species would generate (Pennycuick et al., 1988). However, in this study the measured parasite drag coefficient (eq. 9) was on average 0.26, which is the same as was found for parasite drag coefficient by Lentink et al (2007) for a stuffed bird body.

Since the total drag of the swift was known from the weight of the bird and tilt of the tunnel, parasite drag was measured from the wake and induced drag can be calculated according to eq. 6 (see introduction), it was possible to estimate the profile drag (drag of the wings) by subtraction (cf. eq. 7). Profile drag is the component of aerodynamic forces that has proven most difficult to measure (Pennycuick 2008). The only study where the profile drag has been directly measured in any way was made by

Pennycuick et al. (1992), where they estimated the profile drag of a Harris' hawk by measuring the pressure difference behind the wings and the freestream flow using a 'wake rake'. The profile drag coefficient for the swift was calculated analogously to eq. 9 and the range (0.011 to 0.041) was similar to that found for the Harris' hawk by Pennycuick et al. (1992).

Flight performance

Flight speeds of swifts in the wild

In paper IV swifts were studied during nocturnal spring migration, autumn migration and in roosting flights during summer. The birds were studied in free flight using a tracking radar (see Methods). Spring migration was studied during the month of May, roosting flights were studied during July and autumn migration was studied during August. The objectives for the study were to measure the flight speeds of individual birds during these three different flight scenarios and to relate the results to predictions from flight mechanical theory.

Theory states that the power requirements for level steady flight for a bird varies in a non-linear manner with speed; a relationship commonly called 'the power curve'. It assumes that flying at both low and high airspeeds is relatively costly. Somewhere in between there is a minimum, where the power requirements are the smallest (Fig. 7). This is called the minimum power speed (U_{mp}; Pennycuick, 1968b; Pennycuick, 1989). It is the optimal flight speed if the goal is to minimize the energy consumption *per unit time.* If a tangent is drawn from origin to the power curve, the airspeed at the intersection corresponds to the maximum range speed (U_{mr}; Fig. 7). Flying at this speed minimizes the energy consumption *per unit distance* and is optimal if the objective is to maximize the flight range on a given amount of fuel (Pennycuick, 1968b; Pennycuick, 1989). If the fuel deposition rate at stop-over on migration is taken into account, a third characteristic speed, the time minimization speed (U_{mt}; Fig. 7), can be derived from the curve (Alerstam and Lindstöm, 1990; Alerstam, 1991; Hedenström & Alerstam, 1995). The intercept of this tangent and the x-axis corresponds to the overall speed of migration (U_{migr}; Fig. 7). Very few studies have been made to empirically test these predictions. Hedenström and Alerstam (1996) studied flight speeds of skylarks (*Alauda arvensis)* during display flight and migratory flight. They predicted that the flight speeds during display flights would be close to U_{mp},

Figure 7. A conceptual power curve. It is costly to fly slowly as well as fast. In between, the curve has its minimum, which corresponds to the minimum power speed (U_{mp}). If a tangent is drawn from origin to the curve, the maximum-range-speed (U_{mr}) is obtained. If the fuel deposition rate (P_{dep}) for a bird at stopover sites along the migratory journey is taken into account, the optimal speed is the time-minimizing-speed (U_{mt}). In this case the y-axis is extended downwards to include the fuel deposition rate. Vmt is found by drawing a tangent from the point of the current deposition rate to the power curve. The intercept between the tangent and the x-axis corresponds to the overall speed of migration (U_{migr}).

since the birds are then trying to stay aloft for as long as possible and covering ground is not of importance. During migratory flights, they predicted that the speeds would be similar to U_{mr} or U_{mt}, since the primary objective would be to fly as long of a distance as possible on the fuel available. The results showed that the skylarks flew at airspeeds close to U_{mp} during display flights, but that flight speeds were higher during migration (Hedenström & Alerstam, 1996).

In paper IV it was predicted that the swifts would fly at slowest speeds during roosting flights, since the birds are not trying to cover ground but rather aim to spend the night in the air to a minimum energy cost, i.e. they would fly at U_{mp}. Swifts during spring migration were predicted to fly at the highest speeds of the three, since these birds are assumed to be time restricted, due to e.g. competition for nests or mates at breeding sites, i.e. they would fly at U_{mt}. Flight speeds during autumn migration were predicted to be somewhere intermediate of spring and summer since the birds are assumed to be under less time pressure but have the objective of covering distance, i.e. they would fly at U_{mr}.

The results show that the flight speeds were indeed on average higher during spring migration (U=10.6 ms^{-1}, s.d.=3.9 ms^{-1}) than in the other two periods, which indicates a time-selected migration. However, the speeds recorded during autumn migration (U=9.2 ms^{-1}, s.d.=1.5 ms^{-1}) were similar, i.e. not statistically significantly different, to those recorded during roosting flights (U=9.0 ms^{-1}, s.d.=2.1 ms^{-1}) The general result shows that the swifts changed their flight speeds between different flight scenarios to a smaller extent than expected. It further suggests that swifts in some way are restricted in terms of flight speeds. The range of flight speeds that was found was rather small with the majority of the birds flying between 8-12 ms^{-1} and with no birds flying slower than 6 ms^{-1}. This result fits well with what has been observed in the wind tunnel while doing the experiments for papers I-III. The birds in the tunnel have never been able to fly slower than 6 ms^{-1}. Below this speed, they were unable to produce enough lift and quickly descended to the tunnel floor. In the tunnel no

bird has been able to fly faster than 11 ms^{-1}, but this is most likely a constraint coming from complications of maneuvering in relation to the wind tunnel walls, rather than an aerodynamic limitation per se.

Since this short, restricted, range of flight speeds had been found for the swifts both in wind tunnel flight and free flight during different behaviors, the flight speeds during display flight, or 'screaming parties' (see Introduction) were also measured. During these flights, the birds appear to reach high speeds, so the objective for paper V was to measure the flight speeds of these birds in free flight to see what speeds the birds were capable of achieving. The speeds were measured by filming the birds with two cameras, setup in a stereo configuration. From the stereo sequences, 3D trajectories of the birds in flight could be derived (see Methods). Birds that were filmed were always approaching in level flight, so the speeds they flew at were self-powered, not acquired from converting potential energy to kinetic energy by diving. The flight speeds of the birds were estimated by tracking the beak of the birds over time in the 3D space. This was done by digitizing the position of the beak of the bird in each frame and sequence in both camera views. The time series were then analyzed to calculate the speed of the bird. The results show that the bird during these flights fly at an average of 21 ms^{-1}, i.e. twice the speed otherwise measured on migration or roosting. These flights are, however, quite different from migration and roosting. In the case of the screaming parties, the birds fly at these high speeds for just a short moment, whereas the speeds on migration are assumed to be sustained flight speeds. It is possible that the birds perform anaerobic muscle work during screaming flights. During short bursts of anaerobic muscle work, power output can be increased up to twice the power output of aerobic muscle work (e.g. Weis-Fogh and Alexander, 1977). Flight muscle mass-specific work has been calculated for the swift at sustained flight speeds (Hedenström and Alerstam, 1992). The horizontal speed was on average 10.0 ms^{-1} and the vertical speed 1.34 ms^{-1}. Climbing power was calculated as $P_z = mgU_z$, with m=0.0407g (mass of the bird including 10%

fuel) and U_z=1.34 ms^{-1}, resulting in P_z =0.54 W (due to a calculation error in the original article, the value is different here). Power for horizontal flight was calculated according to the routines provided in Pennycuick (1989) to 0.43 W using a body drag coefficient of 0.4. Total flight power for the birds in that study was thus 0.97 W. From this, flight muscle mass-specific work was calculated by dividing the total power output by the flight muscle mass and the wing beat frequency. Flight muscle mass was estimated to be 20% of lean mass, i.e. 0.0047 kg, wing beat frequency was 6.8 Hz and thus mass-specific work 19 J/kg flight muscle. In this study, paper V, the swifts flew on average at U_h=20.9 ms^{-1} and U_z=4.0 ms^{-1}. The same calculations for these birds result in a total power of 3.96 W and mass-specific work of 51 J/kg flight muscle, a 2.7 time increase compared with sustained flight. These calculations should be viewed as only rough estimates, but they may give an indication of the magnitude of the performance. Lentink et al (2007) provided an empirical measurement of the body drag coefficient and reported an average of 0.26 for a swift body (and in paper III it was estimated to be, on average, the same). Using this value instead of the 0.4 previously used results in a mass-specific work of 17 J/kg for sustained flight and 41 J/kg for sprint flight in the present study. The increase during sprint flight is then 2.4 times that of sustained flight. The mass-specific power (total power divided by flight muscle mass) for blue-breasted quails (*Coturnix chinensis*; about the same weight as the swift) during take-off flight has been estimated to be ,on average, 390 W/kg flight muscle and maximum 531 W/kg flight muscle (Askew et al., 2001). These flights also involve short bursts of high power output. An analogous value for the swifts in this study is 430 W/kg flight muscle, using the estimate based on a body drag coefficient of 0.26. This suggests that swifts are capable of high mass-specific power output and the results fit well into the reasoning by Dial et al. (2008), where they showed that smaller birds are capable of higher mass-specific power than larger birds. Dial et al (2008) suggested that e.g. hummingbirds are capable of extreme maneuverability and vertical flight because of their high mass-specific power. That the muscle mass specific work/power for the swifts approaches that of a galliform species during take-off supports the notion that the display flight of swifts represents performance at or near the maximum possible by the vertebrate muscle.

Compensation for wind drift by migrating swifts

In paper VI, the same data set that was used for the flight speed comparison in paper IV was used to examine if and how swifts compensate for side winds during spring and autumn migration, respectively. This is a central problem for migrating birds, both in terms of being able to detect the direction and speed of the wind and in terms of being able to compensate for deviations from the intended flight path due to it. For nocturnal passerine birds, full or partial wind drift appears to be most common (e.g. Cochran & Kjos 1985, Liechti 1993, Zehnder et al. 2001, Bäckman & Alerstam 2003).

Because of the swifts' adaptations to a life in the air (see Introduction), it was expected that they would be more efficient in their wind drift/compensation behavior than other nocturnal migrants. Another reason for using swifts to investigate the wind drift/compensation issue is that the birds can be reliably identified when tracked by the radar. By studying a specific species, which is not commonly feasible in radar studies, we can minimize the risk of bias due to pseudo-drift that may arise in the analysis as a consequence of species and/or populations having different preferred migratory mean directions (e.g. Alerstam 1978; Green & Alerstam, 2002). A common way of analyzing wind drift/compensation is to plot track (average or individual) against difference between track and heading (track-heading; average or individual) for different wind direction categories and to derive a linear regression equation for the data. The slope of this line will correspond to the proportion of drift/compensation, where 0 corresponds to full compensation and 1 corresponds to full drift. However, for such

an analysis to produce a reliable estimate, the data need to be evenly spread over different wind directions (see e.g. Green & Alerstam, 2002). The trackings of migrating swifts were not spread evenly enough to fulfill this criterion and therefore the drift/compensation behavior was examined by dividing the data into two categories: birds flying in westerly winds and birds flying in easterly winds. This method is a robust way to analyze drift/compensation, but gives a qualitative rather than quantitative answer (Green & Alerstam, 2002). The results showed that the swift compensated almost completely for wind drift. Track directions were very similar between the two wind categories, whereas heading directions were clearly adjusted towards the wind direction (Fig. 8).

As a second analysis, the effect of the side wind component on flight speed was examined. This was done with a general linear model analysis. The analysis was performed on airspeeds as the dependent variable and included season as a fixed factor and vertical speed, tailwind component, side wind component (calculated as the component of the wind vector that was perpendicular to the heading direction) and potential interactions between season and side wind component as covariates. The result showed that side wind had a significant effect on flight speed. Airspeed increased with a factor

of 1.012 for every 1 ms^{-1} increase in side wind. Liechti et al. (1994) and Liechti (1995) described theoretically that increasing flight speed with increasing crosswind is an adaptive compensation for drift when maintaining a constant track. The study presented in paper VI is possibly the first case of empirical confirmation of this theoretical prediction (cf. Liechti, 2006).

Concluding remarks

The ability to fly is one of the key features of birds. It has a central role in birds' ecology and behavior and by understanding the aerodynamics of different birds we can start to uncover pieces of the complete picture of flight as locomotion. We can learn about its potential and its constraints. The study of animal flight has been ongoing for several hundreds of years, but it is only in rather recent times that we have the technical ability to reveal the underlying mechanisms, both in terms of kinematics and aerodynamics. The studies done so far focusing on the mechanistic base of animal flight are quite few, although the collection of species studied is increasing quickly nowadays. We are still in the beginning of understanding animal flight and the studies performed so far, including those
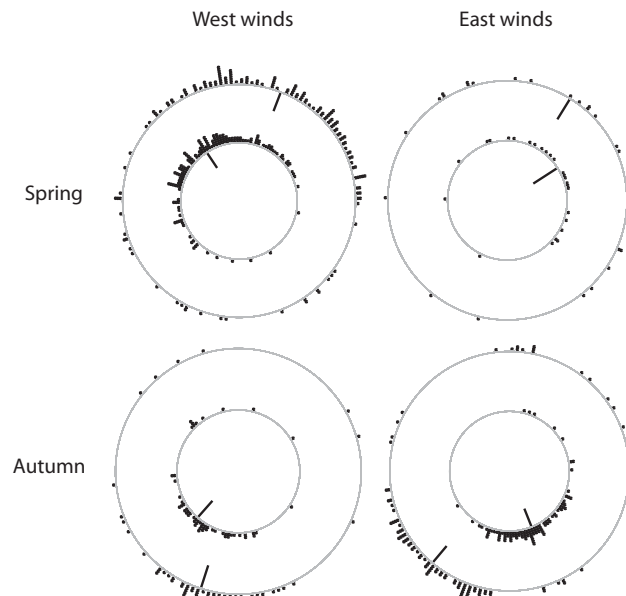

Figure 8. Flight directions (outer circles: track; inner circles: heading) for swifts flying in westerly and easterly winds, respectively, during spring and autumn. Track is maintained in both wind situations, while heading is shifted towards the winds, suggesting a large amount of compensation.

in this dissertation, represent a first glance at a set of different species in order to get an overview of what is 'out there'. The next step is to try to relate these different species and their corresponding aerodynamics and kinematics to each other and to morphology, ecological function and evolutionary history. To do this we probably need to continue to explore more species, but study by study we are getting closer to completing the puzzle of animal flight.

Summary

This dissertation is on the flight of birds. The study species is the common swift (*Apus apus* L.), or swift for short. The swift is a migratory species that breeds in Eurasia and winters in tropical Africa. Swifts are extremely aerial birds: they spend almost their entire lifetime in the air, day and night. The only time these birds land for any considerable time period is during breeding. Such an extreme lifestyle is naturally linked to special adaptations. This is why the flight performance and the aerodynamics of this species are interesting to study. In papers I-III the wake of swifts is studied in a wind tunnel. The airflow behind the bird is visualized by the use of digital particle image velocimetry and the flight behavior is recorded using high-speed cameras.

In paper I, flapping flight was examined at cruising speed and the results showed that the wake of the swift differed from the wakes previously described for other birds. The swift left, in the wake, a pair of trailing vortices behind the wingtips, similar to what had been seen before on other animals, but it also shed vortex filaments between these in an almost continuous manner, indicating a gradual change in the forces produced (Fig. 3). This wake structure was new and it was called the 'continuous change' wake due to this smooth variation in force production over the wingbeat.

In paper II the wake of swifts was revisited and this time the bird was flown over a range of speeds. The system for flow visualization had been upgraded since paper I and now allowed

for high-speed stereo recordings. Due to the high speed, it further allowed for a time resolved wake representation (Fig. 4). The new results showed that in addition to the wake structures found in paper I, a pair of trailing tail vortices and a pair of trailing 'wing root' vortices were found. The wing root vortices had a rotation opposite to that of the wingtip vortices and they appeared to originate from the wing/body junction. The existence of these wing root vortices suggests that the two wings do not operate as one joint wing, but rather are to some degree aerodynamically detached from each other.

In paper III the gliding flight of swifts was examined. The bird was flown over a range of flight speeds and the tunnel was tilted as to simulate different sink rates. The tunnel was initially tilted downwards (air stream from below) to its maximum and then gradually tilted backwards towards horizontal until the bird was just able to glide steadily in the tunnel. That angle then corresponded to the minimum tilt angle for that speed. From this the minimum sink speeds for different flight speeds could be compiled into a glide 'super-polar'. This describes the bird's glide efficiency, which is closely linked to its energy consumption in flight (although flapping flight is different from gliding flight). The wake was also sampled at the minimum tilt angle at each speed and the results show a simpler wake than had been seen in the flapping flight studied in papers I and II. The wake consisted of a pair of trailing wingtip vortices and a pair of trailing tail vortices (Fig. 6).

In paper IV swifts were studied in free flight in their natural habitat using tracking radar. The birds were studied during three different flight scenarios: spring migration, autumn migration and roosting flight. Swifts do not roost, as most birds do, on the ground or perched in a tree; they spend the night in the air. The objective for the study was to compare flight speeds between the three different behaviors and relate them to predictions made based on flight mechanical theory. The results showed that the birds did not change their flight speeds between behaviors to the extent predicted from theory. However, the speed during spring migration was higher than both during autumn migration and roosting

flights, which was in line with predictions, suggesting that that the birds are under time selected migration during spring.

In paper V the peak performance in terms of the flight speeds of the swifts were studied. This was done by measuring the flight speeds of the birds during their display flights, commonly called 'screaming parties'. In both the wind tunnel studies and the radar studies, the range of flight speeds that were recorded were rather narrow, suggesting that the swifts were in some way restricted in terms of available flight speeds. Therefore it was of interest to measure the birds' capability. The results showed that the birds during the screaming parties pushed themselves to perform flight speeds, on average, twice as fast as during migration. This is maybe an unexpected result, that birds that otherwise seem restricted in terms of flight speeds, at the same time are capable of flying at flight speeds higher than most other birds of similar size. It is likely that the swifts perform anaerobic muscle work during these short bursts of high speed flights, compared to the aerobic muscle work during the sustained flight speeds measured during migration.

In paper VI the swifts were again studied using tracking radar and the objective was to examine how these birds respond to wind drift. This is a central concern for any migrating bird that wishes to keep a preferred track direction towards its destination. Side winds will drift the bird away from this if the bird does not compensate for the wind in some way. The most intuitive solution is to orient into the winds and thereby compensate for the side wind component, but it has been shown theoretically that increasing the flight speed with increasing side wind is a way to compensate too. The results showed that the swifts used both these strategies. From the analysis it was clear that the birds compensated to a large extent (almost completely) for side winds by changing their heading direction towards the wind, but it was also shown that the birds increased their flight speed as a response to increased side winds. This was the first time this theoretical prediction was empirically confirmed.

References

Alerstam, T. (1978) A graphical illustration of pseudodrift. *Oikos*, **30**, 409-412.

Alerstam, T. (1991) Bird flight and optimal migration. *Trends Ecol. Evol.* **6**, 210-215.

Alerstam, T. & Lindström, Å. (1990). *Optimal bird migration: the relative importance of time, energy, and safety. In: Bird Migration.* Gwinner, E. (ed.). Springer-Verlag, Heiderlberg,

Bomphrey, R. J. (2006) Insects in flight: direct visualization and flow measurements. *Bioinsp. Biomim.* 1:S1-S9.

Bomphrey, R. J., Lawson, N. J., Harding, N. J., Taylor, G. K. and Thomas, A. L. R. (2005) The aerodynamics of *Manduca sexta*: digital particle image velocimetry analysis of the leading-edge vortex. *J. Exp. Biol.* 208, 1079-1094.

Bomphrey, R. J., Taylor, G. K. and Thomas, A. L. R. (2009) Smoke visualization of free-flying bumblebees indicates independent leading-edge vortices on each wing pair. *Exp. Fluids*, **46**, 811-821.

Bristol, R. L., Ortega, J. M., Marcus, P. S. and Savas, Ö. (2004) On cooperative instabilities of parallel vortex pairs. *J. Fluid Mech.* **517**, 331-358.

Bruderer, B. (1997) The study of bird migration by radar. Part 1: The technical basis. *Naturwissenschaften,* **84**, 1-8.

Bruderer, B. and Weitnauer, E. (1972). Radarbeobachtungen über Zug und Nachtflüge des Mauerseglers (*Apus apus*). *Rev. Suisse Zool.,* **79**, 1190-1200.

Buchanan, K. L. and Evans, M. R. (2000). The effect of tail streamer length on aerodynamic performance in the barn swallow. - *Behav. Ecol.,* **11**: 228-238.

Bäckman, J. and Alerstam, T. (2001) Confronting the winds: orientation and flight behaviour of the roosting swift, *Apus apus. Proc. R. Soc. Lond.* B, **268**, 1081-1087.

Bäckman, J. and Alerstam, T. (2002) Harmonic oscillatory orientation relative to the wind in nocturnal roosting flights of the swift *Apus apus. J. exp. Biol.*, **205**, 905-910.

Bäckman, J. and Alerstam, T. (2003). Orientation scatter of free-flying nocturnal passerine migrants: components and causes. *Animal Behaviour* **65**, 987-996.

Cochran, W. W. and Kjos, C. G. (1985). Wind drift and migration of thrushes: a telemetry study. *Illinois Natural History Survey Bulletin* **33,** 297-330.

Crow, S. C. (1970) Stability theory for a pair of trailing vortices, *AIAA J.* **8**, 2172-2179.

del Hoyo, J., Elliott, A. and Sargatal, J. (1999) *Handbook of the birds of the world.* Vol. 5. Lynx Edicions, Barcelona.

Dial, K. P., Greene, E. and Irschick, J. (2008) Allometry of behavior. *TREE* **23**, 394-401.

Ellington, C. P., van den Berg, C., Willmott, A. P. and Thomas, A. (1996) Leading-edge vortices in insect flight. *Nature*, **384**, 626-630.

Green, M. and Alerstam, T. (2002) The problem of estimating wind drift in migrating birds. *J. Theor. Biol.* **218**, 485-496.

Greenwalt, C. H. (1961) *Hummingbirds.* Doubleday, New York, USA.

Hedenström, A. and Alerstam, T. (1992) Climbing performance of migrating birds as a basis for estimating limits for fuel-carrying capacity and muscle work. *J. Exp. Biol.* **164**, 19-38.

Hedenström, A. and Alerstam, T. (1995) Optimal flight speed of birds. *Phil. Trans. R. Soc. B.* **348**, 287-299.

Hedenström, A., Johansson, L. C., Wolf, M., von Busse, R., Winter, Y. and Spedding, G.R. (2007). Bat flight generates complex aerodynamic tracks. *Science* **316**, 894-897.

Hedenström, A., Muijres, F. T., von Busse, R., Johansson, L. C., Winter, Y. and Spedding, G. R. (2009) High-speed stereo DPIV measurements of wakes of two bat species flying freely in a wind tunnel. *Exp. Fluids* **46**, 923-932.

Holmgren, J. (2004). Roosting in tree foliage by Common Swifts *Apus apus. Ibis* **146**, 404-416.

Hubel, T. Y., Hristov, N. I., Swartz, S. M. and Breuer, K. S. (2009) Time-resolved wake structure and kinematics of bat flight. *Exp. Fluids*, **46**, 933-943.

Kokshaysky, N. V. (1979). Tracing the wake of a flying bird. *Nature* **279**,146-148.

Lack, D. (1956). *Swifts in a tower.* Methuen, London.

Lentink, D., Müller, U.K., Stamhuis, E.J., Kat, R., Gestel, W. Van, Veldhuis, L. L. M., Henningsson, P., Hedenström, A., Videler, J.J. & Leeuwen, J.L van. (2007) How swifts control their glide performance with morphing wings. *Nature* **446**, 1082-1085.

Liechti. F. (1993). Nächtlicher Vogelzug im Herbst über süddeutschland: Winddrift und Kompensation. *J. Orn.* **134**, 373-404.

Liechti, F. (1995). Modelling optimal heading and airspeed of migrating birds in relation to energy expenditure and wind influence. *J. Avian Biol.* **26**, 330-336.

Liechti, F. (2006) Birds: blowin' by the wind? *J. Ornithol.* **147**, 202-211.

Liechti, F., Hedenström, A. & Alerstam, T. (1994) Effects of sidewinds on optimal flight speeds of birds. *J. Theor. Biol.*, **170**, 219-225.

Lindhe Norberg, U. M. (2002) Structure, form, and function of flight in engineering and the living world. *J. Morph.* **252**, 52-81.

Muijres, F. T., Johansson, L. C., Barfield, R., Wolf, M., Spedding, G. R. and Hedenström, A. (2008) Leading-edge vortex improves lift in slow-flying bats. *Science* **319**, 1250-1253.

Pennycuick, C. J. (1968a) A wind tunnel study of gliding flight in the pigeon *Columba livia. J. exp. Biol.*, **49**, 509-526.

Pennycuick, C. J. (1968b) Power requirements for horizontal flight in the pigeon *Columbia livia. J. exp. Biol.*, **49**, 527-555.

Pennycuick, C. J. (1971a). Soaring behaviour and performance of some east African birds, observed from a motor-glider. *Ibis* **114**, 178–218.

Pennycuick, C. J. (1971b) Gliding flight of the white-backed vulture *Gyps africanus. J. Exp. Biol.* **55**, 13–38.

Pennycuick, C. J. (1988) On the reconstruction of the pterosaurs and their manner of flight, with notes on vortex wakes. *Biol. Rev.* **63**, 299-311.

Pennycuick, C. J. (1989) *Bird Flight Performance: A Practical Calculation Manual.* Oxford: Oxford University Press.

Pennycuick, C.J. (2008) *Modelling the Flying Bird.* Elsevier.

Pennycuick, C.J, Obrecht, H. H. and Fuller, M. R. (1988) Empirical estimates of body drag of large waterfowl and raptors. *J. exp. Biol.*, **135**, 253-264.

Pennycuick, C. J., Heine, C. E., Kirkpatrick, S. J. and Fuller, M. R. (1992) The profile drag of a hawk's wing, measured by wake sampling in a wind tunnel. *J. Exp. Biol.* **165**, 1-19.

Pennycuick, C. J., Klaassen, M., Kvist, A. and Lindström, Å. (1996) Wing beat frequency and the body drag anomaly: Wind tunnel observations on a thrush nightingale (*Luscinia luscinia*) and a teal (*Anas crecca*). *J. exp. Biol.*, **199**, 2757-2765.

Pennycuick, C. J., Alerstam, T. and Hedenström, A. (1997). A new low-turbulence wind tunnel for bird flight experiments at Lund University, Sweden. *J. Exp. Biol.* **200**, 1441–1449.

Riskin, D. K., Willis, D. J., Iriarte-Díaz, J., Hedrick, T. L., Kostandov, M., Chen, J., Laidlaw, D. H., Breuer, K. S., and Swartz, S. M. (2008) Quantifying the complexity of bat wing kinematics. *J. Theor. Biol.* **254**, 604-615.

Rosén, M. and Hedenström, A. (2001) Gliding flight in a jackdaw: a wind tunnel study. *J. Exp. Biol.* **204**, 1153-1166.

Rosén, M. and Hedenström, A. (2002) Soaring flight in the eleonora's falcon (*Falco eleonorae*).*The Auk*, **119**, 835-840.

Rosén M., Spedding, G. R. and Hedenström, A. (2007). Wake structure and wingbeat kinematics of a house-martin *Delichon urbica. J. R. Soc. Interface*, 10.1098/rsif.2007.0215.

Spaar, R. and Bruderer, B. (1996) Soaring migration of steppe eagles *Aquila nepalensis* in southern Israel: flight behaviour under various wing and thermal conditions, J*. Avian Biol.*, **8**, 288-297.

Spaar, R. and Bruderer, B. (1997) Optimal flight behavior of soaring migrants: a case study of migrating steppe buzzards, *Buteo buteo*

vulpinus. Behav. Ecol., **8**, 288-297.

Spedding, G. R. (1986) The wake of a jackdaw (*Corvus monedula*) in slow flight. *J. exp. Biol.*, **125**, 287-307.

Spedding, G. R. (1987a) The wake of a kestrel (*Falco tinnunculus*) in gliding flight. *J. exp. Biol.*, **127**, 45-57.

Spedding, G. R. (1987b) The wake of a kestrel (*Falco tinnunculus*) in flapping flight. *J. exp. Biol.*, **127**, 59-78.

Spedding, G.R., Rayner, J.M.V. & Pennycuick, C.J. (1984) Momentum and energy in the wake of a pigeon (*Columba livia*) in slow flight. *J. Exp. Biol.*, **11**, 81-102.

Spedding, G. R., Hedenström, A. and Rosén, M. (2003a). Quantitative studies of the wakes of freely flying birds in a low-turbulence wind tunnel. *Exp. Fluids* **34**, 291-303.

Spedding, G. R., Rosén, M. & Hedenström, A. (2003b). A family of vortex wakes generated by a thrush nightingale in free flight in a wind tunnel over its entire natural range of flight speeds. *J. Exp. Biol.* **206**, 2313–2344.

Spedding, G. R., Hedenström, A. and Johansson, L. C. (2009) A note on wind-tunnel turbulence measurements with DPIV. *Exp. Fluids.* **46**, 527-537.

Tobalske, B. W., Warrick, D. R., Clark, C. J., Powers, D. R., Hedrick, T. L., Hyder, G. A. and Biewener, A. A. (2007) Three-dimensional kinematics of hummingbird flight. *J. Exp. Biol.*, **210**, 2368-2382.

Torre-Bueno, J. R and Larochelle, J. (1978) The metabolic cost of flight in unrestrained birds. *J. exp. Biol.*, **75**, 223-229.

Tucker, V. A. (1987). Gliding birds: the effect of variable wingspan. *J. Exp. Biol.* **133**, 33–58.

Tucker, V. A. (1988). Gliding birds: descending flight of the whitebacked vulture, *Gyps africanus. J. Exp. Biol.* **140**, 325–344.

Tucker, V. A. (1990) Body drag, feather drag and interference drag of the mounting strut in a peregrine falcon, *Falco peregrinus. J. exp. Biol.* **149**, 449-468.

Tucker, V. A. and Parrot, G. C. (1970). Aerodynamics of gliding flight in a falcon and other birds. *J. Exp. Biol.* **52**, 345–367.

Tucker, V. A. and Heine, C. (1990). Aerodynamics of gliding flight in a Harris' hawk, *Parabuteo unicinctus. J. Exp. Biol.* **149**, 469–489.

Tucker, V. A., Cade, T. J. and Tucker, A. E. (1998). Diving speeds and angles of a gyrfalcon (*Falco rusticolus*). *J. Exp. Biol.* **201**, 2061–2070.

Warrick, D. R., Tobalske, B. W. And Powers, D. R. (2005) Aerodynamics of the hovering hummingbird. *Nature* **435**, 1094-1097.

Weis-Fogh, T. & Alexander, R. McN. (1977). *The sustained power output from striated muscle.* - In: T.J. Pedley (ed.) Scale Effects in Animal Locomotion, London Academic Press., London, pp. 511-525.

Zehnder, S., Åkesson, S., Liechti, F. & Bruderer, B. (2001). Nocturnal fall bird migration at Falsterbo, south Sweden. *Journal of Avian Biology* **32**, 239-248.

Tornseglarens flykt

Populärvetenskaplig sammanfattning

Figurer återfinns i den engelska sammanfattningen

Fåglars flykt är något som i alla tider fascinerat oss människor. Vi har nog alla någon gång stått och förundrats över hur elegant en tornfalk ryttlar över en äng, eller med vilken enastående precision en fiskgjuse kan fånga sin fisk i en sjö. Inom vetenskapen har man studerat fåglars flykt under mycket lång tid. Redan Leonardo da Vinci var intresserad av hur fåglar och andra djur bar sig åt för att kunna flyga. Förutom ren och skär nyfikenhet, var Leonardo också intresserad av att försöka bygga flygande maskiner. På den tiden visste man ingenting om hur luftflöden beter sig för olika objekt som till exempel en liten fladdermus och ett flygplan. Därför trodde man att svaret låg i att imitera djuren så bra som möjligt. Numera vet vi att det inte fungerar så, men vid den tiden var det en logisk slutsats. Efter Leonardo skulle det dröja ungefär 400 år innan bröderna Wright 1903 lyckades bygga sin första flygmaskin som verkligen fungerade. Sedan dess har det hänt mycket med flygplansutvecklingen, men hur fantastiskt avancerade de flygplan som görs nu än är, så är de inte i närheten av någon av naturens flygare vad gäller manövrerbarhet, precision eller energieffektivitet. Vi har fortfarande mycket att lära från fåglars flykt.

Denna avhandling representerar ett försök att förstå en aning mer om fåglar flykt genom att studerar en av naturens mest avancerade flygare, tornseglaren (*Apus apus*, L.). Tornseglaren är en flyttande fågel som vi här i norra Europa endast har på besök under några månader varje sommar, resten av året spenderar tornseglaren i tropiska Afrika eller på flyttning. Tornseglarna är väldigt speciella fåglar, de spenderar nästan hela sitt liv i luften. De jagar sin föda i luften, sover i luften (!), samlar bomaterial i luften och det händer även att de parar sig i luften. Den enda gång som dessa fåglar landar för en längre tidsperiod är under häckningen. Denna livsstil är naturligtvis kopplad till speciella evolutionära anpassningar. Tornseglaren är olik andra fåglar vad gäller kropp- och vingform. Kroppen är strömlinjeformad och vingarna är långa, smala och hålls ofta bakåtsvepta. Anledningen till att studera en sådan fågel är att den, på ett sätt, är essensen av en fågel. En så pass avancerad flygare kan lära oss mycket om fåglars flykt även i en vidare bemärkelse, dess potential och dess begränsningar.

När en fågel flyger genom luften lämnar den bakom sig ett "spår" av virvlar (ofta kallat vaken). Dessa virvlar reflekterar de krafter som bildats av vingen och genom att lyckas fånga dessa på bild och analysera deras egenskaper, kan man räkna ut styrkan på de krafter som fågeln bildar när den flyger. För att kunna göra detta krävs att man flyger med fågeln

under ordnade former, dvs det är inte möjligt att göra detta i det vilda. För experimenten i artikel I, II och III användes en vindtunnel där fåglarna fick flyga. Med en vindtunnel kan man simulera naturlig flykt genom att låta fågel flyga stationärt i förhållande till vindtunneln och istället låta en vind blåsa mot fågeln (Fig. 2). Detta kan låta märkligt, men aerodynamisk sett är denna situation identisk med att fågeln i stället flyger genom stilla luft med motsvarande hastighet.

I artikel I studerades vaket av en tornseglare i aktiv flykt, dvs när fågeln genererar kraft genom att slå med vingarna. Luften visualiserades och analyserades och på så vis kunde luftvirvlarna, vaken, bakom fågeln återskapas i förenklad form. Bakom sina vingspetsar lämnade tornseglaren virvlar som fanns med genom hela vingslaget, vilket är något man sett tidigare på andra flygande djur. Utöver dessa släpptes dock även, genom hela vingslaget, virvlar vinkelrätt mot de två vingspetsvirvlarna. Dessa virvlar sammanband vingspetsvirvlarna och varierade mycket mjukt i styrka över vingslaget (Fig. 3). Denna typ av vak hade man inte sett tidigare hos andra fåglar.

För artikel II studerades tornseglarens aktiva flykt ännu en gång och denna gång flögs fågel över ett hastighetsintervall. Resultaten från den studien visade att, förutom de vakstrukturer som beskrevs i artikel I, bildades ett virvelpar av fågelns stjärt och ett virvelpar någonstans där vingarna möter kroppen. Att det bildas virvlar vid vingfästena tyder på att de två vingarna tillsammans med kroppen aerodynamiskt sett inte fungerar som en enda vinge utan att vingarna till viss del arbetar skilt från varandra. Detta beror troligen på att kroppen bildar mindre lyftkraft än vingarna och på så vis omöjliggör en mjuk lyftkraftsfördelning från vingspets till vingspets. Det är energetiskt sett mindre effektivt att fågeln bildar dessa extra virvlar, men det är inte nödvändigtvis bara negativt. Genom att var vinge arbetar till viss del aerodynamiskt skilt från den andra kan eventuellt manövrerbarheten öka för fågeln.

I artikel III presenteras en studie av tornseglarens glidflykt. Även om det rör sig om samma typ av fågel som i artikel I och II, är

sättet att flyga ganska olikt mellan aktiv flykt och glidflykt. I glidflykt slår fågeln inte med vingarna och därmed bildar den inte heller någon egen kraft. I stället skapas aerodynamisk kraft genom att omvandla lägesenergi till kinetisk energi genom att fågeln sjunker. I studien som presenteras i artikel III flögs en tornseglare åter igen i vindtunneln och genom att vinkla tunneln nedåt så att vinden kom snett underifrån kunde fågeln lockas att glida stationärt. När fågeln glider på samma ställe motsvarar den vinkel vindtunneln ställs in på precis den vinkel mot horisontalplanet som fågeln hade glidflugit med i det fria. Eftersom alla krafter är i balans, kan man baserat på vindtunnelns lutningsvinkel och fågelns vikt räkna fram den lyftkraft som bildas av fågeln och det luftmotstånd som fågeln utsätts för vid olika hastigheter. Förhållandet mellan lyft och luftmotstånd är ett mått på fågelns effektivitet som glidflygare: ju mer lyft som bildas i förhållande till luftmotstånd desto mer effektiv är fågeln. I jämförelse med andra arter visade sig tornseglaren vara relativt effektiv i detta avseende.

I artikel IV lämnade jag vindtunneln och studerade i stället tornseglarnas flykt i det vilda. Detta gjordes med hjälp av en målsökande radar. En sådan radar kan följa enskilda objekt med hög noggrannhet på upp till ca fem kilometers avstånd. Målet för studien var att undersöka vilka flyghastigheter tornseglarna valde att flyga med under tre olika beteenden: vårflytten, höstflytten och när fåglarna sover i luften. Det finns teorier om vilka hastigheter som bör vara bäst vid dessa tre beteenden, så idén var att jämföra prediktioner från dessa teorier med vad tornseglarna verkligen gjorde. Enligt teorin borde tornseglarna flyga snabbast på vårflytten eftersom de då är tidspressade och långsammast när de sovflyger eftersom de då inte behöver försöka komma någonstans. Under höstflytten borde de flyga med hastigheter någonstans mitt emellan. Resultatet visade att tornseglarna mycket riktigt flög fortare på vårflytten, men mellan höstflytt och sovflygningar fanns det ingen större skillnad. Det generella resultatet visade att tornseglarna ändrade sina flyghastigheter mindre än vad som predikterats från teorin, som om de på något sätt var begränsade vad gällde

möjliga flyghastigheter.

Artikel V knyter mycket an till föregående artikel, men infallsvinkeln var ganska olik. Eftersom tornseglarna verkade vara begränsade med avseende på flyghastigheter studerades fåglarna under deras spelflykt. Tornseglarnas spelflykt är en typisk sommarföreteelse, du har säkert någon gång sett dem när de snabbt flyger runt skrikande i täta flockar lågt över hustaken i kvällningen. Eftersom fåglarna verkar flyga fort under detta beteende, kunde det vara intressant att se hur fort de egentligen flyger och vad det krävs för att göra detta. Detta studerades med hjälp av stereofilmning. Två höghastighets-kameror monterades på ett avstånd från varandra för att skapa "stereo-syn" och riktades mot en tornseglarkoloni där många individer ofta flög förbi i spelflykt. Genom att filma i stereo kunde fåglarnas tredimensionella flygbanor räknas fram i efterhand så att det inte spelade någon roll hur fåglarna flög i förhållande till kamerorna. Från dessa flygbanor beräknades sedan varje fågels flyghastighet. Det visade sig att tornseglarna, precis som man skulle tro, flög snabbt under detta beteende, upp till 110 km/h och i medel 75 km/h vilket är ungefär dubbelt så fort som medel under vår- eller höstflytten. Så, helt plötsligt var fåglarna som annars verkade vara begränsade, kapabla att prestera flyghastigheter som ligger högre än de flesta andra fåglar i deras storleksklass. Uppskattningar gjordes även för vad som krävs av fåglarnas flygmuskulatur för att prestera dessa exceptionella flygningar och resultaten antydde att musklerna under den korta tid som fåglarna blixtrar förbi kolonin arbetar nära gränsen för vad vertebratmuskler är kapabla till.

Artikel VI handlar om hur tornseglare kompenserar för vindarna under flyttingen. Detta är ett centralt problem för alla flyttande fåglar, eftersom de oftast har ett mål de siktar på. Om de tar sikte mot målet och flyger utan att ta hänsyn till och korrigera för rådande vindarna kommer de att drivas bort från sin flygrutt. Eftersom tornseglare hade visat sig vara välutvecklade flygare i flera andra avseenden, var prediktionen att de även skulle vara skickliga på att kompensera för vindarna. Återigen var det radardata som låg till grund för analysen och resultatet visade att tornseglarna, till väldigt stor del, kompenserade för vindarna genom att ändra sin flygriktning in mot vinden och på så vis bibehöll sin riktning. Detta skedde både under vår- och höstflyttning vilket tyder på att även unga, oerfarna tornseglare, besitter denna färdighet. Om unga fåglar inte hade kunnat detta hade fåglarnas spridning under hösten varit större än under våren eftersom en stor andel av de höstflyttande tornseglarna är ungfåglar som beger sig ut på sin första resa mot Afrika. Ett annat resultat från denna studie var att tornseglarna, förutom att kompensera för vindarna genom att ändra sin flygriktning, även kompenserade genom att öka sin flyghastighet. Detta har tidigare beskrivits teoretiskt som en möjlig vindrespons bland flyttande fåglar, men denna studie är den första att visa detta empiriskt.

Thanks!

Even though only one name is featured on the cover of this book, it far from means that all the work has been done by only one person. I have had the privilege to work with, and be surrounded by, many wonderful people.

First of all I wish to thank my supervisor, Anders Hedenström. To me, you are the perfect supervisor! I was always free to work on my own and make my own decisions, but you were always there for me whenever I needed your help. I thank you for your firm guidance along the crooked paths of Science, for reading and improving all of my manuscripts and for "quality checking" my work. I have appreciated your honesty and thoroughness when giving me feedback very much. You have taught me so much these years and I am forever grateful for that.

I also wish to thank my co-supervisor, Thomas Alerstam. It has always been a pleasure to meet with you and discuss the results of our studies. Your enthusiasm has always given me new energy to tackle the next analysis.

I have been blessed with the opportunity to work in a research group with amazing people, the Animal Flight Lab. You are all like beacons of knowledge to me and I have enjoyed every minute of the time together with you. I thank you all! Florian. My friend and colleague. You are a brilliant guy. I think you are one of the most honest persons I know. If you ever thought something I was working on did not meet the standards, you told me so without hesitation. This is a rare quality and something I have appreciated a lot. Thank you also for all the "off-work" activities we have done together. Christoffer, your knowledge of our research field and your creativity have been an inspiration to me from the very beginning. Your ability to give a suggestion on what to do after only two minutes of briefing about a tricky problem has always impressed me. I thank you for all the spontaneous discussions that many times have led to the next step of analysis or even new experiments. Melissa, Rhea, Marta and Sophia. You are all such nice people and you possess so much knowledge. It has always been a pleasure to talk with you about research or about whatever. I especially thank you, Marta for helping me in the beginning when I did not know the first thing about PIV. Your handwritten step-by-step, do-it-yourself PIV-guide was my lifeline in the beginning.

I wish to thank Jan Holmgren for lending us his beloved swifts for flights in the tunnel and for all the help. It has always been interesting to listen to everything you tell me about swifts. You know so much more about these birds than I will ever do. Thank you also for letting me do the high-speed stereo-filming experiments in your backyard and for afterwards helping me with measuring the calibration cube for four hours in one of the hottest days of the year.

I wish to thank Melissa Bowlin, Sara Henningsson, Håkan Karlsson, Teresa Kullberg and of course Anders Hedenström for proofreading my drafts of the introductory part of this thesis.

Håkan! Min västgötske broder! You are a true friend. I am very glad that you and I ended up in Lund both of us and that we even did two studies together. Your enthusiasm for the masses of

migrating birds that appeared on the radar screen when I in the beginning only saw green blips made me quickly appreciate the fantastic possibilities of the radar technique. I soon also saw beyond the green fluttering curve and started to see the beautiful image appearing on the radar screen. Those were some magical nights! Thank you.

Johan. Thank you for all those hours of working on improving your excellent radar software (and for making it in the first place for that matter). Your vast knowledge is sometimes even intimidating! I don't think I've been more impressed by many more persons in my life! Thank you also for your refreshing and ironic humor, it has many times made my day.

Sara, my sister. I am so happy that we ended up doing our PhD-studies in Lund at the same time, despite our very different ways getting here. I was afraid that we forever had lost you to that country across the Atlantic, but you returned and for that I am very glad. It has been so nice to have you here, not the least in the beginning, when I was getting my bearings. It was much because of you I started planning to come here to Lund and doing my PhD, so for that I am very thankful. Thank you also for our childhood together. You and I have always been such good friends! Soo many memories...

Anna, my oldest sister. Isn't it quite funny that all three of us kids have been doing our PhD during more or less the same time? You have always inspired me, ever since we were little. I remember that you, being my oldest sister, very much "set the standards" and I think that it was largely because of you I started studying to begin with. You were a role model. I thank you for that and wish you good luck on finishing your own thesis!

Jennie, my office roommate for almost the whole time. Sharing office with you has been great. I was very lucky that you also used an "open", "multi-layer" archive structure on you desk, which made my desk look a little bit less messy (that hybrid zone by the phone where our paper piles met was rather interesting). Thank you!

The department. Were to begin? The four years I've spent here has been some of the best in my life. This department has been such a wonderful work place. This place is oozing creativity! The warm and nice atmosphere has made me enjoy every day. All those impossible discussions during coffee breaks, midnight swimming in places were no man is meant to go swimming and all the humor of the people here has added to the already fun work of doing research. I thank you all!

Many thanks to the people of the Migration Group and CAnMove for all the interesting presentations during our meetings.

I wish to thank Gunilla Lindquist and Anne Fogelberg for helping me with all those (for me) completely incomprehensible administrative things and for both being such nice and colourful people.

Thanks to the staff at the Biology library. You were all very helpful whenever I needed your help to find some obscure article or book.

I also want to thank my former teacher at University of Skövde, Noél Holmgren, for inspiration and for encouraging me to apply for a PhD.

Mamma och Pappa!

Mamma. Du är utan tvekan en av de visaste personer jag känner. Din nyfikenhet på livet och optimistiska inställning har alltid varit en stor inspiration för mig i vad än jag tagit mig för. Jag tror nog att lite av dessa två egenskper spillt över en aning på mig och det är jag evigt tacksam för. Jag har så många trevliga minnen från allt vi gjort tillsammans. Alla de där sakerna som du sysslat med under åren har verkligen fått mig att inse hur mycket roligt det finns att göra i livet! Det har varit allt från oljemåleri, till släktforskning, till botanik, till antikviteter, till keramik, ja det finns ingen ände. Du är fantastisk!

Pappa. Du har ända sedan jag var liten fått mig att känna att allt är möjligt att göra om man bara tar sig tiden att lära sig. Sedan får man väl säga att du är extrem i detta avseende, det är inte många som hänger med (att gå från flygplanstekniker till överläkare i klinisk kemi hör inte till de

allra vanligaste karriärsutvecklingarna). Men, hur som helst, så har din oerhörda kunskap och törst efter ännu mer kunskap (jag har väldigt nyfikna föräldrar) alltid inspirerat mig. Dessutom minns jag precis det tillfälle som utan tvekan ledde mig in på den väg jag nu tagit. Jag minns hur du lärde mig gärdsmygen sång när vi var ut och promenerade i skogen en gång. Jag blev fullständigt fångad direkt! Efter det har fåglar alltid varit närvarande i mitt liv. Jag tackar er båda två för att ni alltid trott på min förmåga och stöttat mig i mina val!

Tea. I am convinced. Newton was wrong. You are the reason the planets revolve around the sun (at least in my Universe). My life is so bright because of you. I love you deeply.
You have also directly contributed to the making of this thesis by all the discussions (or sometimes just listening to my monologues about some tricky analysis problem), all the proofreading or other help with finding the right words when I was writing and not to say the least, all the enormous help you gave me when I was caring for the swifts and doing experiments. Without you this thesis would never had been written. I am forever thankful.

Per Henningsson
Helsingborg, 20 December 2009

List of contributions to the papers

Paper I. The study was planned together with Anders Hedenström (AH). I did the experiments, data processing and the major part of the analysis. The results were discussed with AH and Geoffrey Spedding (GS). I wrote the paper together with AH and GS.

Paper II. The study was planned together with AH. I did the experiments. I did the data processing and analysis with help from Florian Muijres (FM). The results were discussed with AH, FM and Christoffer Johansson (CJ). I wrote the paper together with AH and FM.

Paper III. The study was planned together with AH. I did the experiments, data processing and data analysis. The results were discussed with AH and FM. I wrote the paper together with AH.

Paper IV. The study was planned together with all of the authors. Parts of the data were collected by me together with Håkan Karlsson (HK) and parts of the data were collected by Johan Bäckman (JB) and Thomas Alerstam (TA). I processed and analyzed the data with help from JB and HK. The results were discussed by all of the authors. I wrote the paper with help from all of the co-authors.

Paper V. The study was planned together with CJ and AH. I did the experiments, processed the data and did the analysis. The results were discussed together with AH and CJ. I wrote the paper together with AH and CJ.

Paper VI. The study was planned together with all of the authors. The data were the same as for paper IV. HK did the analysis with input from me and all of the other authors. The results were discussed by all of the authors. I participated in writing the paper.

Vortex wake and flight kinematics of a swift in cruising flight in a wind tunnel

P. Henningsson[1,*], G. R. Spedding[2] and A. Hedenström[1]

[1]Department of Theoretical Ecology, Lund University, SE-223 62 Lund, Sweden and [2]Department of Aerospace and Mechanical Engineering, University of Southern California, Los Angeles, CA 90089-1191, USA

*Author for correspondence (e-mail: per.henningsson@teorekol.lu.se)

SUMMARY

In this paper we describe the flight characteristics of a swift (*Apus apus*) in cruising flight at three different flight speeds (8.0, 8.4 and 9.2 m s^{-1}) in a low turbulence wind tunnel. The wingbeat kinematics were recorded by high-speed filming and the wake of the bird was visualized by digital particle image velocimetry (DPIV). Certain flight characteristics of the swift differ from those of previously studied species. As the flight speed increases, the angular velocity of the wingbeat remains constant, and so as the wingbeat amplitude increases, the frequency decreases accordingly, as though the flight muscles were contracting at a fixed rate. The wings are also comparatively inflexible and are flexed or retracted rather little during the upstroke. The upstroke is always aerodynamically active and this is reflected in the wake, where shedding of spanwise vorticity occurs throughout the wingbeat. Although the wake superficially resembles those of other birds in cruising flight, with a pair of trailing wingtip vortices connected by spanwise vortices, the continuous shedding of first positive vorticity during the downstroke and then negative vorticity during the upstroke suggests a wing whose circulation is gradually increasing and then decreasing during the wingbeat cycle. The wake (and implied wing aerodynamics) are not well described by discrete vortex loop models, but a new wake-based model, where incremental spanwise and streamwise variations of the wake impulse are integrated over the wingbeat, shows good agreement of the vertical momentum flux with the required weight support. The total drag was also estimated from the wake alone, and the calculated lift:drag ratio of approximately 13 for flapping flight is the highest measured yet for birds.

Key words: swift, *Apus apus*, aerodynamics, flight, wake, kinematics, wind tunnel, digital particle image velocimetry (DPIV).

INTRODUCTION

When an animal flies through the air it leaves behind a region of modified fluid motions, known collectively as a wake, which reflects the magnitude and time history of aerodynamic forces generated by the wings and body. Newton's third law requires that the forces exerted by a solid body upon a surrounding fluid be exactly equal and opposite to the forces exerted by the fluid on the body, and studying the wake is an elegant practical method for examining the forces produced with minimal interference with the flying animal. In principle, the consequences of all wing, tail and body actions are to be found in the wake. In steady motions, the flow fields responsible for lift generation of an aerofoil can conveniently be characterized by the strength and geometry of compact regions of shear and rotation, idealized mathematically as line vortices. Then a description of the wake vorticity is entirely sufficient for quantitative description and prediction of the forces on the body. As Dabiri (Dabiri, 2005) [summarized in Peng and Dabiri (Peng and Dabiri, 2008)] has recently stressed, in unsteady flows there can be another significant component of the force that appears as an acceleration of the line vortices themselves. The accelerating component itself does not have vorticity, but is a purely potential flow, and both types of flowfield need to be measured in order to account for all forces acting on the fluid. In many cases of moderate amplitude flapping animal flight, however, it is likely that the unsteady accelerations of the vortices themselves are comparatively small compared with the rotational acceleration of the fluid around them. We will return to this point later but, for now, we will consider the wake vorticity as the primary and important distinguishing characteristic of wakes in animal flight.

Idealized vortex wake models have been developed describing wakes found at different flight speeds. The discrete loop wake (Rayner, 1979a; Rayner, 1979b; Rayner, 1979c) postulates that during each downstroke a single vortex loop is formed and shed, and the resulting momentum flux provides the force required to support the weight and overcome viscous and induced drag forces. In this model the upstroke is considered inactive. This model corresponds well (at least qualitatively) to the wakes found in slow forward flight of small passerines, pigeons and jackdaws (Kokshaysky, 1979; Spedding et al., 1984; Spedding, 1986; Spedding et al., 2003b). At higher, cruising flight speed a model different from the discrete loop model was found to be a better approximation of the wake. This model is called the constant circulation model (Spedding, 1987; Rayner et al., 1986) and approximates the wake disturbance as a pair of trailing wingtip vortices of nearly constant circulation that undulate up and down, roughly following the wingtip trace. In this case both down- and upstroke are active, where the downstroke produces lift and thrust and the upstroke produces lift and negative thrust (drag). Because the wings are flexed during the upstroke, the aerodynamic forces are smaller in magnitude, and the resulting net horizontal force is the thrust. An interesting characteristic of this wake model is that since the circulation of the wake vortices does not change, then neither can the wing circulation, and so there is no large-scale shedding of spanwise vorticity during the wingbeat cycle. This would appear, but has never been proven, to be an efficient form of locomotion.

A third type of wake, called the ladder wake, has been proposed for animals that fly with rigid, relatively inflexible wings, such as

humming birds and swifts (Pennycuick, 1988; Pennycuick, 1989). As noted above, for animals flying with upstroke wing flexion, the net forward thrust is achieved by an asymmetry in the effective span of the downstroke and upstroke. If the wings do not flex, then positive thrust must be achieved by some other means. The ladder wake model provides the required asymmetry by variation of circulation, rather than wake width. As with the constant circulation wake, the wings leave continuous trailing wingtip vortices, but in this case they are connected by spanwise vortices shed during both wingbeat turning points. At the transition from the upstroke to the downstroke a distinct vortex with positive (counter-clockwise) circulation is shed from the wings as the circulation of the bound vortex on the wings increases. Then, at the transition from downstroke to upstroke, the wing circulation decreases and so a corresponding vortex with negative (clockwise) circulation is shed. The upstroke–downstroke asymmetry required for net thrust comes from the different circulation values. The ladder wake has been proposed but never observed, perhaps because no equivalent wake studies have been made of comparatively rigid-winged birds.

Studies of birds and bats in wind tunnel flight show that real wakes differ from these idealized wake models (Spedding et al., 2003b; Hedenström et al., 2006a; Hedenström et al., 2007; Rosén et al., 2007). In this paper we investigated the wake properties of the swift *Apus apus* L., since it has been suggested as a candidate species for the ladder wake. The swift is unlike most bird species, with respect both to its biology and to its body design. It spends almost its entire lifetime on the wing, day and night, landing only to breed (Lack, 1956) and only occasionally roosting in trees (Holmgren, 2004). This extreme lifestyle is naturally coupled to a specialized body and wing design. The swift has a streamlined body and long, relatively slender, aft-swept wings. This design and its aerodynamic function potentially contain features that, if understood, would widen our knowledge of animal flight.

MATERIALS AND METHODS
The wind tunnel
Experiments were performed in the low turbulence wind tunnel at Lund University, Sweden. The wind tunnel has an octagonal test section, 1.22 m wide and 1.08 m high. The 1.2 m upstream part of the test section, where the actual measurements are performed, has Plexiglas walls and the 0.5 m downstream part is open, providing quick and easy access to the flying animal during experiments. The air speed across 97.5% of the test section is within ±1.3% of the mean and the turbulence level in the upper test section part is on average 0.04% of the wind speed (Pennycuick et al., 1997). The x-, y- and z-axes of a rectangular coordinate system lie in the streamwise, spanwise and vertical directions, respectively.

Birds, housing and flight training
Two juvenile swifts were captured on 2nd August, 2006, in their nest, the day before their expected fledging. The timing of capture was decided based on cues such as restlessness and intense flight muscle training inside the nest boxes. The birds were then kept for 12 days and during this time, when not flying in the wind tunnel, they were kept in a lidless plastic box with a nest bowl. They were hand fed with a mixture of maggots, crickets, dried insects and supplementary vitamin powder for birds every second hour throughout daytime. The mass and overall health status of the birds were monitored carefully. The flight training required was minimal and both birds made their premier flight in life in the wind tunnel the day after capture with impressive success. The birds quickly learned to fly stably in the test section, within the first 2 days of

training. The birds were guided in the tunnel by a marker (a fly on a string suspended from the ceiling) upstream and to the side of the measuring volume. One of the birds, however, started to fly into the contraction section upstream of the test section and could therefore not be used for quantitative measurements, but for visual observation only. Both birds were released into the wild with normal body weights and in good condition on 13th August, 2006. Morphological details of the single bird used in the experiments are presented in Table 1.

Wingbeat kinematics
Flight kinematics of the swift were recorded in the wind tunnel using a high-speed camera (NAC Hotshot 1280, Simi Valley, CA, USA) filming from a posterior position, *ca* 1.2 m downstream of the test section to ensure negligible disturbance of the flow in the test section. The camera recorded sequences of 2.75 s in duration at 60 frames s^{-1} and with an exposure time of 1/60 s. The sequences were recorded as 24 bit grayscale AVI-files with a resolution of 640 pixels×510 pixels and a pixel aspect ratio of 1:1. The swift was filmed in steady flight at three wind speeds at which the bird was found to be able to fly in a natural manner: 8.0, 8.4 and 9.2 m s^{-1}. Numerous sequences were initially recorded for each wind speed (in total N=460) and then each sequence was carefully and critically studied so only sequences or parts of sequences showing perfectly stable flight and where both the upper and the lower wingtip turning points could be seen were used for further analysis (N=7, 12 and 6 for 8.0, 8.4 and 9.2 m s^{-1}, respectively).

For each of the remaining sequences the position of the shoulder joint and the wingtip in each frame were digitized in a custom-written MatLab program (The MathWorks, Inc., Natick, MA, USA), recording the *ix*- and *iy*-position (in camera pixel coordinates) of these two reference points, respectively ($p1$, $p2$ in Fig. 1). The horizontal camera axis was aligned with the mean flow in the wind tunnel, and on corresponding reference grids. The position of the shoulder joint was in every sequence clearly distinguished, while for the wingtip, moving much more rapidly, the blur sometimes prevented accurate positioning. In these cases the position of the wingtip was interpolated from a cubic smoothing spline function to the total vector of positions for the sequence. To calculate the amplitude and the wingspan in real coordinates (m), a reference length was determined by finding the time of the upper turning point in each wingbeat and calculating the length between the shoulder joint and wingtip in pixels at this moment. Turning points are the transitions from down- to upstroke and *vice versa* and were found from the locations of zero derivatives of the spline-fitted time series of shoulder-to-tip angles. At the upper turning point of the wingbeat the swift's wing is completely outstretched and gives an accurate reference length. The measured length (m) of the swift wing (shoulder–wingtip; Table 1) was divided by the mean of the distances in pixels to obtain a conversion factor, unique for every sequence.

Table 1. Morphological details of the bird used in the experiment

Total mass (kg)	0.039
Wingspan (m)	0.38
Wing area[a] (m^2)	0.015
Aspect ratio[b]	9.6
Shoulder–wingtip (m)	0.1789
Body frontal area (m^2)	0.0017

[a]Defined as the area of both wings including the body area in between.
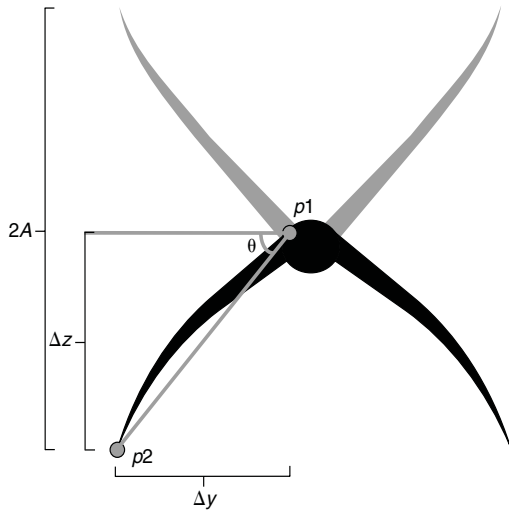[b]Defined as wingspan squared divided by wing area.

Fig. 1. Rear view of the flying swift showing the method of digitizing from high-speed films. The shoulder joint (*p*1) and wingtip (*p*2) are located and with the measurements of distance in the horizontal (Δ*y*) and vertical (Δ*z*) direction between these, the stroke angle (θ) can be calculated. The peak-to-peak amplitude, 2*A*, is the distance between the wingtip at the upper and lower turning point.

The uncertainty in estimating wing marker positions is determined by the pointing accuracy of the human operator and by the discretization of the data in space and time. The wingbeat frequency was around 9 Hz and the framing rate was 60 Hz. The relatively coarse temporal resolution is why smooth functions were fitted to the data before analysis. Note that measurements such as semispan and wingtip amplitude are not necessarily systematically underestimated because the spline fitting function is as likely to overshoot the data as to underestimate it. Overall uncertainties in the kinematic data may be estimated to be less than 5%.

From each digitized sequence the following kinematic data were derived.

Wingbeat frequency (*f*): the wingbeat frequency was derived from the angle between the shoulder joint and the wingtip, which was calculated for each frame in each flight sequence (Fig. 1). The sequence of angles was used as a signal from which the dominant frequency was derived using a discrete Fourier transform. A dominant frequency was distinct in every sequence analysed and the mean of these was calculated.

Wingbeat angular amplitude (θ_{tot}): the total wingbeat angular amplitude was calculated by recording the absolute angle between the shoulder joint and the wingtip at the turning points of the wingbeat. The upper and lower angles are added to yield the peak-to-peak angular amplitude in each wingbeat cycle ($\theta_{tot}=\theta_u + \theta_l$), and a mean was calculated for each sequence (Fig. 1).

Wingbeat amplitude (2*A*): the peak-to-peak wingbeat amplitude was calculated from the absolute distance in *z* between the shoulder joint and the wingtip (Fig. 1), for both upper and lower wingtip excursions ($2A=A_u + A_l$). The mean of the measured amplitude of each wingbeat for the complete sequence was calculated.

Wingbeat angular velocity ($\dot{\theta}_{u,d}$): the angular velocity during mid-upstroke and -downstroke was derived from the derivative of the spline function of the angular time series. The mid-stroke was defined as the moment at which the angle between the shoulder joint and the wingtip was zero, i.e. when the wing was passing the

horizontal plane with respect to the shoulder joint. The mean angular velocities during mid-upstroke ($\dot{\theta}_u$) and -downstroke ($\dot{\theta}_d$) were calculated for each sequence.

Downstroke duration and fraction (T_d, τ): the downstroke duration, T_d, was defined as the time for the wing to travel from the upper turning point to the lower one. The downstroke fraction was $\tau=T_d/T$, where *T* is the period of one entire wingbeat cycle.

Wing semispans (b_d,b_u) and span ratio, (*R*): the local semispan in each frame was measured by multiplying the absolute distance in the horizontal direction from the shoulder joint to the wingtip in pixels by the conversion factor described above, and adding half the body width to the result. As with the mid-stroke angular velocity, $\dot{\theta}_{u,d}$, the mid-stroke span was calculated when the wing passed through the horizontal plane. The semispan is therefore defined as the horizontal component of the distance between the body centreline and wingtip. This is the length that best approximates the aerodynamically significant quantity. The span ratio was calculated as the ratio between the semispans at mid-upstroke and -downstroke, $R=b_u/b_d$.

Flow visualization

The method of quantitative flow visualization is a custom variant of digital particle image velocimetry (DPIV) known as CIV, as presented in Spedding et al. (Spedding et al., 2003a). A thin fog (particle size 1 μm) is continuously introduced downstream of the test section and re-circulates in the tunnel until evenly distributed. During measurements, the fog is illuminated by a double-pulsed laser (Spectra Physics Quanta Ray PIV II, dual head Nd:YAG, with Q-switch-controlled 200 mJ per pulse energy) at a repetition frequency of 10 Hz. The laser produces a 3 mm thick vertical light sheet, aligned with the flow, entering from beneath the test section floor. The time between pulse pairs is controlled by a delay generator (Stanford Research System DG535) that can be set to introduce an arbitrary time delay, δ*t*. For any given flow speed, δ*t* was tuned carefully to allow the maximum possible mean particle image displacement without losing data from complex parts of the flow. A CCD array camera (Redlake, Megaplus II ES 4020, Tallahassee, FL, USA), with focal plane positioned parallel to the laser sheet, captures images in synchrony with the pulsed laser. The camera is operated in binning mode (1024 pixels×1024 pixels) and the images are transferred via a digital interface (DVR Express 1.23, IO Industries, London, ON, Canada) to a parallel SCSI disk array on a PC, where CIV processing takes place.

Calculated displacements of rectangular windows in the pixel image plane are converted to velocities in the plane of the laser sheet, using a pixel conversion factor and the known time δ*t*. The laser sheet is always oriented vertically and streamwise, so the velocity components are {*u,w*} in {*x,z*}. The wake structure is described in terms of the spanwise component of vorticity:

$$\omega_y = \frac{\partial w}{\partial x} - \frac{\partial u}{\partial z} .$$

In a well-run experiment, uncertainties in {*u,w*} of 1–2% are realizable, which typically gives uncertainties in gradient quantities of ±5–10%.

A rear-view camera (described above) is positioned downstream of the test section recording film sequences used for classifying the position of the bird with respect to the laser. The position of the bird in relation to the light sheet was classified discretely as, first, left wing (L), right wing (R) or body (LR) and, second, as inner wing (X), mid-wing (Y) or outer wing (Z). For example, an image

corresponding to the inner left wing would be denoted as 'LX' (Fig. 2). The bird typically flew 0.4 to 0.5 m upstream of the laser sheet, which resulted in a small time delay between the motion recorded by the downstream camera and the wake images recorded by the PIV camera. When flight speed U=8.4 m s^{-1}, the delay would be around 0.05 s. This is compensated for by linking the wake images to positions of the bird in the high-speed camera two to three frames before the laser flashes occur.

Force balance

For a bird to fly level, the vector sum of thrust and lift must be equal to the vector sum of drag and the weight. It is convenient to analyse the wake by comparison with two idealized wake models, one at each end of a spectrum of possible intermittency. The first model describes the wake as a discrete shedding of vortex loops during each downstroke. In this intermittent model the upstroke is inactive and leaves no wake signature (Spedding et al., 2003b). The projected area of an elliptical vortex loop is:

$$S_e = \pi b \frac{\lambda_d}{2},\qquad(1)$$

where b is the wing semispan (m) and λ_d is the downstroke wavelength (the length travelled in a streamwise direction during the downstroke). The vertical impulse, I_z, contained in the structure is the product of its area and the circulation:

$$I_z = \rho S_e \Gamma_1,\qquad(2)$$

where ρ is the air density and Γ_1 is a reference circulation that is sufficient to support the weight for one wingbeat period T, from a single elliptical loop with area S_e. This can be readily calculated as:

$$\Gamma_1 = \frac{WT}{\rho S_e},\qquad(3)$$

where W is body weight. The second model, found at the other end of the intermittency spectrum, is a 'power-glider'. A rectangular wake is continuously extended at speed U, and over an interval T it grows by $UT \times 2b$. The reference circulation required for weight support in this case is thus:

$$\Gamma_0 = \frac{W}{\rho U 2b}.\qquad(4)$$

The reference circulations Γ_0 and Γ_1 are likely to bracket the actual circulation values in the real wake. Γ_0 would be the minimum circulation required if the bird had to do no work against drag, and the flat, rectangular wake were to provide only weight support. Γ_1 would be the value required if only the downstroke were active and all the momentum flux for lift (ignoring drag) had to be produced during the downstroke alone.

RESULTS
Wingbeat kinematics

A total of 25 high-speed film sequences at three different flight speeds were obtained, 8.0 m s^{-1} (N=7), 8.4 m s^{-1} (N=12) and 9.2 m s^{-1} (N=6) containing 30, 30 and 20 complete wingbeats, respectively. Even though the range of flight speeds was quite narrow, the wingbeat frequency of the swift showed a clear decrease with increasing flight speed, dropping from 9.1 to 8.3 Hz (Fig. 3A). The shoulder-to-wingtip angle, θ_u, of the wing at the upper turning point increased with flight speed, while the angle at the lower turning
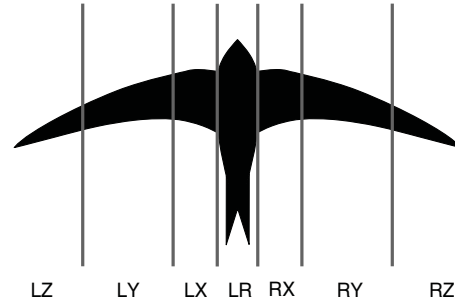

Fig. 2. The discrete classification system and notation. The LR position corresponds to the body, X is the arm section of the wing, and Y and Z are the inner and outer parts of the hand wing, respectively.

point, θ_d, did not (Fig. 3B). The downstroke duration, T_d, increased with increasing flight speed (Fig. 3D), but the angular velocity of both the up- and downstrokes, $\dot\theta_{u,d}$, did not vary greatly (Fig. 3E). The downstroke fraction (τ, Fig. 3D), down- and upstroke semispans (b_d, b_u, Fig. 3F), and consequently span-ratio (R, Fig. 3F) also all remained approximately constant across U.

The primary change in observed wingbeat kinematics with increasing flight speed was an increase in wingbeat amplitude. Since the measured wing angular velocity remained approximately constant, the result was a decrease in observed flapping frequency.

Wake velocity and vorticity fields

The wingbeat frequency of the swift at the flight speed examined (8.4 m s^{-1}) was 8.6 Hz, with wake wavelength λ=UT= 8.4/8.6=0.98 m. Each frame recorded by the PIV camera covers only 0.2 m in x, so approximately five full frames were needed to cover a complete wingbeat. The recording frequency of the camera is 10 Hz and with the swift wingbeat frequency, f=8.6 Hz, sequences of progressively decreasing phase of the wingbeat were obtained. Images were phase-ensembled to reconstruct the representative wake of a complete wingbeat at each spanwise position on the wing in Fig. 4. Since the swift flies between 0.4 and 0.5 m upstream of the laser sheet, the wake was sampled approximately 10 chord lengths away from its physical origin at the wings and body.

Steady flapping flight

Fig. 4A–C shows the wake shed behind the wings during one complete wingbeat cycle at three positions, moving from inner (Fig. 4A) to outer wing (Fig. 4C). All three sections show that vorticity of predominantly positive sign is shed during the downstroke, and that this changes to vorticity of mostly negative sign during the upstroke. The amplitude of the vertical excursions of the wake increases from base to tip (Fig. 4A–C) of the wing, as one would expect. The patterns of shed vorticity and associated velocity vectors on the upstroke of the outer wing section (Fig. 4C) are more complex than further inwards.

The uniformity in sign and gradual change in strength of the shed vorticity are quite different from those of previously studied birds at moderate-/high-speed flight. When combined with the absence of any large-scale spanwise structure at the turning points, the shed wake vorticity implies a time-history of circulation change on the wing itself that is also gradually and constantly changing. During the downstroke, the circulation on the wing increases to reach a maximum at, or just before, the lower turning point. The circulation
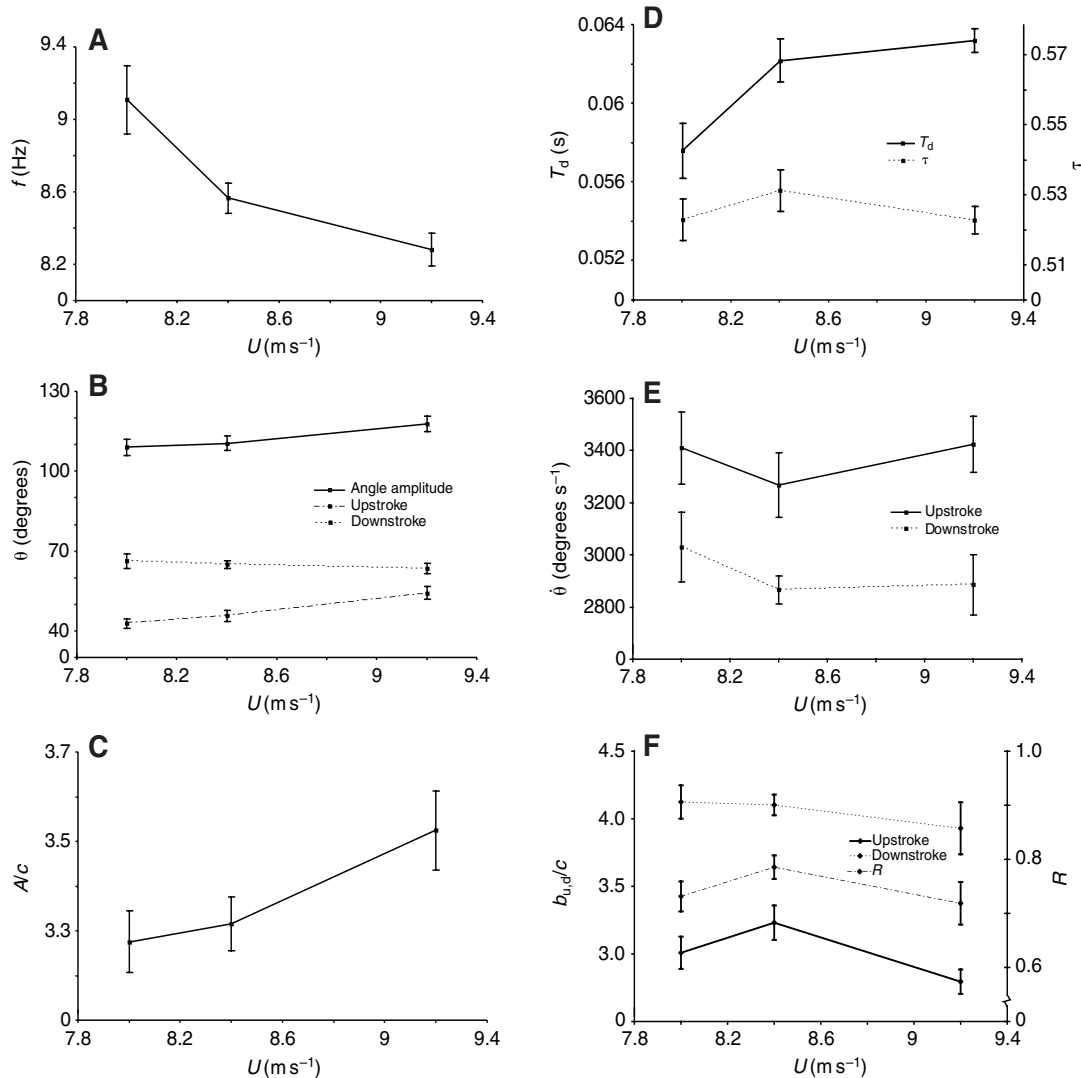
Fig. 3. (A) The wingbeat frequency, f, decreases with increasing flight speed, U, from 9.1 Hz at 8.0 m s^{-1} to 8.3 Hz at 9.2 m s^{-1}. (B) Upper (u), lower (d) and total (tot) angular excursion, θ, of the wing in the vertical plane as a function of flight speed, U. The increase in $\theta_{tot}(U)$ comes only from the increase in $\theta_u(U)$. (C) Amplitude, A, normalized by mean chord length, c. (D) The downstroke duration, T_d, increases with flight speed, U. The downstroke fraction, τ, does not vary with flight speed, U. (E) The wing angular velocity at mid-upstroke and -downstroke, $\dot{\theta}_{u,d}$, does not vary greatly with flight speed, U. (F) Wing semispans, $b_{u,d}$ at mid-upstroke and -downstroke normalized by mean chord length (c) *vs* flight speed, U. Wing semispan does not vary with flightspeed. The span ratio, R, does not change with flight speed, U. Error bars represent ±s.e.m.

then gradually decreases again during the upstroke. At the end of the upstroke, the shed vorticity is weakly negative, and the magnitude of the associated induced velocity field in the vicinity is also weak.

The direction and magnitude of the induced velocity field (we presume it is a global flow that can be thought of as being caused by the compact vortices in the wake) is consistent with a downwash from a wing that is lifting throughout the wingbeat, but the lift and thrust on the downstroke are stronger than the lift and drag on the upstroke. The net positive thrust propels the bird forward.

Interpreting three-dimensional vortex structure from stacks of two-dimensional velocity fields can be arduous, but certain checks are also possible. For example, wingtip trailing vortices should induce a downwash between them (as noted above) but should also be associated with an upwash in the outer wake, as the airflow is

swept from high to low pressure around the wingtips. This is seen in Fig. 5. These characteristics of wingtip vortices are found in all phases of the wingbeat.

Body drag

The most prominent feature of the body wake (Fig. 4D) is a mean flow from right to left (towards the bird's body). A velocity profile in this direction is commonly called a velocity defect, since it is a region where the local flow speed is lower than ambient. It is lower because friction between the body and the mean flow reduces the local flow speed, and consequently exerts a drag force on the body. Although there is a region of significant downwash towards the end of the downstroke and the beginning of the upstroke, it is notable that the body wake was modulated only weakly by the induced flow of the lifting wings further away from the centreline. The wake and
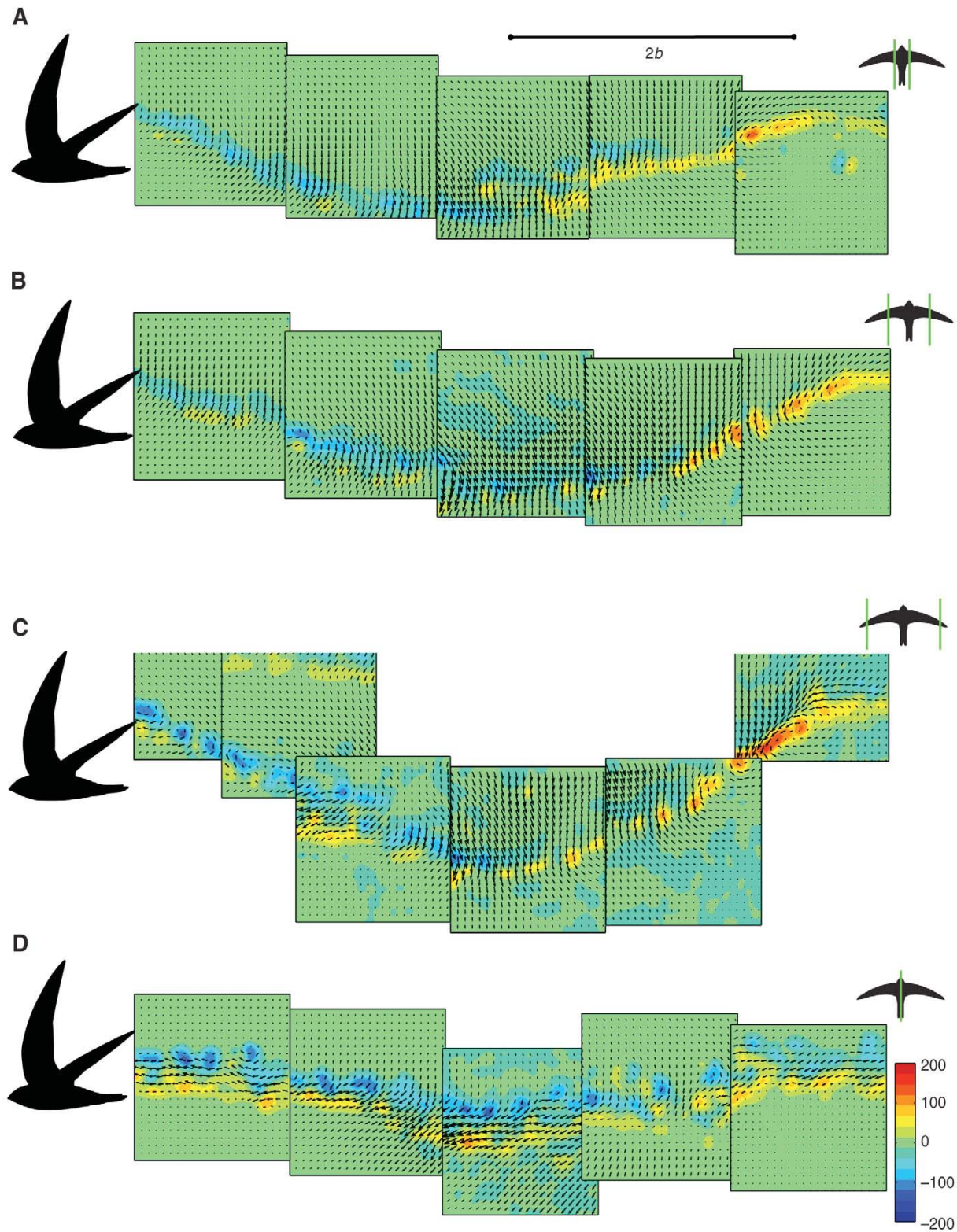
Fig. 4. Reconstruction of the vortex wake from a complete wingbeat at different spanwise locations: (A) arm wing (X in Fig. 2), (B) mid-hand (Y in Fig. 2), (C) outer-hand (Z in Fig. 2), and (D) body (LR in Fig. 2). The mean flow has been subtracted so the reference frame is in still air, as though the bird has passed from right to left. The spanwise vorticity, $\omega_y(x,z)$, is colour coded on a constant scale, symmetric about 0 s^{-1}. Velocity vectors are drawn with 1/3 of the actual density.
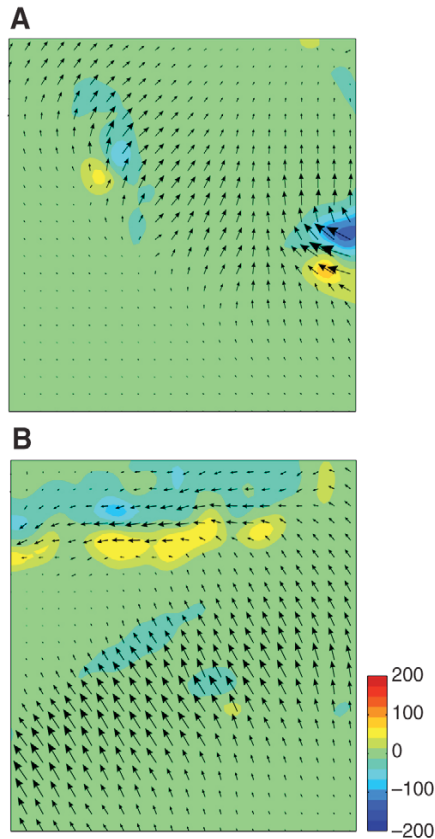
Fig. 5. $\omega_y(x,z)$ for outboard cuts through the edge of wingtip vortices on the upstroke (A) and downstroke (B).

Fig. 6. $\omega_y(x,z)$ for wakes generated during short gliding phases: (A) body (LR in Fig. 2) and (B) mid-hand (Y in Fig. 2).

induced downwash of the two wings has not merged across the body, whose drag component still persists, even at x/c=10.

The velocity defect was accompanied by chains of opposite-signed patches of vorticity, but we cannot say whether these were shed at the body or whether they developed as free shear-layer instabilities in the wake. Similarly, the possible contribution of the tail towards the wake structure is not easily ascertained. While the tail area is reduced in stable, steady, level flight, small control movements, and their subsequent wake signature, cannot be ruled out.

Gliding flight

A small number of individual frames showed a wake generated during brief, intermittent gliding phases. The central velocity defect behind the body in Fig. 6A is not unlike that seen behind the body in flapping flight, but the far field is much more regular, with a weak global downward flow. The mid-wing section in Fig. 6B is dominated by a global downward motion, which can be predicted as a consequence of lift on the wings. The downflow is deflected slightly to the left, and associated with strips of opposite-signed spanwise vorticity. This local defect profile must come from the friction drag on the wing section.

Quantitative wake analysis

Fig. 4 shows that the wake of the swift consists of almost continuous shedding of wake vortices throughout the wingbeat, implying that the strength of the circulation on the wing, the bound vortex, is also changing continuously. The phenomenon can be quantified,
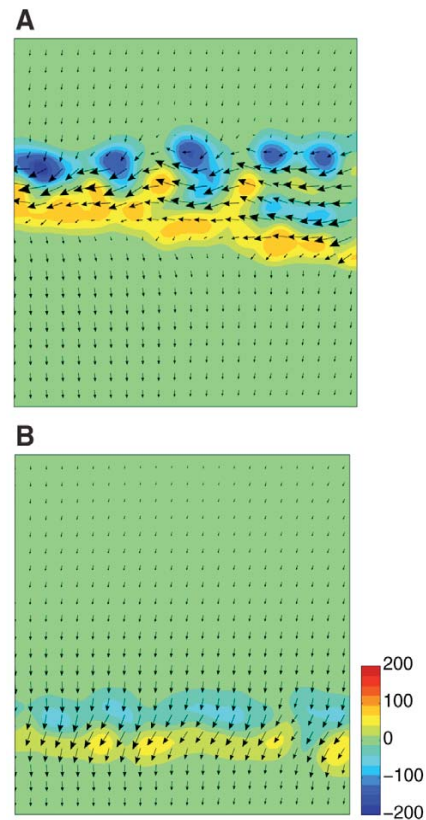
and U=8.4 m s^{-1} can be used as an example. The circulation at different phases of the wingbeat was measured by splitting the data at each spanwise location into five discrete phases of the wingbeat: phase 1 is the end of the upstroke; phase 2 is mid-upstroke; phase 3 is the lower turning point between down- and upstroke; phase 4 is mid-downstroke; and phase 5 is the beginning of the downstroke. Frames were sorted by phases that correspond to a tiling, from left to right, of subwindows covering the ensemble velocity fields such as those shown in Fig. 4. The results appear in Fig. 7A–D. The circulation deposited into the wake in each phase matched a change of circulation of the bound vortex on the wing, with positive wake circulation corresponding to an increase in wing circulation magnitude and negative wake circulation implying a decrease. At all four locations, from body to wingtip, the downstroke is dominated by positive circulation and the upstroke was dominated by negative circulation, consistent with the idea that absolute circulation in the bound vortex accumulates during the downstroke and diminishes during the upstroke. At each location, the maximum positive wake circulation occured at mid-downstroke (phase 4) and the strongest negative circulation occured at mid-upstroke (phase 2).

The peak positive circulations at phase 4 (mid-downstroke) in panels A–C of Fig. 7 all have similar values, suggesting that the circulation variation along the wing was small. The positive wake circulation dropped sharply in the transition from phase 4 to phase 3, over the second half of the downstroke. This was followed by the most rapid rise in negative circulation (at all spanwise locations)

from phase 3 to phase 2, the beginning of the upstroke. The wake behind the outer wing (Fig. 7B,C) had a higher increase in negative circulation than the inner wing (Fig. 7A). Although the relatively
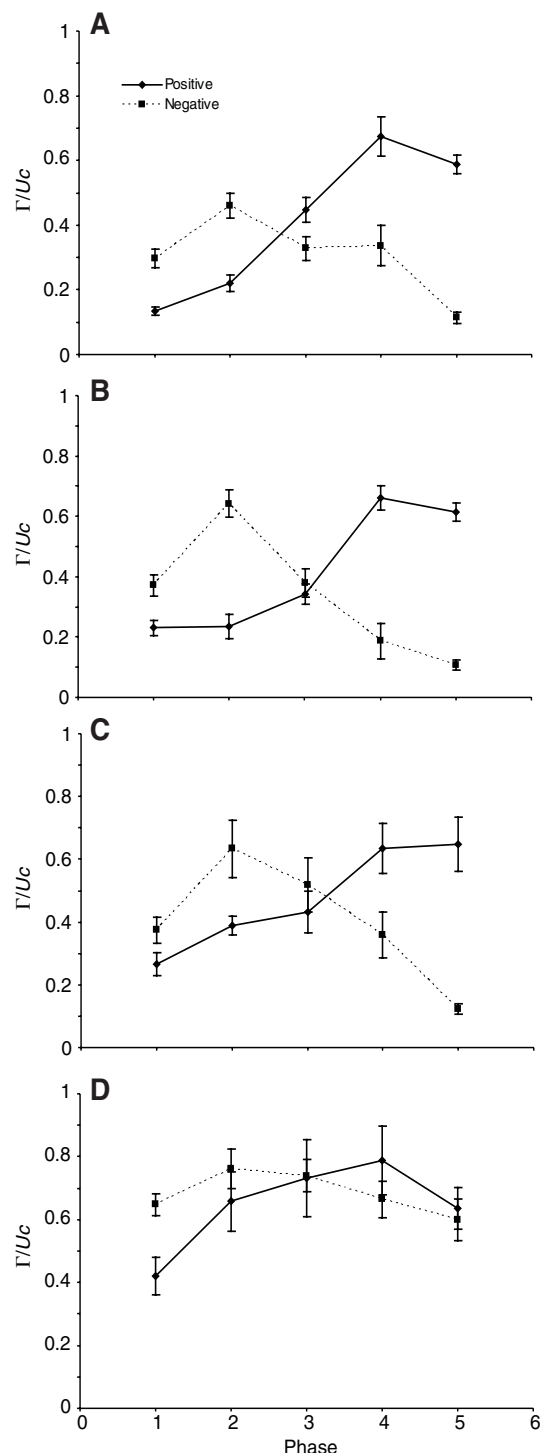

Fig. 7. Normalized total circulation in each phase of the wingbeat, where phase 5 at the right of the abscissa is the beginning of the downstroke and phase 1 at the left marks the end of the upstroke: (A) inner wing (X in Fig. 2), (B) mid-hand (Y in Fig. 2), (C) outer-hand (Z in Fig. 2) and (D) directly behind the body (LR in Fig. 2). Error bars represent ±s.e.m.

unflexed wing appeared to remain aerodynamically active during the upstroke, the outer wing appeared to be more lightly loaded.

The body–tail-generated drag wake (Fig. 7D) had a higher strength cross-stream vorticity than the wing sections. Variation of circulation magnitude with phase similar to that for the wing sections was seen, but the amplitude of the variation was much less. Alongside the observed undulation of the centreline wake (Fig. 4D), the data suggest a coupling of some kind between the body wake vortices and the spanwise vorticity shed from the wing. The data are too far downstream of the body to say more.

The continuous shedding of vorticity into the wake means that no distinct starting or stopping vortices are identifiable, at any point in the wake. In the Introduction, Γ_0 and Γ_1 were introduced as likely limiting values of the wake circulation strengths for wakes composed of rectangular wakes (Γ_0) or discrete, pulsed loops (Γ_1). In practice, however, although the swift generates a wake that might most closely be approximated by a constantly growing rectangular area, the most coherent and strongest vortices could well be trailing wingtip vortices, whose properties are not readily measured in streamwise slices. Fig. 8 shows that the peak circulation of the strongest patches of spanwise vorticity were always significantly less than either reference circulation value. In fact, the strongest vortices were those associated with the body wake. In summary, there were no abrupt changes in circulation on the wing that make it possible to construct a meaningful discrete vortex model of the wake, given the measurements available. We must therefore search for an alternative.

DISCUSSION
Flight characteristics

Both swifts in this study were juveniles and their first flight in the wind tunnel was also their first flight in life. Juvenile swifts leaving their nests must be prepared for constant, day-and-night flight from the moment they drop over the edge. They exercise their flight muscles in the nest prior to fledging, but have no chance to practice the actual technique of flying (Lack, 1956). This could potentially be an explanation for why the swifts of this study so quickly learned to fly in the wind tunnel. Their capacity for controlled and stable flight was the most obvious difference compared with descriptions of other species presented in previous studies, which normally have required lengthy training prior to the actual experiments (e.g. Park et al., 2001; Spedding et al., 2003b; Hedenström et al., 2006a; Rosén et al., 2007). The next obvious difference was the extremely narrow

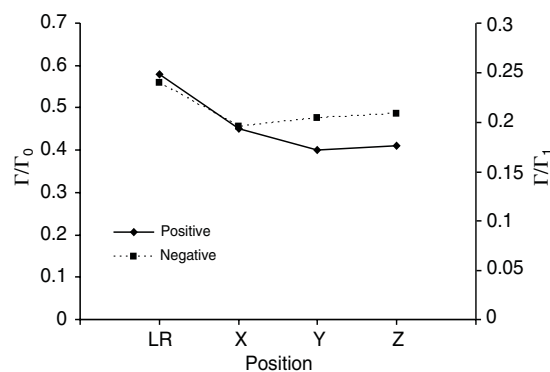Fig. 8. Maximum observed circulation of any coherent structure in the swift wake relative to two reference circulations, Γ_0 and Γ_1, for the power-glider and pulsed ring generator, respectively. On the abscissa, LR to Z are positions given in Fig. 2.

range of speeds at which the birds would fly. Below approximately 7.5 m s^{-1} the birds seemed unable to sustain stable flight, but dropped to the floor of the test section within a few seconds. A swift flying relaxed and at a natural flight speed flies with its feet held up close to the body and completely tucked in under the feathers (P.H., unpublished obervation). When the swifts of this study were exposed to airspeeds from 7.5 to 9 m s^{-1} this was the case, but when the wind speed exceeded 9 m s^{-1} the feet were extended, indicating that the flight speed was in some way troublesome. The range of natural flapping flight speeds for swifts may be narrow compared with those of other similar-sized bird species.

Wingbeat kinematics

The swift beats its wings at a similar angular velocity at each flight speed. The only direct response to the higher flight speed is an extension of the wingbeat by increasing the shoulder-to-wingtip angle of the upper turning point, resulting in increased wingbeat amplitude. Since the angular velocity does not vary significantly, the downstroke duration, T_d, increases. In the case of the swift, T_d always exceeds T_u, in contrast with findings for passerines where $T_u > T_d$ (e.g. Rosén et al., 2007; Hedenström et al., 2006a; Rosén et al., 2004; Park et al., 2001). The barn swallows of Park et al. (Park et al., 2001) increased their flight speed by increasing angular velocity and decreasing T_d over 8–9.2 m s^{-1}. The curve of $f(U)$ was quadratic over the entire range of flight speeds (4–14 m s^{-1}) with a minimum close to 9 m s^{-1}, but around this minimum (7–11 m s^{-1}) f varied little. A study on robins (*Erithacus rubecula*) showed that the wingbeat frequency and wingbeat amplitude increased slightly (although statistically insignificantly) with increasing flight speed (Hedenström et al., 2006a). A house martin (*Delichon urbica*) showed, like the swift, a decrease in wingbeat frequency with increasing flight speed, but a decreasing downstroke duration (Rosén et al., 2007). The rufous hummingbird (*Selasphorus rufus*) adapts to increasing U in a wind tunnel by varying both amplitude and wing angular velocity, keeping f almost constant at 42 Hz (Tobalske et al., 2007).

The wingbeat frequency measured for this swift ranged from 8.3 to 9.1 Hz, overlapping a predicted value of 8.9 Hz from a semi-empirical relationship derived by Pennycuick (Pennycuick, 1996) as:

$$f = m^{3/8} g^{1/2} b^{-23/24} S^{-1/3} \rho^{-3/8} , \qquad (5)$$

where m is the mass of the bird, g is the gravitational acceleration, b is the wingspan, S is the wing area and ρ is the air density. Variable values were based on the morphology of this specific bird (see Table 1) and $\rho = 1.19$ kg m^{-3}. These f values are slightly higher than those derived from the radar studies of Bäckman and Alerstam (Bäckman and Alerstam, 2001; Bäckman and Alerstam, 2002), who found a frequency range of 7.0 to 8.3 Hz, and Bruderer and Weitnauer (Bruderer and Weitnauer, 1971), who observed a range of 6 to 8 Hz.

The span ratio, R, was higher in the swift compared with that in previously studied species in the wind tunnel. It did not change significantly with flight speed but remained at approximately 0.7. Hence, the swift flexes its wings relatively little during the upstroke, which is consistent with visual observation of swifts in free flight (P.H., unpublished observations). Over the same range of absolute flight speeds, $0.2 \leq R \leq 0.3$ for the barn swallow (Park et al., 2001), $R = 0.4$ for the thrush nightingale (Rosén et al., 2004), $R = 0.4$ for the robin (Hedenström et al., 2006a) and $R = 0.3$–0.4 for the house martin (Rosén et al., 2007). From data on mid-downstroke and -upstroke wingspan presented in Tobalske et al. (Tobalske et al., 2003), estimates of span ratios for ringed turtle doves (*Streptopelia risoria*), budgerigars (*Melopsittacus undulatus*), cockatiels (*Nymphicus*

hollandicus) and black-billed magpies (*Pica hudsonia*) can be derived. Span ratios at 9 m s^{-1} for these birds were approximately 0.6, 0.5, 0.4 and 0.3 for the ringed turtle doves, the budgerigars, the cockatiels and the magpies, respectively. The rufous hummingbird of Tobalske et al. (Tobalske et al., 2007) reduces R from 0.98 at $U = 0$ m s^{-1} to 0.9 at $U = 12$ m s^{-1}, and so while the hummingbird also has relatively little wing flexion on upstroke, the opposing trend of $R(U)$ cautions against generalizing the swift results to all rigid-winged birds.

Wake topology

The swift wake shows no obvious similarities to the ladder wake even though the swift has been proposed to be a candidate for this wake type (Pennycuick, 1988; Pennycuick, 1989). The ladder wake model supposes that the circulation changes abruptly between down- and upstroke with the shedding of a distinct vortex in each of the upper and lower turning points, but this was not found in the swift. The wake shows both similarities and differences compared with those of previously examined passerine species.

The continuous shedding of spanwise vorticity is similar to the wake structure of the thrush nightingale, robin and house martin in cruising flight (Spedding et al., 2003b; Hedenström et al., 2006a; Rosén et al., 2007), but here the change in sign is much more regular and systematic (Fig. 4), with positive vorticity shed on the downstroke, transitioning to negatively signed vorticity in the trailing wake from the upstroke. The transition is gradual, with its mid-point at the lower turning point. As an example, the contrasting spatial variation of net wake circulation in the swift and thrush nightingale is shown in Fig. 9. The thrush nightingale circulations at both medium and high flight speeds are relatively sharply peaked at phases 1 and 3, at the upper and lower wingstroke turning points. By contrast, the swift-generated wake circulations vary more gradually, and the negative peak is not at the lower turning point, but in mid-upstroke, at phase 2. These studies are based on far-wake data only and so the mechanisms underlying the continuous shedding of spanwise vorticity in the swift cannot easily be traced back to the local wing motions or aerodynamics. There could be continuous changes in several concomitant or isolated properties such as local angle of attack, camber, wing section geometry and/or relative velocity. However, the contrast between the two species in

Fig. 9. The variation in normalized circulation over the five wingbeat phases for the swift and for the thrush nightingale (TN) at two flight speeds, $U = 7$ and 10 m s^{-1}, that describe medium- and high-speed flight, respectively, in wind tunnel conditions. The swift data come from Fig. 7A and the thrush nightingale data from the database described in Spedding et al. (Spedding et al., 2003b). The data from both species come from the inner wing.
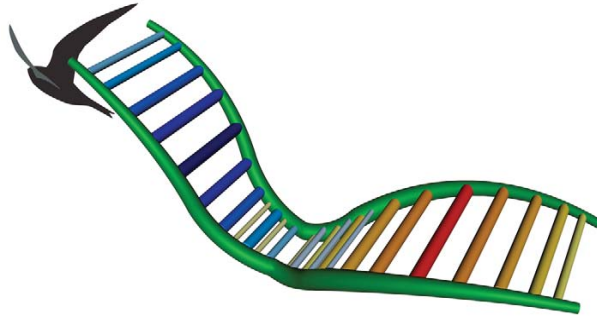
Fig. 10. Three-dimensional wake structure of the swift in cruising flight. The image frame is as if the bird flew obliquely from right to left and slightly into the paper, leaving the trace of one wingbeat in still air, starting at the upper turning point. Green tubes show the wingtip vortices, cylinders in shades of red are spanwise vortices with positive circulation and cylinders in shades of blue have negative circulation. The colour intensities and tube diameters are proportional to the strengths of each component. The geometry is deduced from a combination of wingbeat kinematics and streamwise plane section data.

Fig. 9 is consistent with larger amplitude variations in wings that flex significantly during the upstroke.

Insects also fly with comparatively rigid wings, having no distal joints or articulations, although passive elastic deformation makes them significantly non-planar. The wake of a hawkmoth (*Manduca sexta*) has certain characteristics similar to those of previously studied passerines such as the thrush nightingale, with intermediate wake formations between isolated vortex loops and constant circulation wakes (Bomphrey, 2006). The composite wake of the hawkmoth flying at $3.5\,\mathrm{m\,s^{-1}}$ shows continuous shedding of spanwise vorticity but, unlike the swift, both the down- and upstroke generate a mix of positive and negative vorticity. Furthermore, a part of the hawkmoth wake appears to form a distinct vortex loop (Bomphrey et al., 2006), which is not found in the swift wake.

A schematic summary of the three-dimensional swift wake topology is given in Fig. 10. The picture is a somewhat stylized summary of information from qualitative and quantitative spanwise vorticity distributions at different locations along the wing, combined with the measured kinematics. Cylinders in hues of red denote positive circulation and cylinders in hues of blue represent negative circulation. The distribution of the circulation intensity is based on data in Fig. 7. The green trailing, streamwise vortices are drawn by inference from figures such as Fig. 5.

Force balance

The continuous shedding of spanwise vortices illustrated in Fig. 10 cannot be adequately modelled by discrete vortex loop models derived either from the power-glider or from a pulsed ring generator, so neither reference circulations Γ_0 or Γ_1 are very useful (Fig. 8). Here we present an empirical model that integrates the accumulated wake circulation changes over the wingspan and over one wake wavelength. The completeness of the modelling effort can then be checked by comparing the calculated integrated vertical force with the known weight of the swift.

The continuous change model

The measured wake contains a time history of the circulation changes on the wing. In order to calculate the total integrated circulation we must add one further assumption about the absolute circulation value at some point. As a starting estimate, we shall assume that the circulation falls to zero at the end of the upstroke. This is a consistent interpretation of the very weak vorticity in phases 1 and 5 in Fig. 4, but others are possible and we must await further support from the force balance calculation itself. The net circulation (positive minus the absolute value of negative) found in each phase from the beginning of the downstroke to the end of the upstroke can be added to derive the accumulated circulation in the bound vortex and subsequently the vertical and horizontal impulse.

The measured wake circulations have been discretized at four spanwise locations and over five time intervals or wake phases (as shown in Fig. 7, for example). At the jth spanwise location, a local span section of width b_j can be identified, and then the vertical impulse, I_z, for that segment, over the phases comprising the downstroke part of the wake is:

$$I_{z,\mathrm{d},j} = \rho 2b_j \frac{\lambda}{5}\left(\Gamma_5 + \Gamma_4 + \frac{\Gamma_3}{2}\right),\qquad(6)$$

where the j indices are LR, X, Y, Z for the locations noted in Fig. 2. The local span-lengths, b_j, are measured from the centreline out to the wingtip. Each phase of the wake covers 1/5th of its wavelength λ, and Γ_5 to Γ_3 are the total accumulated circulations in phases 5 to 3, proceeding in order from the beginning of the downstroke to the lower turning point. Γ_3 marks the transition from downstroke to upstroke and appears also in the equivalent calculation of the upstroke wake impulse:

$$I_{z,\mathrm{u},j} = \rho 2b_j R \frac{\lambda}{5}\left(\frac{\Gamma_3}{2} + \Gamma_2 + \Gamma_1\right).\qquad(7)$$

The upstroke spans are reduced uniformly by the span ratio, R. If a more detailed, localized, accounting of the wing flexion were required, then it could be written directly into specific values for b_j, or into localized corrections, R_j.

The calculation includes the circulation contribution from the body wake (Fig. 7D), whose vortex wake signature is not easily extracted from that of the wing root. However, even though the wake vortices are as strong, or stronger than their counterparts further out on the wing, their net effect is approximately zero because there are equal amounts of positively and negatively signed vorticity. If the circulation increment is instead calculated from interpolating the LX and RX components across the body, the numerical result is the same within the calculation uncertainty.

Now the total impulse of a wake tiled by rectangular elements ($I_{z,\mathrm{rect}}$) of area $b_j(\lambda/5)$ (or $b_j(\lambda/5)R$ for the upstroke) is the sum of the downstroke and upstroke components over all span stations:

$$I_{z,\mathrm{rect}} = \sum_j (I_{z,\mathrm{d},j} + I_{z,\mathrm{u},j}),\quad j \in \{\mathrm{LR,X,Y,Z}\}.\qquad(8)$$

The wake geometry is better approximated by elliptical shapes on both the down- and upstroke (Fig. 11), and so the wake area, and its impulse, should be modified by the area ratio of an ellipse to a rectangle, which is $\pi/4$. Since we use the wingspan as a measure of wake width (rather than the wake measurements themselves, which are too sparsely distributed in the spanwise direction) then an improved measure of the actual width for an elliptically loaded wing is $2b(\pi/4)$ (Milne-Thompson, 1966) and so the final total vertical impulse is:

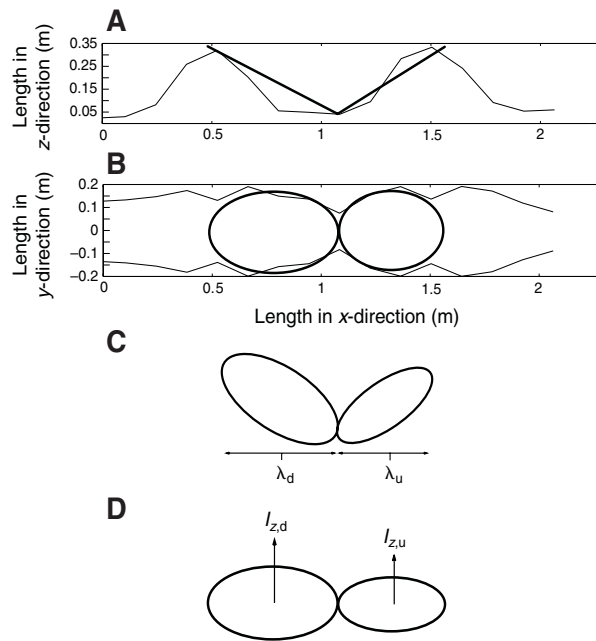$$I_z = \frac{\pi^2}{16} I_{z,\mathrm{rect}}.\qquad(9)$$

Fig. 11. Approximating the wake shape by ellipses. Flight direction is from right to left, and wingtip traces are viewed from the side (A) and above (B). Heavy lines denote ellipses fitted to the down- and upstroke wake geometry. The ellipses are seen from above in B and obliquely from the side in C, and their projection onto the horizontal plane is shown in D.

Substituting measured wake circulation values yields I_z=0.047 Ns. The uncertainty in estimating I_z is dominated by the uncertainty in Γ values. These form a population of repeated measurements of the same kind and so a total relative uncertainty in I_z can be estimated from the root mean square:

$$\frac{\Delta I_z}{I_z} = \left[\frac{1}{n_s n_p} \sum_{j=1}^{n_s} \sum_{i=1}^{n_p} \left(\frac{\Delta \Gamma_{i,j}}{\Gamma_{i,j}} \right)^2 \right]^{1/2}, \qquad (10)$$

where j is the same index over span stations {LR,X,Y,Z}, n_p=5 is the number of wingbeat phases and n_s=4 is the number of spanwise stations. $\Delta I_z/I_z$=0.3, and so the result for I_z can be written I_z=0.05±0.015 Ns (mean ± s.d.). In level, unaccelerated flight, I_z supports the weight W for a time T, and WT=0.044±0.003 Ns. Within experimental uncertainty WT=I_z and the wake-based calculation gives a result that is consistent with the observed experiment – that is, the bird flies level. Indirectly, therefore, the initial assumption that the circulation on the wing drops to zero at the end of the upstroke is also supported.

The approximate balance of forces implies, but does not prove, that vortex-induced flows measured in the wake are sufficient to explain the forces from the beating wing. As noted in the Introduction, additional terms could still be encountered from acceleration of the vortex elements themselves, leading to a contribution from the vortex added-mass. Dabiri (Dabiri, 2005) proposed a vortex–wake ratio, Wa, as a measure of the importance of flow unsteadiness when such terms might be important, with a corrected formulation in Dabiri et al. (Dabiri et al., 2006). Wa is proportional to the difference between the true convection of a vortex structure and its own self-induced velocity (the velocity it would have in the absence of external influences) and can be estimated

from the wake data in experiments like these. Hedenström et al. (Hedenström et al., 2006b) estimated Wa for a thrush nightingale at its slowest flight speed of 4 m s^{-1}, when unsteady effects are most likely to be important, and found that Wa=0.06, about 7 times less than the suggested threshold criterion. In the swift wake, there are no strong, single coherent wake structures and no simple description of line vortices (such as rings) can be given. The unsteady, time-varying terms describing the wake evolution will be smaller still, and added mass terms can be ignored. Such is the case in the far wake described here, and we await further studies of the near-wake dynamics when the question can be re-examined.

The continuously varying wake circulation, and its implied continuous variation of loading on the wing itself points to a wing that generates thrust not by flexing greatly on the upstroke, but by reducing the local aerodynamic angle of attack. This rigid-wing wake, and the quite simple kinematics that produce it, make the numerical modelling much different from that of previously studied birds. The simple empirical integration model presented here is self-consistent and suggests that a more sophisticated wake model with constantly varying spanwise and streamwise vorticity, somewhat analogous to Prandtl's horseshoe vortex model (Prandtl and Tietjens, 1934) but following a slowly varying wing path, could be successful too. The unsteady lifting-line model of Phlips et al. (Phlips et al., 1981) has a prescribed wake geometry that is quite similar to that assumed here, as does that of Hall et al. (Hall et al., 1997), where the wake geometry is that produced by the time-varying wing circulation distribution, which minimizes the power consumption. The wakes in both studies are qualitatively similar to the one modelled here (Figs 10, 11), partly because the swift wing is relatively rigid.

Hall et al. (Hall et al., 1997) predicted a trade-off between flapping amplitude and flapping frequency, with a ridge of optimum power requirements from amplitudes θ_h=35° at k_b=4 to θ_h=20° at k_b=10, where θ_h=(θ_u + θ_d)/2 and k_b is a reduced frequency based on span, reading:

$$k_b = \frac{\omega 2b}{U},$$

in our notation. However, k_b for the swift never reaches the values predicted by Hall et al., varying from 2.2 to 2.7. Flapping amplitudes are also significantly higher, with $\theta_h \approx$ 55° being typical, and the model does not predict the kinematics observed here. Phlips et al. (Phlips et al., 1981) did not perform an optimization study but investigated the propulsive efficiency while varying independent parameters prescribed by a particular kinematics/wake. They also describe a balance between flapping amplitude and frequency, and reported that time-averaged unsteady effects were only beneficial when the equivalent frequency parameter kb>2. While this criterion is met by the swifts, the modelling effect of collecting together vortex elements at the extremes of the wingbeat, we now see, is not supported by the data.

In both cases, further quantitative progress might depend more on the correct modelling of viscous terms, most particularly the drag on the wings and body, which is difficult to measure and predict even for steady wings at this Reynolds number, *Re* (Spedding et al., 2008).

Estimating drag and L/D ratio

The measurement of wing and body drag in animal flight is notoriously difficult, and the sensible outcome of the model with respect to weight support encourages its extension to the estimation of horizontal forces from the wake properties, as in Hedenström et

al. (Hedenström et al., 2006a). Let us suppose that the identified wake structure (Fig. 4A–C) accounted for in the calculations above is distinct from the drag wakes that also must be present (i.e. Fig. 4D, Fig. 6). Projecting the ellipses of down- and upstroke (Fig. 11) onto the vertical (rather than horizontal) plane yields the impulse directed in the horizontal direction, analogous to Eqns 6 and 7, as:

$$I_{x,d,j} = \rho 2 b_j \frac{A}{5} \left(\Gamma_5 + \Gamma_4 + \frac{\Gamma_3}{2} \right), \tag{11}$$

and

$$I_{x,u,j} = \rho 2 b_j R \frac{A}{5} \left(\frac{\Gamma_3}{2} + \Gamma_2 + \Gamma_1 \right), \tag{12}$$

for the downstroke and upstroke, respectively, where A is the wingbeat amplitude. The net horizontal impulse, defined as positive in the direction of flight, comes from the difference between the down- and upstroke components over all span locations:

$$I_{x,rect} = \sum_j (I_{x,d,j} - I_{x,u,j}), \quad j \in \{LR,X,Y,Z\}. \tag{13}$$

The same correction is made for wake shape and span efficiency, and so the net horizontal force is:

$$F_x = \frac{I_x}{T} = \frac{\pi^2}{16} \frac{I_{x,rect}}{T}. \tag{14}$$

Since flight speed is constant, the net forward force is equal and opposite to the total drag, D, on the wings and body.

In steady horizontal motion there is no net horizontal momentum in the wake, and the local velocity defects caused by friction and pressure drag on the wings and body will be exactly balanced by the net thrust. In making analytical models (e.g. Rayner 1979a; Phlips et al., 1981; Spedding, 1987) it is common to construct a wake composed of relatively few vortex elements and to suppose that the net forward momentum flux in this wake balances the viscous drag, which itself is not explicitly modelled. Similarly, one might imagine that the simple wake models derived from experiments such as these represent the thrust wake generated by the wings, but not the drag component. As a very simple example, Fig. 10 and Eqns 11–14 do not include the observed body drag wake patterns seen in Fig. 6A. Note that Eqns 11 and 12 use amplitudes from kinematics and not from the observed wake geometry. The latter could be used but are known with less certainty as the self-induced wake deformations would complicate simple geometric measures. The idea that the identified wake structure corresponds to a pattern that balances a separate drag component is plausible but difficult to test because accounting for all components of the wake would require tracing their origin back to particular events on the wings and body.

Making the assumption above, Eqn 14 can now be used to calculate the drag of the whole bird in flight, and for the swift this value is $D=F_x=0.029$ N. In steady flight, the lift, L, is equal to the weight, $L=W=0.383$ N, and so at a flight speed $U=8.4$ m s^{-1}, the effective $L/D=13.3$.

A similar approach (with the same assumptions) gave $L/D=7.5$ for a robin in flapping flight at 9 m s^{-1} (Hedenström et al., 2006a). The higher L/D for the swift suggests that the aerodynamic design of the swift is better optimized for energy-efficient flight, and the streamlined body and the high aspect ratio wings are obvious morphological indicators that would make such a finding unsurprising. The L/D estimate applies only to the specific flight speed for which it is measured, and even though the bird was allowed to fly at its preferred flight speed, this does not necessarily correspond to the maximum L/D. Further, we may note that L/D for flapping flight is not obviously related to the same quantity for gliding flight. Due to the flapping motion, both extra lift and extra drag are expected, but their relative change is not known. Previous estimates of L/D in gliding flight are 12.6 for a jackdaw (Rosén and Hedenström, 2001) and 10.9 for a Harris' hawk (Tucker and Heine, 1990). These birds both have less streamlined bodies and lower aspect ratio wings than the swift but have almost as high an L/D in gliding as does the swift in flapping flight. L/D for the gliding swift may yet be higher still, and DPIV studies of the steady gliding flight of swifts are planned. Lentink et al. (Lentink et al., 2007) measured the lift and drag forces of preserved swift wings with varying sweep and at different airspeeds, and L/D of the swift wing–body assembly was approximately equal to 10 at $U=9$ m s^{-1}. L/D at each fixed sweep angle was a very sensitive function of flight speed. Although care was taken to allow passive deformation in response to the aerodynamic loading, working with inanimate animal parts is always problematic and the higher measurement from flapping flight suggests that the free gliding value could rather be higher still.

Based on the same assumptions as for the L/D estimate, one may also define time-averaged lift and drag coefficients for the entire wing/body assembly as:

$$C_L = \frac{L}{qS}, \quad C_D = \frac{D}{qS}, \tag{15}$$

where $q=\rho U^2/2$ is the dynamic pressure and S is the wing planform area (given in Table 1). The required/measured $C_L=0.61$, which is readily obtained in well-designed wings at these Reynolds numbers ($Re=Uc/\nu$, where c is the mean chord length and ν is the kinematic viscosity; for $U=8.4$ m s^{-1}, $Re=2.2\times10^4$) but higher than the value of approximately 0.4 inferred from wake measurements of other species flying close to their preferred flight speed (Spedding et al., 2008). Defined as above, $C_D=0.05$. Caution is required in comparing C_D values because the reference area must (1) be specified precisely, and (2) be the same between cases. Here we use wing planform area simply for convenience. Alternatives include total wetted surface area and projected frontal surface area, neither of which is readily calculated from the data available. The Lentink et al. (Lentink et al., 2007) experiments measured lift:drag polars of pairs of fixed swift wings glued together, calculated a drag coefficient from the force balance measurements and then added a drag coefficient for the body. Since the wing calculation used S as the reference area, the measurements are roughly comparable to those given here. The wing pairs occupied a family of lift:drag polars with varying sweep angle, and for the $C_L=0.6$ calculated here, values of C_D ranged from 0.045–0.08. Our value of 0.05 lies at the lower end of the range, even though it was calculated for flapping flight.

Cost and benefit of the flight style

During downstroke the forward force is $I_{x,d}/T=0.07$ N and during the upstroke the opposite force is $I_{x,u}/T=0.04$ N. Thus, the counteracting negative thrust during the upstroke is approximately 60% of the thrust generated during the downstroke, implying that the active upstroke is expensive from a thrust generation point of view. However, similar calculations show that the lift produced during the upstroke is also 60% of that produced during the downstroke. This relatively high upstroke contribution to the lift

may be why the active upstroke is favoured despite the cost in reduced thrust. Moreover, there could be benefits in control and manoeuvrability if a large part of the wing is always active, and agility may well be as important in the ecological balance as steady flight efficiency.

CONCLUDING REMARKS

Swifts are renowned for their extreme aerial lifestyle, and also for their curved, relatively inflexible wings. The lunate planform has been shown to be efficient in analytical models of unsteady, low amplitude propulsion (Lighthill, 1970; Cheng and Murillo, 1984; Karpouzian et al., 1990), originally applied to bony fish, sharks, whales and dolphins. The rigidity of the wings may indicate an attempt to maintain this efficient shape in straight and turning flight. Because the wings do not flex on the upstroke as in many other birds of comparable size, their wakes are different too, reflecting an upstroke that seems to be a slightly feathered (local incidence angles on the wing are reduced to reduce the magnitude of the forces) version of the downstroke.

The almost continuous shedding of spanwise vorticity into the wake is very different from that of birds studied thus far, and requires a different empirical model of the vortex wake. The simple integration of the wake components presented here appears to be successful in accounting for the gross, time-averaged forces in steady flight. Although it is still difficult to deduce wing properties from these far-wake measurements, the estimated effective L/D=13.3 is quite respectable for flapping flight at these Reynolds numbers, and is higher than yet measured for any other live bird.

The variation of local wing loading by variation in local angle of attack of a comparatively rigid wing is much more similar to something that might be emulated when constructing a micro air vehicle (MAV), where excess flexibility can lead to prediction and resonance problems (e.g. Shyy et al., 1999; Lian and Shyy, 2007). Not only is the basic mechanical design easier but also the reduced amplitude of variation of the aerodynamic forces leads to much easier design for stable flight. MAV-sized ornithopters may be more swift-like than any other bird studied so far.

LIST OF ABBREVIATIONS AND SYMBOLS

A	wingbeat amplitude
b	wing semispan
b_j	width of local span section
c	mean wing chord
C_D	coefficient of drag
C_L	coefficient of lift
D	drag force
f	wingbeat frequency
$\mathbf{g}$	gravitational acceleration
I_x	horizontal wake impulse
I_z	vertical wake impulse
L	lift force
m	mass of the bird
q	dynamic pressure
R	span ratio
S	wing area
S_e	projected area of wake ellipse
T	wingbeat period
T_d	downstroke duration
U	flight speed
W	body weight
Γ	circulation
Γ_0	reference circulation for weight support in steady gliding flight
Γ_1	reference circulation for weight support by downstroke vortex loop
θ	stroke angle
λ	wake wavelength
ρ	air density

Subscripts u and d indicate upstroke and downstroke, respectively.

REFERENCES

Bäckman, J. and Alerstam, T. (2001). Confronting the winds: orientation and flight behaviour of the roosting swift, *Apus apus*. *Proc. R. Soc. Lond. B Biol. Sci.* **268**, 1081-1087.

Bäckman, J. and Alerstam, T. (2002). Harmonic oscillatory orientation relative to the wind in nocturnal roosting flights of the swift *Apus apus*. *J. Exp. Biol.* **205**, 905-910.

Bomphrey, R. J. (2006). Insects in flight: direct visualization and flow measurements. *Bioinspir. Biomim.* **1**, S1-S9.

Bomphrey, R. J., Lawson, N. J., Taylor, G. K. and Thomas, A. L. R. (2006). Application of digital particle image velocimetry to insect aerodynamics: measurements or the leading-edge vortex and near wake of a Hawkmoth. *Exp. Fluids* **40**, 546-554.

Bruderer, B. and Weitnauer, E. (1972). Radarbeobachtungen über Zug und Nachtflüge des Mauerseglers (*Apus apus*). *Rev. Suisse Zool.* **79**, 1190-1200.

Cheng, H. K. and Murillo, L. (1984). Lunate-tail swimming propulsion as a problem of curved lifting line in unsteady flow. Part 1. Asymptotic theory. *J. Fluid Mech.* **143**, 327-350.

Dabiri, J. O. (2005). On the estimation of swimming and flying forces from wake measurements. *J. Exp. Biol.* **208**, 3519-3532.

Dabiri, J. O., Colin, S. P. and Costello, J. H. (2006). Fast-swimming hydromedusae exploit velar kinematics to form an optimal vortex wake. *J. Exp. Biol.* **209**, 2025-2033.

Hall, K. C., Pigott, S. A. and Hall, S. R. (1997). Power requirements for large-amplitude flapping flight. AIAA 1997-0827, http://www.aiaa.org.

Hedenström, A., Rosén, M. and Spedding, G. R. (2006a). Vortex wakes generated by robins *Erithacus rubecula* during free flight in a wind tunnel. *J. R. Soc. Interface* **3**, 263-276.

Hedenström, A., van Griethuijsen, L., Rosén, M. and Spedding, G. R. (2006b). Vortex wakes of birds: recent developments using digital particle image velocimetry in a wind tunnel. *Anim. Biol.* **56**, 535-549.

Hedenström, A., Johansson, L. C., Wolf, M., von Busse, R., Winter, Y. and Spedding, G. R. (2007). Bat flight generates complex aerodynamic tracks. *Science* **316**, 894-897.

Holmgren, J. (2004). Roosting in tree foliage by Common Swifts *Apus apus*. *Ibis* **146**, 404-416.

Karpouzian, G., Spedding, G. R. and Cheng, H. K. (1990). Lunate-tail swimming propulsion. Part 2. Performance analysis. *J. Fluid Mech.* **210**, 329-351.

Kokshaysky, N. V. (1979). Tracing the wake of a flying bird. *Nature* **279**, 146-148.

Lack, D. (1956). *Swifts in a Tower*. London: Methuen.

Lentink, D., Müller, U. K., Stamhuis, E. J., de Kat, R., van Gestel, W., Veldhuis, L. L. M., Henningsson, P., Hedenström, A., Videler, J. J. and van Leeuwen, J. L. (2007). How swifts control their glide performance with morphing wings. *Nature* **446**, 1082-1085.

Lian, Y. and Shyy, W. (2007). Laminar-turbulent transition of a low Reynolds number rigid or flexible airfoil. *AIAA J.* **45**, 1501-1513.

Lighthill, M. J. (1970). Aquatic animal propulsion of high hydromechanical efficiency. *J. Fluid Mech.* **44**, 265-301.

Milne-Thompson, L. M. (1966). *Theoretical Aerodynamics*. New York: Dover.

Park, K. J., Rosén, M. and Hedenström, A. (2001). Flight kinematics of the barn swallow *Hirundo rustica* over a wide range of speeds in a wind tunnel. *J. Exp. Biol.* **204**, 2741-2750.

Peng, J. and Dabiri, J. O. (2008). An overview of a Lagrangian method for analysis of animal wake dynamics. *J. Exp. Biol.* **211**, 280-287.

Pennycuick, C. J. (1988). On the reconstruction of pterosaurs and their flight manner, with notes on vortex wakes. *Biol. Rev.* **63**, 299-331.

Pennycuick, C. J. (1989). *Bird Flight Performance: A Practical Calculation Manual*. Oxford: Oxford University Press.

Pennycuick, C. J. (1996). Wingbeat frequency of birds in steady cruising flight: new data and improved predictions. *J. Exp. Biol.* **199**, 1613-1618.

Pennycuick, C. J., Alerstam, T. and Hedenström, A. (1997). A new low-turbulence wind tunnel for bird flight experiments at Lund University, Sweden. *J. Exp. Biol.* **200**, 1441-1449.

Phlips, P. J., East, R. A. and Pratt, N. H. (1981). An unsteady lifting line theory of flapping wings with application to the forward flight of birds. *J. Fluid Mech.* **112**, 97-125.

Prandtl, L. and Tietjens, O. G. (1934). *Fundamentals of Hydro- and Aeromechanics*. New York: Dover.

Rayner, J. M. V. (1979a). A vortex theory of animal flight. I. The vortex wake of a hovering animal. *J. Fluid Mech.* **91**, 697-730.

THE JOURNAL OF EXPERIMENTAL BIOLOGY

Rayner, J. M. V. (1979b). A vortex theory of animal flight. II. The forward flight of birds. *J. Fluid Mech.* **91**, 731-763.

Rayner, J. M. V. (1979c). A new approach to animal flight mechanics. *J. Exp. Biol.* **80**, 7-54.

Rayner, J. M. V., Jones, G. and Thomas, A. (1986). Vortex flow visualization reveal change in upstroke function with flight speed in bats. *Nature* **321**, 162-164.

Rosén, M. and Hedenström, A. (2001). Gliding flight in a jackdaw: a wind tunnel study. *J. Exp. Biol.* **204**, 1153-1166.

Rosén, M., Spedding, G. R. and Hedenström, A. (2004). The relationship between wingbeat kinematics and vortex wake of a thrush nightingale. *J. Exp. Biol.* **207**, 4255-4268.

Rosén, M., Spedding, G. R. and Hedenström, A. (2007). Wake structure and wingbeat kinematics of a house-martin *Delichon urbica. J. R. Soc. Interface* **4**, 659-668.

Shyy, W., Berg, M. and Ljungquist, D. (1999). Flapping and flexible wings for biological and micro air vehicles. *Prog. Aerosp. Sci.* **35**, 455-505.

Spedding, G. R. (1986). The wake of a jackdaw (*Corvus monedula*) in slow flight. *J. Exp. Biol.* **125**, 287-307.

Spedding, G. R. (1987). The wake of a kestrel (*Falco tinnunculus*) in flapping flight. *J. Exp. Biol.* **127**, 59-78.

Spedding, G. R., Rayner, J. M. V. and Pennycuick, C. J. (1984). Momentum and energy in the wake of a pigeon (*Columba livia*) in slow flight. *J. Exp. Biol.* **111**, 81-102.

Spedding, G. R., Hedenström, A. and Rosén, M. (2003a). Quantitative studies of the wakes of freely flying birds in a low-turbulence wind tunnel. *Exp. Fluids* **34**, 291-303.

Spedding, G. R., Rosén, M. and Hedenström, A. (2003b). A family of vortex wakes generated by a thrush nightingale in free flight in a wind tunnel over its entire natural range of flight speeds. *J. Exp. Biol.* **206**, 2313-2344.

Spedding, G. R., Hedenström, A., McArthur, J. and Rosén, M. (2008). The implications of low-speed fixed-wing aerofoil measurements on the analysis and performance of flapping bird wings. *J. Exp. Biol.* **211**, 215-223.

Tobalske, B. W., Hedrick, T. L. and Biewener, A. A. (2003). Wing kinematics of avian flight across speeds. *J. Avian Biol.* **34**, 177-184.

Tobalske, B. W., Warrick, D. R., Clark, C. J., Powers, D. R., Hedrick, T. L., Hyder, G. A. and Biewener, A. (2007). Three-dimensional kinematics of hummingbird flight. *J. Exp. Biol.* **210**, 2368-2382.

Tucker, V. A. and Heine, C. (1990). Aerodynamics of gliding flight in a Harris' hawk, *Parabuteo unicinctus. J. Exp. Biol.* **149**, 469-489.

Time-resolved vortex wake of a common swift flying over a range of flight speeds

Per Henningsson, Florian T. Muijres and Anders Hedenström

Department of Theoretical Ecology, Ecology Building, Lund University, SE-223 62 Lund, Sweden

The wake of a freely flying common swift (*Apus apus* L.) is examined in a wind tunnel at three different flight speeds, 5.7 ms^{-1}, 7.7 ms^{-1} and 9.9 ms^{-1}. The wake of the bird is visualized using high-speed stereo digital particle image velocimetry (DPIV). Wake images are recorded in the transverse plane, perpendicular to the airflow. The wake of a swift has been studied previously using DPIV and recording wake images in the longitudinal plane, parallel to the airflow. The new high-speed DPIV system allows for time-resolved wake sampling and the result show features that were not discovered in the previous study. As the earlier study also reviled, a pair of wing tip vortices are trailing behind the wingtips, but in addition a pair of tail vortices and a pair of 'wing root vortices' are found that appear to originate from the wing/body junction. The existence of wing root vortices suggest that the two wings are not acting as a single wing, but are to some extent aerodynamically detached from each other. It is proposed that this is due to the body disrupting the lift distribution over the wing by generating less lift than the wings.

Introduction

As a flying animal in active flapping flight propel itself through the air it generates periodic disturbances to it that are left behind the animal as trailing wake vortices. Newton's third law dictates that the forces exerted by the animal on the fluid are equal and opposite to the forces exerted by the fluid on the animal. Thus, the wake represents the combined consequences of all wing, body and tail actions. In wakes where vertical flow is dominant over accelerated potential flow (see Dabiri, 2005) and wake dissipation and interactions are assumed negligible, the quantitative properties of the vortices in the wake and their orientation relative to each other, i.e. the wake topology, are sufficient to describe the forces exerted by the flying animal. Studying the wake of an animal to examine the forces produced is a convenient and rather elegant approach as it involves minimal disturbance to the animal. Digital Particle Image Velocimetry (DPIV) is a technique that has been used to visualize the wake of flying animals (e.g. Spedding et al. 2003a; b; Bomphrey et al., 2005; Bomphrey, 2006; Warrick et al, 2005; Hedenström et al., 2007; Henningsson et al., 2008; Johansson et al., 2008; Muijres et al., 2008; Spedding and Hedenström, 2009). The technique has been greatly developed in recent years and today stereo systems with high repetition rate exist. In this paper the results of high speed stereo DPIV measurements of flapping flight in the common swift (*Apus apus* L.) using such a system are reported. The

flapping flight of the swift at cruising speed has been previously studied in the Lund wind tunnel using a two-dimensional DPIV system with 10 Hz repetition rate (Henningsson et al. 2008). The high repetition rate of the system used in the current study allows for increased time resolution compared with the previous study, which results in higher detail of the final wake representation, both qualitatively and quantitatively. The topology and variation of the quantitative properties of the vortex wake can be sampled within wing beats instead of, as in the previous study, having to patch together the complete wake from frames originating from separated wing beats (for examples of high-speed DPIV see e.g. Hedenström et al., 2008; Johansson and Hedenström, 2009; Hubel et al., 2009). The main objective of the present study was to explore a wider speed range and to derive a time-resolved wake representation by the use of high speed stereo DPIV system. The bird was flown at three speeds, covering the complete range of flight speeds possible for the swift in the wind tunnel.

Materials and methods

Birds

Two juvenile common swifts were captured in their nest in the early morning on their assumed fledging day 4th of August 2008 and immediately transported to the wind tunnel facility at Lund University, Sweden. Between flight episodes they were kept in a lidless plastic box (0.5×0.4 m) with an artificial nest bowl. They were hand fed every other hour from morning to evening with a mixture of insects, vitamins and water using a syringe. The masses of the birds were monitored carefully throughout the day. Only one of the birds turned out to be usable for experiments (flying steadily and at the appropriate location) and therefore all data presented in this paper were collected from this bird. The morphological details of the bird are presented in Table 1. Wing area and wing span were measured using Scion Image (Scion

Corporation) from top-view digital photographs of the bird with fully spread wings held over a background with a reference grid. Body mass was measured with an electronic balance and averaged over the time of the complete study. On 14th of August both birds were released into the wild.

Wind tunnel

The Lund University wind tunnel is a closed-circuit, low-turbulence, low-speed wind tunnel designed for experiments with live animals. Details and specifications about the tunnel are described in Pennycuick et al. (1997). The air speed across 97% of the test section is within ±1.3% of the mean (Pennycuick et al. 1997) and the baseline turbulence is approximately 0.03% (Spedding et al. 2009).

Stereo DPIV

Specifications, setup and calibration

Flow field areas of approximately 20×20 cm were captured using two CMOS-sensor cameras (High-SpeedStar3: 1024×1024 pixles) connected to frame grabber PCI boards in a pc host. The cameras were equipped with 60 mm lenses (AF Micro Nikkor 60 mm f/2.8D) set to aperture 2.8. The tunnel was filled with a thin fog (particle size 1 μm) that was illuminated by a pulsed 50 mJ laser (Litron LPY732 series, Nd:YAG, 532

Table 1.Morphological details of the bird used in the experiments

Total mass (g)	0.042
Wingspan (m)	0.38
Wing area[a] (m²)	0.014
Mean wing chord[b] (m)	0.037
Aspect ratio[c]	10.3
Body frontal area (m²)	0.0011

[a]Area of both wings including the body area in between
[b]Wing area divided by wingspan
[c]Wingspan squared divided by wing area

Figure 1. Experimental setup for visualizing the wake of the flying swift. The tunnel is filled with a thin fog which is illuminated by the pulsed laser emitting 200 pulse pairs per second. The laser is synchronized with the two CMOS DPIV cameras that capture images of the smoke at each laser pulse. The images are stored in the host PC. The light emitted from the laser is guided via an optical arm that by the end of it has a lens that spreads the light beam into a thin light sheet. The light sheet was for this experiment positioned perpendicular to *U*. The position camera is used for recording the flight behavior of the bird and its location relative to the laser sheet during measurements. The laser and the cameras are triggered and synchronized by the high speed controller box (HSC).

nm) at a repetition rate of 200 Hz. The laser beam was spread by a cylinder lens into a thin sheet shining from above through the glass roof of the test section and transverse to the flow covering the view of the two cameras (Fig. 1). The cameras were equipped with band pass filters (530 ± 5 nm) blocking light from any other light sources than the laser. The system was operated using DaVis 7.2.2 software package (LaVision, Göttingen, DE). A high-speed camera (NAC Hotshot 1280) was filming the bird from above at 250 fps to record flight behavior and the position of the bird in relation to the laser sheet during each measurement.

The DPIV cameras were calibrated using the calibration routine in DaVis ©. The routine involved a calibration plate (20×20 cm, type 22) used to calculate the orientation of each of the two cameras. The calibration was also fine-tuned with a self-calibration routine, also included in DaVis, which compensates for any misalignments between the laser sheet and the calibration plate.

In order to optimize pixel displacement between image pairs the time delay between these images (d*t*) was tested on background flow. The time delay was chosen that resulted in 3-5 pixels displacement.

Data acquisition

The stereo DPIV cameras, the laser and the position high-speed camera were all triggered by a common trigger signal manually executed by the operator. Triggering was done when the bird was flying steadily in the appropriate location, i.e. in view of the cameras and 0.3-0.4 m (▯8-11 chord lengths) upstream of the laser sheet. Each triggering event lasted one second, i.e. recording 200 image pairs. If the bird showed any tendency to move too close to the laser sheet during the measurement the light was blocked for the safety of the bird by activating an electronic internal shutter in the laser control. The bird was flown at wind tunnels speeds $U_\infty = 5.9$ ms[-1], 7.8 ms^{-1} and 10.1 ms^{-1}, or expressed as equivalent air speed, $U_{eq} = 5.7$ ms[-1], 7.7 ms^{-1} and 9.9 ms^{-1} ($U_{eq} = U_\infty \sqrt{\rho/\rho_0}$, where ρ is the average air density measured over the experimental period: 1.17 kg/m³ and ρ_0 is the standard air density at sea level; 1.225 kg/m³).

Data analysis

The DPIV data were analyzed using DaVis software. The raw images were pre-processed prior to vector computations, images were filtered by subtracting a sliding minimum over 5 frames (2 before and 2 after the current frame). This operation filters out any irrelevant structures such as streaks in the light due to imperfections in the glass roof, or if the bird was visible in the background of the images. For image correlation, multi-pass stereo cross-correlation was used (64×64 in initial step and 32×32 in final step, 50 % overlap). The resulting vector fields were post-processed, first by deleting vectors that showed a peak ratio <1.01, when dividing the highest correlation peak with the second highest correlation peak. Secondly, vectors were deleted if the magnitude was 2 times the neighborhood RMS and recalculated if the magnitude was 3 times the neighborhood RMS. Thirdly, empty spaces were filled in by interpolation and a 3×3 smoothing average was applied. For each sequence, background velocities based on measurements of background flow were subtracted to obtain images showing only velocities induced by the bird.

The velocity vectors in x- (streamwise), y- (spanwise) and z- (vertical) direction (Fig. 1) were used to calculate the vorticity normal to each plane. Circulation was calculated for distinct structures in the wake, wingtip vortex, tail vortex and a vortex shed from the wing/body junction (see below), using a custom written Matlab analysis program (The MathWorks, Inc., Natick, MA, USA) and otherwise following the same procedure as described in Spedding et al. (2003).

In order to visualize the wake topology the images were compiled into a 3D representation of the wake by converting the time delay between images (Δt=1/200 s) into spatial displacement (Δx=$\Delta t U_\infty$) assuming a constant convection solely contributed by the freestream velocity (U_∞). The compiled 3D models were used to generate vorticity iso-surface plots of wakes. The iso-surface plots show the normalized constant streamwise vorticity, $\omega_x^* = \pm 2$, where

$$\omega_x^* = \omega_x / \overline{|\omega_x|} .$$

Model formulation and force derivations

Circulation was calculated on distinct and identifiable wake structures, namely wing tip vortices, wing root vortices and tail vortices. All of these structures were assumed to reflect consequences of the force generated by the flying bird. Instantaneous force generated as a function of time within the wingbeat is according to the Kutta-Joukowski theorem

$$F_{\text{inst}}(t) = \rho 2 b(t)\Gamma(t)U_\infty, \qquad (1)$$

where ρ is air density, $b(t)$ is wake semi-span over time of wingtip-, root- and tail-vortices and $\Gamma(t)$ is circulation over time of wingtip-, root- and tail-vortices. Wake period was normalized so that $\tau = t/T$, where T is the wingbeat time duration. Beginning and end of the wingbeat was defined as the upper turning point. The total force over the wingbeat is then

$$F_{\text{tot}} = \int_{\tau=0}^{1} F_{\text{inst}}(\tau)\,d\tau . \qquad (2)$$

The resulting net force was calculated as the sum of the total force contributed by each of the three vortex structures, wingtip-, root- and tail-vortex. The total force is then

$$F_{\text{tot}}^* = F_{\text{tot,tip}} + F_{\text{tot,root}} + F_{\text{tot,tail}} . \qquad (3)$$

This force corresponds to the total net force vector generated by the bird, including both lift and thrust. A bird flying level and at constant speed, which was the case with this bird during recording, needs to produce lift and thrust to balance the counter acting weight and drag. For simplicity thrust/drag force will hereafter be referred to as drag. In order to tease apart lift and drag, the geometry of the wake was taken

into account. By tracing the spatial location of the centre of wingtip-, root-, and tail vortices over time (t) and space ($x = tU_\infty$) the three dimensional path of each of the structures could be estimated. The path was smoothed by the use of a cubic smoothing spline (MatLab, CSAPS, smoothing parameter set to 0.9999). The derivative of this spline was used to estimate the wake plane angle over time (defined as the inclination angle between the wake plane and the horizontal, β). The direction of the total force vector previously calculated was assumed to always be normal to the wake plane and subsequently lift (L) was calculated as

$$L = \sum_i \int_{\tau=0}^{1} F_{\text{inst,i}}(\tau)\cos(\beta_i(\tau)) \ d\tau \qquad (4)$$

and drag (D) as

$$D = \sum_i \int_{\tau=0}^{1} F_{\text{inst,i}}(\tau)\sin(\beta_i(\tau)) \ d\tau , \qquad (5)$$

where i denotes wingtip-, root- and tail forces calculated according to eq. (1) and $\beta_i(\tau)$ is the wake plane angle over time for wingtip and wing root. For the tail, the angle is assumed to be zero, ($\beta_{\text{tail}} = 0$), so only lift is produced.

Results

Overall wake topology

The fundamental structure of the swift wake consists of pairs of wingtip vortices, wing root vortices and tail vortices. Figure 2 shows a typical sequence for each speed, 5.7, 7.7 and 9.9 ms⁻¹, of selected wake images of the left wing and tail.

The beginning of downstroke is similar for all speeds, the wingtip vortex is starting to form but no root vortex is present (Fig. 2a,f,k). At 5.7 ms⁻¹ tail vortices are visible during the start of the downstroke (Fig. 2a). At mid downstroke both the wingtip vortex and the wing root vortex are the strongest at all speeds (Fig. 2b,g,l). The end of downstroke shows weaker wingtip and root vortices than previously in the wing stroke and a tail vortex is present at 5.7 ms⁻¹ (Fig. 2c), which is absent at 7.7 ms⁻¹ at this stage of the wingbeat (Fig. 2h). Also at 9.9 ms⁻¹ a tail vortex is present, but counter-rotating to the wingtip vortex (Fig. 2m). Mid upstroke shows wingtip vortices at all speeds, but no root vortices (Fig. 2d,i,n). At 5.7 ms⁻¹ the tail vortex has grown stronger than previously in the wingbeat (Fig. 2d) and at 9.9 ms⁻¹ the opposite signed tail vortex is still present (Fig. 2n). At the end of upstroke, at all speeds, the wingtip vortex has decreased in strength from the peak earlier in the wingbeat to a point where it is hardly distinguishable. The tail vortex is present at 5.7 ms⁻¹ (Fig. 2e) and 7.7 ms⁻¹(Fig. 2j), but not at 9.9 ms⁻¹(Fig. 2o).

Within one wingbeat on average 21, 22 and 23 number of frames was sampled for 5.7 ms⁻¹, 7.7 ms⁻¹ and 9.9 ms⁻¹, respectively. The vorticity iso-surface plots show the streamwise vorticity trailing the swift during a little over one wingbeat, starting from the beginning of the downstroke (Fig. 3). At 5.7 ms⁻¹ wingtip vortices are prominent during the downstroke (Fig. 3a). Wing root vortices are formed at an early stage of the downstroke, but decreases to a non-visible below threshold strength by the end of the downstroke. During the early upstroke the tail vortices are increased to a considerable strength and are by the end of the upstroke the only visible structure above the threshold. During the course of the final half of the upstroke, wingtip vortices merge with the tail vortices (Fig. 4). At 7.7 ms⁻¹ the downstroke shows similar features as that of 5.7 ms⁻¹ (Fig. 3b), although the wing root vortices appear to be present for a larger portion of the downstroke, especially at the end of downstroke, as compared with 5.7 ms⁻¹. The upstroke at 7.7 ms⁻¹, similar to 5.7 ms⁻¹, also shows how the root vortices fall below the threshold value and the wingtip vortices merge with the tail vortices, but at this speed the tail vortices are weaker compared with those at 5.7 ms⁻¹. The tail is less spread at 7.7 ms⁻¹ compared
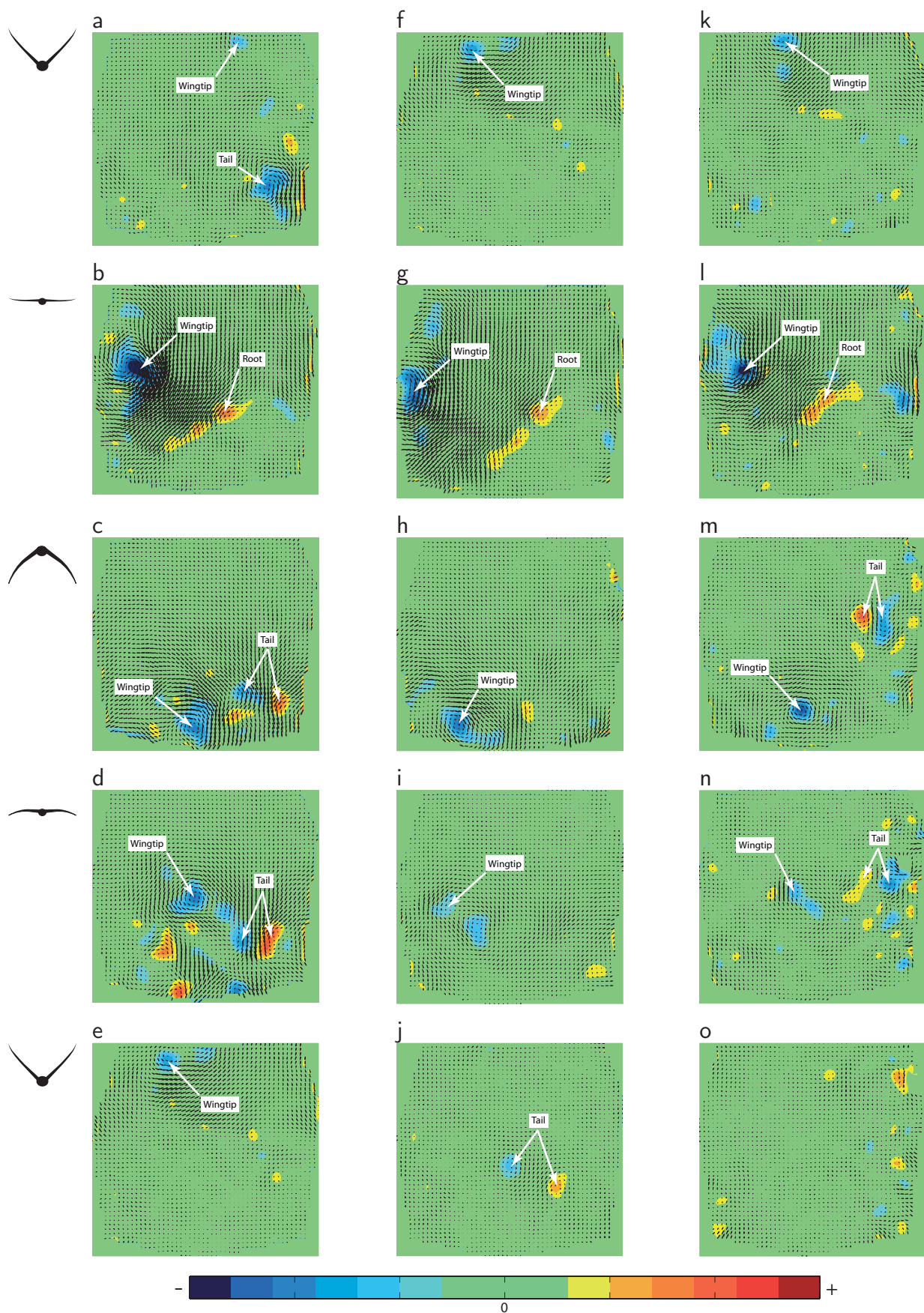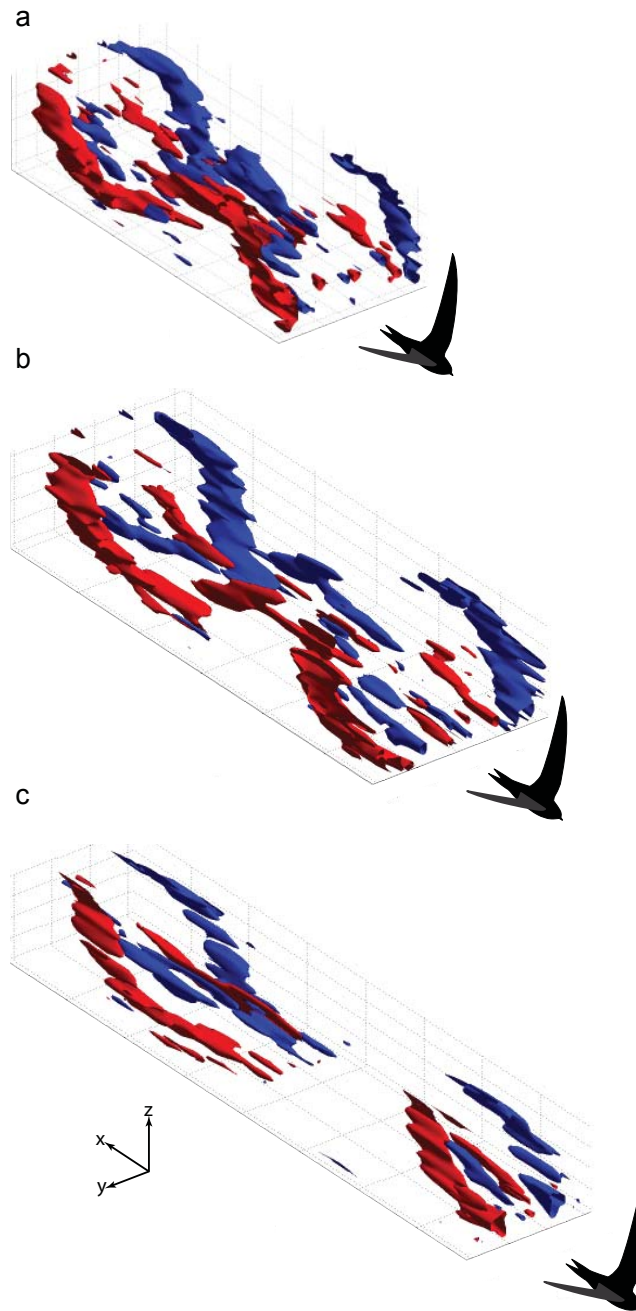
Figure 2. Legend on next page.

Figure 2 (previous page). Velocity vector field superimposed on color-coded vorticity field of key phases of the wingbeat for each speed. First column of panels shows 5.7 ms^{-1}, second column shows 7.7 ms^{-1} and third column shows 9.9 ms^{-1}. First row of panels show beginning of downstroke, second row show mid downstroke, third row show end of downstroke, forth row show mid upstroke and fifth row show end of upstroke. Bird silhouettes symbolize the different phases of the wingbeat. Distance from the swift to the image plane was between 0.3 to 0.4 m, which corresponds to 8-11 chord lengths. The color map scales from -350 s^{-1} (blue) to +350 s^{-1} (red). Reference scale of 5 ms^{-1} for the velocity vectors are shown in upper left corner.

Figure 3. Iso-surfaces showing 1.5 wingbeats for each speed. a) 5.7 ms^{-1}. b) 7.7 ms^{-1}. c) 9.9 ms^{-1}. The view is oriented so as if the bird was flying obliquely towards the observer from left to right. Red colored patches represent positive circulation (clockwise rotation as seen in direction of flight) and blue colored patches represent negative circulation (counter-clockwise rotation as seen in direction of flight).

with 5.7 ms^{-1}. At 9.9 ms^{-1}, the circulation is overall clearly lower than at 5.7 ms^{-1} and 7.7 ms^{-1}. During the beginning of the downstroke wing root vortices are formed and stay present throughout the downstroke, similarly to 7.7 ms^{-1} (Fig. 3c). The wingtip vortices that can be seen in the vorticity vector field images during the mid upstoke (Fig 2n) are too weak to appear in the iso-surface plots and hence the upstroke shows no wake structures.

Quantitative wake measurements

At all speeds the dominant wake structures were the wingtip vortices, the wing root vortices and the tail vortices. Measured circulation of these vortex structures are presented in figure 5, where the fitted lines show the cubic spline functions used in the model. All three speeds show a rapid increase of wingtip circulation during the first half of the downstroke, reaching a peak at mid downstroke (Fig. 5a,d,g). At 5.7 ms^{-1}, there is a steeper increase of Γ compared with 7.7 ms^{-1} and 9.9 ms^{-1} (Fig. 5a). The wing root circulation follows the pattern of the wingtip circulation, although with opposite sign, i.e. a rapid increase in $|\Gamma|$ during the first half of the downstroke

and with peak at the same time as the wingtip circulation, suggesting that the two structures are correlated (Fig. 5b,e,h). The overall magnitude of wingtip circulation and wing root circulation show a decrease with increasing speed. Tail circulation, for all speeds, follow an opposite pattern to the wingtip circulation, i.e. when wingtip circulation is low, as in beginning and end of the wing stroke, the tail circulation is high and vice versa. Tail circulation is on average higher at 5.7 ms^{-1} than at 7.7 ms^{-1} and 9.9 ms^{-1} (Fig. 5c,f,i).

Force derivations

The model used to estimate forces generated by the bird included the three major structures of the wake, i.e. wingtip, wing root and tail vortices. The total aerodynamic force was calculated according to eq (1) - (3) and evaluated to 0.39 N for 5.7 ms^{-1}, 0.34 N for 7.7 ms^{-1} and 0.48 N for 9.9 ms^{-1}. The weight of the bird was 0.41 N, calculated based on its average mass during the experimental period (Table 1). The total force vector represents both lift and drag combined of the bird and therefore an attempt was made to separate these components according to eq.

Figure 4. Illustration showing how the wingtip vortex merges with the tail vortex during the upstroke at the slowest speed, 5.7 ms^{-1}. The left image (a) shows the two structures when they still are distinctly separated. The centre image (b) was captured three frames later than the left (dt=3/200 sec.) and shows how the tail vortex has moved towards the tail vortex and has started to merge with it. The right image (c) was, in turn, captured three frames later than the left (dt=3/200 sec.) and shows when the two vortex structures have merged completely.

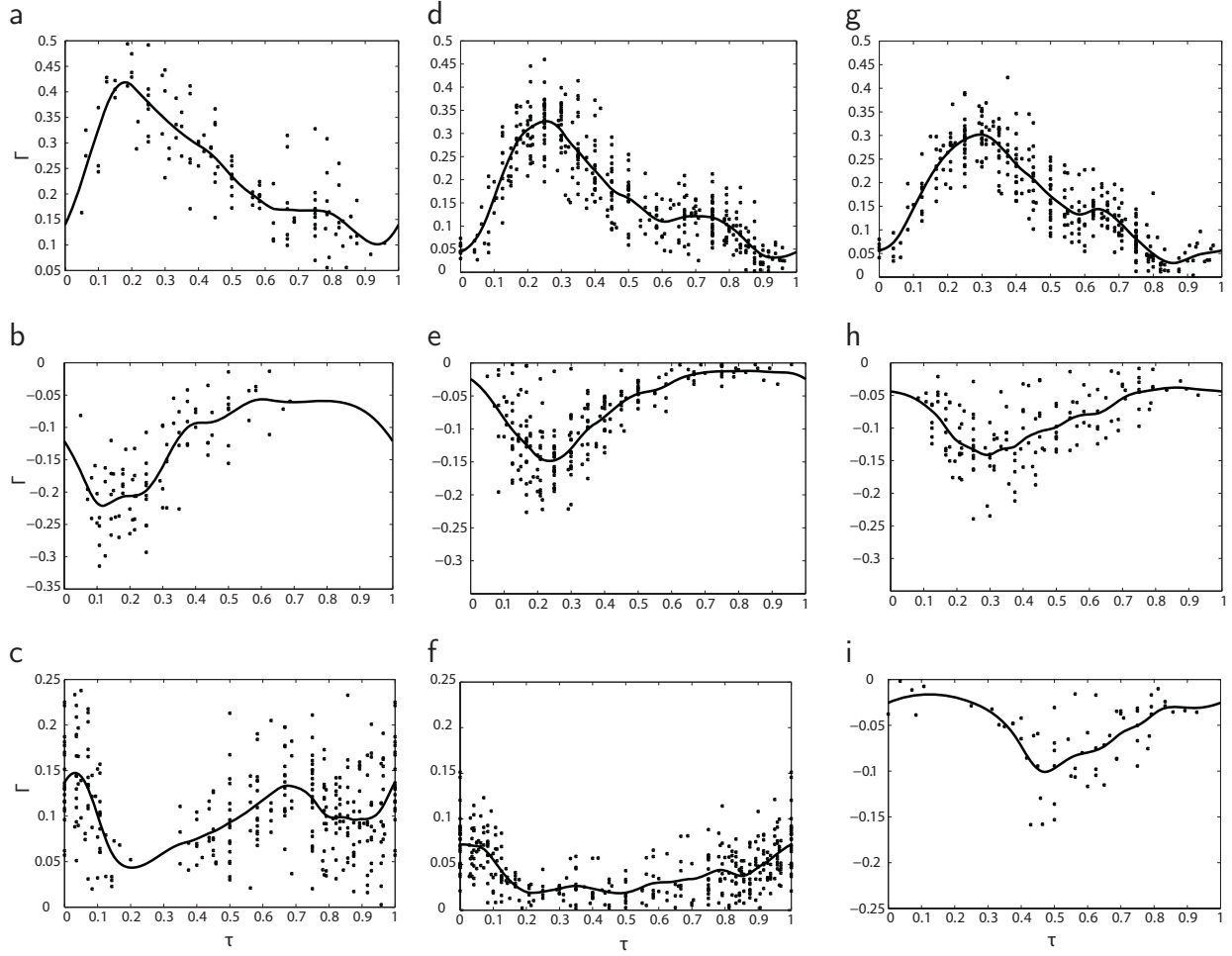Figure 5. Circulation over the wingbeat in wingtip vortex, wingroot vortex and tail vortex. The cubic smoothing splines used when calculating forces from the model are plotted in each panel. First column of panels show the results for 5.7 ms^{-1}, second column show results for 7.7 ms^{-1} and third column show results for 9.9 ms^{-1}. First row of panels show wingtip circulation, second row show wing root circulation and third row show tail circulation.

(4) and eq. (5). Lift was then calculated to 0.20 N (49% of weight) for 5.7 ms^{-1}, 0.24 N (58 % of weight) for 7.7 ms^{-1} and 0.23 N (56% of weight) for 9.9 ms^{-1}. Drag was estimated to 0.046 N for 5.7 ms^{-1}, 0.041 N for 7.7 ms^{-1} and 0.030 N for 9.9 ms^{-1}. Consequently, the lift-to-drag ratio (L/D) for the swift according to this model was 4.4 for 5.7 ms^{-1}, 5.9 for 7.7 ms^{-1} and 7.7 for 9.9 ms^{-1}, respectively. Lift and drag coefficients for the entire wing/body assembly can be calculated as

$$C_{\mathrm{L}} = \frac{L}{qS}, \qquad\qquad (6a)$$

$$C_{\mathrm{D}} = \frac{D}{qS}, \qquad\qquad (6b)$$

where $q = \rho U_{\infty}^{2}/2$ is the dynamic pressure (ρ=1.17 kg m^{-3}, averaged over the complete experimental period) and S is the wing planform area (Table 1). For 5.7 ms^{-1} C_{L} was 1.31 and C_{D} was 0.28, for 7.7 ms^{-1} C_{L} was 0.68 and C_{D} was 0.12 and for 9.9 ms^{-1} C_{L} was 0.56 and C_{D} was 0.07.

Discussion

Flight characteristics

The flight characteristics of the swift used in this experiment was largely similar to that described for the experimental bird by Henningsson et al. (2008). The bird flew well already after just one day of training. Unlike the bird used by Henningsson et al. (2008) the current bird would fly at a slightly wider range of flight speeds, from 5.7 ms^{-1} to 9.9 ms^{-1}, which allowed for an extension of the examined range. At 5.7 ms^{-1}, the bird was clearly struggling to stay aloft, with spread tail and high body angle. Below this speed it would descend to the floor of the test section within a few seconds. At 9.9 ms^{-1}, the bird was flying more relaxed than at 5.7 ms^{-1}, but at this speed maneuvering in relation to the wind tunnel walls started to become challenging for the bird and consequently higher flight speeds were not possible to examine due to safety issues.

Wake topology

The wake topology of the swift as interpreted from the wake images captured at the transverse plane and the corresponding 3D vorticity iso-surface plots show a more complex wake than previously described. In Henningsson et al. (2008) longitudinal (sagittal) wake data led to the conclusion that the wake consisted mainly of a pair of trailing wingtip vortices and between these were interconnecting vortex filaments. The present data suggest that the wake structure consists of some additional features. The wingtip vortices show very similar features as that described in Henningsson et al. (2008). In addition, distinct and clear wing root vortices are found, that appear to originate from a point near the wing/body junction. The root vortices are very consistent and present in every wingbeat at all examined speeds. The existence of root vortices indicates that the wing/body configuration is not acting as a single wing but rather the wings operate to some extent aerodynamically detached from each other. However, since the circulation in the root vortex is lower than that of the wingtip vortex there must be some circulation also over the body/tail and therefore the wakes of the wings are not completely isolated. This is similar to what has been found in the wake of bats (Hedenström et al., 2007; Muijres et al., 2008; Hedenström et al., 2008), a blackcap (*Sylvia atricapilla*; Johansson and Hedenström, 2009) and to some extent in bumblebees (Bomphrey et al., 2009). The fact that this wake structure is found in such a vast range of organisms, both in terms of morphology, taxonomy and size, suggests that the root vortices originate from the constraint of the necessity to incorporating a solid body into a smooth wing design (see Bomphrey et al., 2009). The ability to fly has to our knowledge evolved independently at least four times during the history of evolution: in insects, birds, bats and the extinct pterosaurs. It may be quite counterintuitive to think that the aerodynamics of animal flight should have evolved to such similar solutions. However, the body of a bird, bat or insect is likely to always generate less downwash (lift) compared to the wings (e.g. Tobalske et al., 1999; Tobalske et al. 2009), simply because of the aerodynamic properties of such shapes and therefore there will be a steep pressure gradient from wing to body. This gradient will necessarily introduce some disturbance to the wake, which could be manifested as root vortices. Still, it is not obvious whether the wake topology with separate loops is an advantage or a constraint. Generating two separate vortex loops, one for each wing, will be less efficient than if the two wings together with the body would act as one wing and only shed wingtip vortices. On the other hand, separate wakes may facilitate increased agility, gained from each wing operating aerodynamically detached from the other (see Hedenström et al. 2007).

A previous study of swift wakes consisted of only longitudinal views (Henningsson et al. 2008) and therefore the tail vortices were not well represented and therefore largely ignored. With the current transverse data the tail vortices are more obvious and consistent and

could be incorporated in the wake model. The tail appears to possibly have different functions at the three different speeds. At 5.7 ms^{-1} the tail is widely spread with the circulation of the tail vortices being stronger compared to 7.7 and 9.9 ms^{-1} (Fig. 5c), at 7.7 ms^{-1} the circulation is lower than at 5.7 ms^{-1} (Fig. 5f) and at 9.9 ms^{-1} the circulation is of opposite sign compared to 5.7 and 7.7 ms^{-1} (Fig. 5i). Especially at 5.7 ms^{-1}, but also at 7.7 ms^{-1}, the circulation of the tail vortices follows inversely that of the wingtip vortices. This implies that the tail has the function of contributing lift during periods of the wing stroke when the lift generated by the wings is low. At 9.9 ms^{-1}, the tail show reversely rotating vortices compared with those at 5.7 ms^{-1} and 7.7 ms^{-1}, actually generating negative lift. At that speed it is possible that the tail is used for control, for example, by creating a pitch up moment to counteract a pitch down moment introduced by the wings. This configuration would result in longitudinal static stability (e.g. Anderson, 1989).

Model and force derivations

The model describing the wake of the swift accounts for the three major structural components of the wake, i.e. wingtip-, root- and tail vortices. Weight of the bird is the force best known in this type of experiments and it is used as a reference for the model output. The results show that the lift calculated from the wake based model is only about 50%-60% of the weight of the bird. This deficit is a concern, since it indicates that the wake representation is not fully satisfactory. The method of measuring the circulation, the model formulation and finally the calculations performed have been carefully checked and there is no reason to suspect any methodological errors or calculation errors. A similar problem was addressed by Hubel et al. (2009), where wake circulation yields approximately 50% weight support for a bat in flapping flight. In that study two potential explanations were proposed: firstly, that vortex structures are partly destroyed by background turbulence or other unsteady phenomena, and secondly, that a portion of the vortex sheet is lost due to diffusion before it converges into the wingtip vortex. Both of these explanations are potentially applicable to the current case of the swift. Both Hubel et al. (2009) and the current study of the swift where measuring the far wake behind the animals. It is possible that the wake evolves when convecting downstream of the animal into a structure more or less distorted compared with the original wake created at the wing. The amount of distortion thus depends on how far downstream the wake is sampled. Yet another potential explanation to the wake deficit is that the wingtip vortex and the wing root vortex interact. In aeronautics, there is a well known phenomenon commonly called Crow-instability (Crow, 1970), in which vortex pairs interact as the wake evolves in an increasingly complex way further downstream of a wing. This phenomenon has been empirically investigated at $Re_\Gamma \approx 10^5$ ($Re_\Gamma = (\Gamma_1 + \Gamma_2)/\nu$, where Γ_1 and Γ_2 are the circulation in the two vortices and ν is the kinematic viscosity; corresponding value for the swift was approx. 2.4×10^4) and the results suggest that counter-rotating vortex pairs interact by initially attracting towards each other and subsequently the weaker (in this case root) vortex inter-twists the stronger (in this case wingtip) vortex and finally wraps around it into a complex structure (Bristol et al. 2004). The wake of the swift was sampled approximately 8-10 chord lengths downstream from the bird, which suggest that the wake, when captured, is in its early state of Crow-instability. However, it is likely that the two pairs of vortices, wingtip and root, have interacted so that the wing root vortex has started to move towards the wingtip vortex and vice versa. If this is the case, the effective wake span will be affected in two ways: the wingtip vortex will move inwards the wing and the root vortex will move outwards the wing, resulting in an underestimate of the wingtip vortex span and an overestimate of the root vortex span. These effects will both reduce the positive contribution to lift by the wingtip vortex and increase the negative contribution to lift generated by the root vortex (eq. 1). Even at an early state of Crow-instability this could

potentially cause a misrepresentation of the wake and an underestimate of the forces. To test this, the model was adjusted so that the measured wake span was equal to the span of the bird, i.e. as if no contraction in the wake occurred. Then the calculated lift was 90%, 83% and 115% of the weight for 5.7 ms^{-1}, 7.7 ms^{-1} and 9.9 ms^{-1}, respectively. The L/D ratio was, however, almost the same, 4.7, 5.8 and 8.0, for the three speeds, respectively. This result is probably an overestimate of the forces, since it is expected that the wake contracts downstream the bird (e.g. Milne-Thompson, 1966), but it represents the other extreme, i.e. no wake contraction, and the results from these two calculations (based on actual wake span versus based on wing span) should encircle the true value. If the deficit indeed stems from Crow-instability, the circulation in the wake would be conserved (cf. Spedding et al. 2008) and not lost or destroyed as proposed by Hubel et al. (2009). To examine this, the circulation measured in the wake in the present study was compared to the circulation measured in Henningsson et al (2008), where the wake was measured in a longitudinal plane. The circulation measured in the current study was not different from that found in the earlier study of the wake of a flying swift. This supports the argument that the wake deficit found in the current study is due to some wake distortion, for example Crow-instability. If this is true, it is a general issue when studying far wakes at the transverse plane. It is a dilemma, if the wake is sampled close to, but not on the object, the samples will represent a wake that is still in an intermediate phase of contraction of unknown degree, whereas if the wake is sampled further downstream where the wake has contracted fully, instability becomes an issue. Furthermore, it is difficult to measure wakes using DPIV on, or very close to, a live animal flying freely in a wind tunnel, due to safety issues, which means that one is often restricted to measuring the far wake.

When a bird is flying level at a fixed velocity, the mean thrust and drag are balanced. Thrust, and hence drag, was estimated by taking the geometry of the wake into account. This calculation rests on the assumptions that the

total force (vector sum of lift and thrust) always is generated normal to the wake plane and that the wake plane does not change orientation to a large extent from when it was generated at the wing until it is captured by the DPIV cameras approximately 8-10 wing chords downstream. By comparing near and far wakes of a bat, Johansson et al. (2008) showed that the qualitative and quantitative wake properties show rather small changes with distance from the object. Nevertheless, the drag estimate made here, should be viewed upon as a preliminary estimate, especially considering the above mentioned problem with wake distortion. The drag as estimated from the model was higher than the drag estimate made based on the alternative model by Henningsson et al. (2008). In that study the model used input from longitudinal DPIV images and it was assumed that any shed circulation in the wake corresponded to a change in circulation of the bound vortex on the wing. Otherwise, the calculations were made in a similar fashion as with the current model, by integrating over the wingbeat to calculate the total net force and decomposing this force into lift and thrust based on the geometry of the wake. The outcome of the two models is different. The L/D ratio estimated by Henningsson et al. (2008) was about 13, whereas the highest L/D ratio estimated from the current model was 7.7. The L/D ratio for robins were estimated from the wake and evaluated to 7.5 in flapping flight in a wind tunnel (Hedenström et al., 2005), which suggest that the L/D ratio measured here is an underestimated value considering the morphological differences between the swift and robin (AR_{swift}=10.3, AR_{robin}=4.8). The L/D ratio of the swift in gliding flight in a wind tunnel has been estimated to 12.7 (P. Henningsson and A. Hedenström, in prep.). This represent the true L/D ratio while the L/D ratio calculated here for flapping flight represents the effective L/D (i.e. when the wake geometry due to the flapping motion is taken into account) and is expected to be lower. However, it is maybe unlikely that the L/D ratio is almost half in flapping flight compared with gliding flight. The low L/D ratio found in this study compared with that found by Henningsson et al. (2008) could be a consequence

of vortex interactions as described earlier. By changing the wake span into wing span in the model, weight support was found, but the L/D ratio stayed more or less the same. By adjusting the span in the model the potential changes in span due to Crow-instability is compensated, but if there is also a component of rotation of the two vortices around each other in this instability, it is not compensated for and may potentially change the wake plane angles and subsequently the L/D ratio. Further research is required to investigate wake interactions for this type of configurations at Reynolds numbers in the range for bird flight.

Acknowledgements

References

Anderson, J. D. (1989) Introduction to flight. McGraw-Hill, Inc. New York.

Bomphrey, R. J. (2006) Insects in flight: direct visualization and flow measurements. *Bioinsp. Biomim.* 1:S1-S9.

Bomphrey, R. J., Lawson, N. J., Harding, N. J., Taylor, G. K. and Thomas, A. L. R. (2005) The aerodynamics of Manduca sexta: digital particle image velocimetry analysis of the leading-edge vortex. *J. Exp. Biol.* 208, 1079-1094.

Bomphrey, R. J., Taylor, G. K. and Thomas, A. L. R. (2009) Smoke visualization of free-flying bumblebees indicates independent leading-edge vortices on each wing pair. *Exp. Fluids* **46**, 811-821.

Bristol, R. L., Ortega, J. M., Marcus, P. S. and Savas, Ö. (2004) On cooperative instabilities of parallel vortex pairs. *J. Fluid Mech.* **517**, 331-358.

Crow, S. C. (1970) Stability theory for a pair of trailing vortices, *AIAA J.* **8**, 2172-2179.

Dabiri, J. O. (2005). On the estimation of swimming and flying forces from wake measurements. *J. Exp. Biol.* **208**, 3519-3532.

Hedenström, A., Rosén, M. and Spedding, G. R. (2005). Vortex wakes generated by robins *Erithacus rubecula* during free flight in a wind tunnel. *J. R. Soc. Interface* **3**, 263-276.

Hedenström, A., van Griethuijsen, L., Rosén, M. and Spedding, G. R. (2006b). Vortex wakes of birds: recent developments using digital particle image velocimetry in a wind tunnel. *Animal Biol.* **56**, 535-549.

Hedenström, A., Johansson, L. C., Wolf, M., von Busse, R., Winter, Y. and Spedding, G.R. (2007). Bat flight generates complex aerodynamic tracks. *Science* **316**, 894-897.

Hedenström, A., Muijres, F. T., von Busse, R., Johansson, L. C., Winter, Y. and Spedding, G. R. (2009) High-speed stereo DPIV measurements of wakes of two bat species flying freely in a wind tunnel. *Exp. Fluids* **46**, 923-932.

Henningsson, P., Spedding, G. R. and Hedenström, A. (2008) Vortex wake and flight kinematics of a swift in cruising flight in a wind tunnel. *J. Exp. Biol.* **211**, 717-730.

Hubel, T. Y., Hristov, N. I., Swartz, S. M. and Breuer, K. S. (2009) Time-resolved wake structure and kinematics of bat flight. *Exp. Fluids*, **46**, 933-943.

Johansson, L. C., Wolf, M., von Busse, R., Winter, Y., Spedding, G. R. and Hedenström, A. (2008) The near and far wake of Pallas' long tongued bat (*Glossophaga soricina*). *J. Exp. Biol.* **211**, 2909-2918.

Johansson, L. C. and Hedenström, A. (2009) The vortex wake of blackcaps (*Sylvia atricapilla* L.) measured using high-speed digital particle image velocimetry (DPIV). *J. Exp. Biol.* 212, 3365-3376.

Milne-Thompson, L.M. (1966). *Theoretical Aerodynamics.* New York: Dover.

Muijres, F. T., Johansson, L. C., Barfield, R., Wolf, M., Spedding, G. R. and Hedenström, A. (2008) Leading-edge vortex improves lift in slow-flying bats. *Science* **319**, 1250-1253.

Pennycuick, C. J., Alerstam, T. and Hedenström, A. (1997). A new low-turbulence wind tunnel for bird flight experiments at Lund University, Sweden. *J. Exp. Biol.* **200**, 1441-1449.

Rosén, M., Spedding, G. R. and Hedenström, A. (2004). The relationship between wingbeat kinematics and vortex wake of a thrush nightingale. *J. Exp. Biol.* **207**, 4255-4268.

Rosén M., Spedding, G. R. and Hedenström, A. (2007). Wake structure and wingbeat kinematics of a house-martin *Delichon urbica. J. R. Soc. Interface*, 10.1098/rsif.2007.0215.

Spedding, G. R., Hedenström, A. and Rosén, M. (2003a). Quantitative studies of the wakes of freely flying birds in a low-turbulence wind tunnel. *Exp. Fluids* **34**, 291-303.

Spedding, G. R., Rosén, M. & Hedenström, A. (2003b). A family of vortex wakes generated by a thrush nightingale in free flight in a wind tunnel over its entire natural range of flight speeds. *J. Exp. Biol.* **206**, 2313–2344.

Spedding, G. R., Hedenström, A. H., McArthur, J. & Rosén, M (2008). The implications of low-speed fixed-wing aerofoil measurements on the analysis and performance of flapping bird wings. *J. Exp. Biol.* **211**, 215–223.

Spedding, G. R., Hedenström, A. and Johansson, L. C. (2009) A note on wind-tunnel turbulence measurements with DPIV. *Exp. Fluids* **46**, 527-537.

Tobalske, B. W., Peacock, W. L. and Dial, K. P. (1999) Kinematics of flap-bounding flight in the zebra finch over a wide range of flight speeds. *J. Exp. Biol.* **202**, 1725-1739.

Tobalske, B. W., Jason, W. D., Hearn, W. D. and Warrick, D. R. (2009) Aerodynamics of intermittent bounds of flying birds. *Exp. Fluids* **46**, 963-973.

III

Aerodynamics of gliding flight in common swifts

Per Henningsson and Anders Hedenström

Department of Theoretical Ecology, Ecology Building, Lund University, SE-223 62 Lund, Sweden

The gliding flight performance and wake topology of a common swift is examined in a wind tunnel. The swift was gliding steadily at speeds between 7 and 11 ms^{-1}. The tunnel was tilted to simulate descending flight at different sink speeds. The swift varied its wingspan, wing area and tail span over the speed range. Wingspan decreased linearly with speed over the speed range, whereas tail span decreased in a non-linear manner. At the slowest speed the tail was spread more than on any other speed, while it was otherwise decreasing linearly with speed. For each airspeed, the minimum glide angle was found. These minimum angles showed a curvilinear relationship with airspeed, with a minimum sink speed (U_{ms}) at 8.1 ms^{-1} and a speed of best glide (U_{bg}) at 9.4 ms^{-1}. Lift-to-drag ratio (L:D) was calculated for each airspeed and tilt angle combinations and the maximum for each speed showed a curvilinear relationship with airspeed, with a maximum of 12.5 at an airspeed of 9.5 ms^{-1}. Wake was sampled in the transverse plane using stereo Digital Particle Image Velocimetry (DPIV). The main structures of the gliding flight wake consisted of a pair of trailing wingtip vortices and a pair of trailing tail vortices. The circulation of these was measured and a model was constructed that showed good weight support. Parasite drag was estimated from the wake defect measured in the wake behind the body. Parasite drag coefficient ranged from 0.30 to 0.22 over the range of airspeeds. Induced drag was calculated and used to estimate profile drag coefficient, which was found to be in the same range of what has been previously measured on a Harris' hawk.

Introduction

From an aerodynamic viewpoint animal gliding flight is less complicated than flapping flight because it does not involve any moving actuators. A gliding animal should therefore comply more directly with aerodynamic theory, which has mainly been developed for fixed wing configurations. Yet, there are relatively few wind tunnel studies of gliding flight aerodynamics available (Pennycuick 1968, Tucker and Parrott 1970, Tucker and Heine 1990, Rosén and

Hedenström 2001), probably because it requires a tiltable wind tunnel. Some basic properties about gliding flight can be measured in the field using an aircraft, an optical range finder or a radar (Pennycuick 1971a; 1971b, Tucker, 1988; Tucker et al., 1998; Rosén and Hedenström, 2002, Spaar and Bruderer 1996, 1997), but with the limitation of reduced possibilities to record the body mass, wing morphology, horizontal and vertical winds.

The aerodynamic force generated by a flying bird is reflected by the vortex wake (e.g. Rayner

1979, Spedding 1986), and modern techniques of Digital Particle Image Velocimetry (DPIV) have revealed both qualitative and quantitative properties about bird and bat wakes (e.g. Spedding et al. 2003, Hedenström et al. 2006, Hedenström et al. 2007, Rosén et al. 2007; Johansson et al., 2008; Hubel et al., 2009). However, only one study to date has investigated the wake shed from a gliding bird (Spedding et al. 1987), showing a rather simple wake consisting mainly of two wing tip vortices. In the present study, we used a tiltable wind tunnel (Pennyuick et al 1997) and a stereo DPIV system to record the wake flow behind a common swift *Apus apus* in gliding flight. The advantage of this approach is that the checksum of the aerodynamic forces lift (L) and drag (D) are known properties of a bird in steady gliding flight, and we can use this for direct comparison with the contribution from the vortex wake.

The physics of gliding flight

A steadily gliding bird, i.e. non-powered flight with fixed wings at a constant flight speed, converts potential energy to counteract the aerodynamic forces. It will glide at a certain horizontal forward speed and sink speed. The sink speed (U_s) will depend on the bird's weight, wing morphology and body shape (streamlining). Sink speed is calculated as

$$U_s = U \sin \theta, \tag{1}$$

where U is the flight speed along the glide path (not to be confused with horizontal speed) and θ is the angle of the glide path in relation to the horizontal (Fig. 1). To standardize airspeed measurements, all speeds refer to equivalent air speeds ($U = U_{true} \sqrt{\rho / \rho_0}$, where U_{true} is the true airspeed, ρ is the average air density measured over each day of the experimental period and $\rho_0 = 1.225$ kg/m³ is the standard air density at sea level). At equilibrium gliding, the resultant of lift and drag balances the weight of the bird (mass times gravity; mg). The lift component of the total force is directed perpendicular to the glide path. Note that lift in this case does not refer to the force keeping the bird aloft, but the force generated perpendicular to the wing surface (true lift). Lift is then given by

$$L = mg \cos \theta. \tag{2}$$

Drag of the bird is directed backwards, parallel to the glide path and perpendicular to lift and is calculated as

$$D = mg \sin \theta. \tag{3}$$

Drag calculated in this manner represents the total drag of the bird. Drag of a flying bird is usually separated into three components:
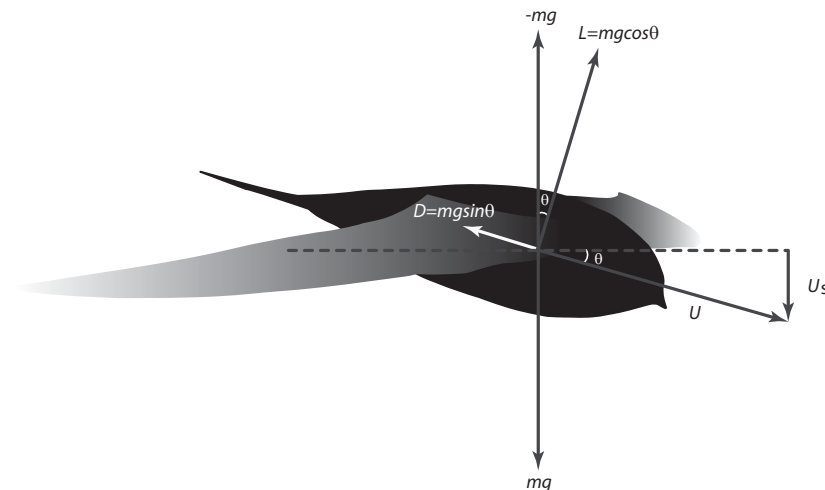

Figure 1. Forces acting on the swift in equilibrium gliding. The glide path is inclined at an angle θ to the horizontal and the resultant of the vectors lift (L) and drag (D) is equal and opposite to the weight of the bird (mg). Total speed (U) involves the component sink speed (U_s), which is directed downwards and perpendicular to the horizontal.

parasite drag, profile drag and induced drag. Parasite drag consists of friction and form drag of the body, caused when propelling the birds' body through the air and is calculated as

$$D_{par} = \tfrac{1}{2}\rho S_b C_{D,par} U^2,$$ (4)

where ρ is the air density, S_b is the body frontal area and $C_{D,par}$ is the parasite drag coefficient. Profile drag is the drag generated when moving the wings through the air and is calculated as

$$D_{pro} = \tfrac{1}{2}\rho S_w C_{D,pro} U^2,$$ (5)

where S_w is the wing area and $C_{D,pro}$ is the profile drag coefficient. The third component is induced drag and is due to the downwash induced by the wings and tail of the bird when creating lift. Induced drag is calculated as

$$D_{ind} = \frac{2kL^2}{\rho \pi b^2 U^2},$$ (6)

where b is the wingspan and k is the induced drag factor. k indicates how much the wing deviates from an elliptical lift distribution. This factor is typically set to 1.1 (e.g. Pennycuick 1975, 1989, 2008; Rosén & Hedenström 2001).

Profile drag is the component of aerodynamic forces that has proven most difficult to measure (Pennycuick 2008). Since the calculation of D_{ind} is relatively well established and D_{par} could be estimated from the wake (see below), D_{pro} could be estimated by subtraction as

$$D_{pro} = D\text{-}D_{ind}\text{-}D_{par}.$$ (7)

Coefficients of lift and drag

In order to make lift and drag of a particular bird comparable to those of others, the forces may be converted into dimensionless coefficients. These coefficients control for size of the bird, the flight speed and the air density. Lift coefficient is calculated as

$$C_L = \frac{2L}{\rho S_w U^2}$$ (8)

and drag coefficient is calculated as

$$C_D = \frac{2D}{\rho S_w U^2}.$$ (9)

Materials and methods

Birds

Two juvenile swifts were captured on 27th August 2009 in their nest on the day they were assumed to fledge. This minimizes the time needed to keep the birds in captivity and maximizes the chance that they are physically fit to fly. Between experiments the birds were kept in a lidless plastic box (30×40 cm) with artificial nest bowls. This housing resembles the nest the birds came from and therefore the birds remained calm in that environment. The birds were handfed with a mixture of mashed insects (both dried and fresh), vitamins, calcium and water with the help of a syringe. Before and after each flight session and each feeding occasion the birds were weighed and these values were used both for calculations of forces and as information about the birds' general condition. The birds required minimal training and only two days were spent on this before data acquisition was initiated. Only one of the birds would glide steadily in the tunnel and consequently all results presented in this paper refer to this bird.

The length from the beak to a white marker on the rump of the bird was measured on images of the bird held next to a reference grid to be used as reference length for accurate pixels-to-meters conversion of high-speed films (see below). Also, from these reference images of the hand held bird, the projected area of the head and the distance between the eyes were measured. These measures were used to test the accuracy of the

scale determined based on the beak-to-marker reference length in each of the image frames of the high-speed films (see below). The maximum wing area and wing span was also measured on the hand held bird with fully spread wing according to figure 2. The morphological details of the bird are presented in Table 1. On 6th of September 2009 the birds were released into the wild in good condition.

Wind tunnel

The Lund wind tunnel has a closed circuit design with an open test section. The design is customized for experiments with freely flying animals. The background turbulence is low, approximately 0.03% (Spedding et al. 2009) and airspeed across 97% of the test section is within ±1.3% of the mean (Pennycuick et al. 1997). Details on the design and specifications of the wind tunnel are presented in Pennycuick et al. (1997). The Reynolds number, calculated as $Re = Uc/\nu$, where c is the mean chord of the wing and ν is the kinematic viscosity, ranged from approximately 18400 at 7 ms^{-1} to 29500 at 11 ms^{-1}. The coordinate system for the tunnel is defined as: x-axis: streamwise, y-axis: spanwise and z-axis: vertical.

Experimental setup

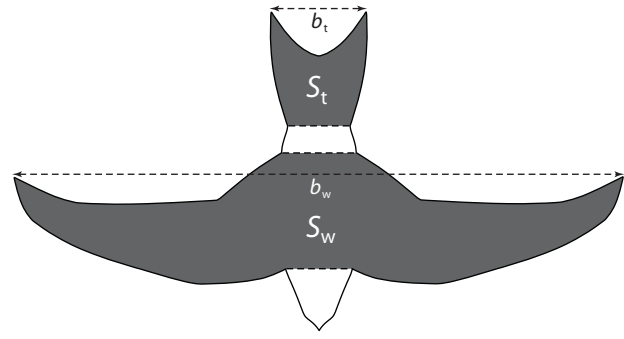The wing morphology during flight was recorded with a high speed camera (NAC Hotshot 1280;

Table 1.Morphological details of the bird used in the experiments

Average mass (g)	0.042
Max wingspan (m)	0.392
Max wing area[a] (m²)	0.0157
Mean wing chord[b] (m)	0.041
Max aspect ratio[c]	9.8
Body frontal area (m²)	0.0011

[a]Area of both wings including the body area in between
[b]Wing area divided by wingspan
[c]Wingspan squared divided by wing area

Figure 2. Body, wing and tail outline of the swift. The grey colored areas show how wing area (S_{w}) and tail area (S_{t}) was measured from top-view high-speed film sequences of the bird during steady gliding. Dashed lines show definition of wing span (b_{w}) and tail span (b_{t}). The distance from the beak to a marker on the rump of the bird (between the dashed line behind the wing and the dashed line at the proximal part of the tail) was used as reference length to determine the scale in each frame. The distance between the eyes of the bird and the projected area of the head (showed white here) were used to test the accuracy of the determined scale.

1280×1024 pixels) filming the bird straight from above. The wake was sampled using stereo digital particle image velocimetry at a plane transverse (y,z) to the free stream flow. The imaging plane was ca 0.3-0.4 m (8-11 wing chord lengths) downstream of the bird. The DPIV and the high-speed camera were triggered when the bird was gliding steadily in the appropriate position. The high-speed camera was, during the DPIV-experiments, used also to record the location of the bird relative to the imaging plane and the flight behavior of the bird.

Experimental protocol

The bird was allowed to fly freely in the wind tunnel and it was not guided by any means. The bird was flown at 5 different flight speeds: 7, 8, 9, 10 and 11 ms^{-1}. For each speed, the tunnel was initially tilted to its maximum, 6.3°, and then tilted back towards horizontal in increments of 0.1° until the bird was just able to glide steadily. This angle corresponds to the minimum decent angle for that particular speed. Once the angle was found the procedure was repeated from the

6.3° position with a new speed. At all speeds it was clear when the minimum angle was found because the bird would not be able to glide steadily at any lower angle, but would either descend or decelerate. For the wake measurements each of the speeds and corresponding minimum tilt angles were revisited and thereby the previous measurements were confirmed. The bird was at all speeds able to glide steadily at all angles steeper than the minimum.

High-speed camera details

The high-speed camera was mounted on top of the test section and thereby always perpendicular to the airflow regardless of the tunnel tilt angle. The camera was triggered manually and captured the bird for 0.75 seconds at 250 frames per second. From each of the recorded sequences, a single frame was used to measure wing area, tail area, wing span and tail span with Scion Image (Scion Corporation; see Fig. 2) using the reference lengths and area described above. The frames were taken only from steady gliding sequences. Images from two to three sequences per angle and speed combination were analyzed and the average was calculated.

SDPIV details

Flow field areas of approximately 0.20×0.20 meters were recorded using two CMOS-sensor cameras (High-SpeedStar3: 1024×1024 pixels) connected to frame grabber PCI boards in a host computer. The cameras were equipped with 60 mm lenses (AF Micro Nikkor 60 mm f/2.8D) set to aperture 2.8. A thin fog (particle size 1 μm) was introduced into the tunnel downstream from the test section and circulated in the tunnel until even. The fog particles were illuminated by a pulsed 50 mJ laser (Litron LPY732 series, Nd: YAG, 532 nm) generating pulse pairs at 200 Hz repetition rate. The laser beams were spread by a cylindrical lens into a thin sheet covering the view of the two cameras. To filter out light from any other source than the laser the cameras were equipped with band pass filters (530 ±

5 nm). The system was operated using DaVis 7.2.2 software package (LaVision, Göttingen, DE). The DPIV cameras were calibrated using a calibration plate (0.20 × 0.20 meters, type 22) and the routine in DaVis. The calibration was fine-tuned using the self-calibration routine in DaVis, by which any misalignment between the laser sheet and calibration plate is corrected.

The DPIV data were analyzed using DaVis software. The raw images were pre-processed prior to vector computations by using subtract-sliding-minimum filter over 5 frames. For image correlation, multi-pass stereo cross-correlation was used (64 × 64 in initial step and 32 × 32 in final step, 50% overlap). Vectors in the resulting vector field showing peak ratios <1.01, when dividing the highest correlation peak with the second highest correlation peak, were deleted. Vectors were also deleted if the magnitude was 2 times the neighborhood RMS and recalculated if the magnitude was 3 times the neighborhood RMS. As a final post-processing stage, empty spaces were interpolated and a 3 × 3 smoothing average was applied. For each sequence, background velocity measured on free stream flow was subtracted from the out of plane velocity. DPIV sequences were only used for further analysis if they corresponded to high speed film sequences showing the bird in steady gliding.

Wake measurements

Vortex circulation and estimate of lift

The processed wake images were used for calculating the circulation (Γ) of identifiable wake structures. This was done for each minimum glide angle at each speed. The wake of the gliding swift consists mainly of a pair of wingtip vortices and a pair of tail vortices (see below). Circulation was measured using a custom written Matlab program (The MathWorks, Inc., Natick, MA, USA) and otherwise following the same procedure as described in Spedding et al. (2003). Averages over all sequences for each speed were calculated for wingtip vortices and tail vortices, respectively. According to lifting

line theory and the Kutta-Joukowski theorem the force generated by a fixed finite wing can be approximated by

$$L = \rho b \Gamma U , \qquad (10)$$

where b is wake span and Γ is circulation. Both the wingtip and tail vortices were assumed to contribute to lift and hence total lift generated by the gliding swift was calculated as

$$L = \rho U \left(b_{w,wake} \Gamma_w + b_{t,wake} \Gamma_t \right), \qquad (11)$$

where $b_{w,wake}$ is the average wingtip vortex wake span, Γ_w is average circulation of the wingtip vortex, $b_{t,wake}$ is the average tail vortex wake span and Γ_t is average circulation of the tail vortex. Since the DPIV cameras, the laser sheet and consequently the orientation of the recorded image plane follow the tilt of the tunnel, the calculated lift will correspond to the lift generated by the bird ($mg\cos\theta$; see Fig. 1) and not the weight of the bird (mg) at any given glide angle (θ; see Fig. 1).

Velocity defect and estimate of parasite drag

The drag of the bird body, called parasite drag, is a quantity for calculating the overall drag of a bird (e.g. Pennycuick 1989, 2008). In order to estimate the drag generated by the body alone, the out-of-plane (x) velocity defect behind the body was measured. When plotting the streamwise velocity of the complete frame the deceleration of the freestream airflow introduced by the bird could be distinguished (cf. Hedenström et al. 2009). Patches of decelerated flow were typically found in the wingtip vortices, the tail vortices and behind the body (Fig 3A). To estimate the drag by the body alone the air velocities were measured in the location of the body, but excluding the drag introduced by the tail vortices (Fig. 3A). These measurements were performed using a custom written Matlab program, which allows the user to manually define an area of interest containing the velocity defect created by the body. Within this area the streamwise velocities of vectors having a velocity less than 20% of the freestream flow were measured. From this the mass flow rate was calculated as
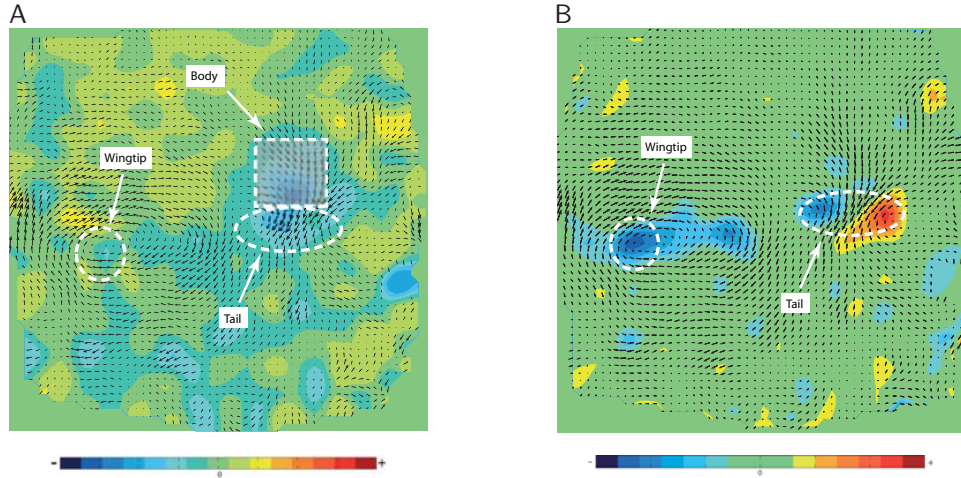
$$\dot{m} = \rho A U_b , \qquad (12)$$

Figure 3. An example of velocity vector fields superimposed on (A) out-of-plane velocities and (B) vorticity at 9 ms^{-1}, illustrating how the velocity defect caused by the body alone was measured. Panel (A) shows the velocity defect over the complete frame and patches of decelerated air are found in the tail vortices, the wingtip vortices and behind the body. Note that the trace of the body as shown clearly in panel (A) is not apparent in the vorticity field of the same frame as shown in panel (B). The shaded rectangle in panel A illustrates how the body velocity defect was typically measured.

where A is the measured wake area and U_b is the air velocity behind the body. Parasite drag was then calculated as

$$D_{\mathrm{par}} = \left| \dot{m} \Delta U \right| , \qquad (13)$$

where ΔU is the difference in velocity between the decelerated air behind the body, U_b, and the unaffected freestream flow, U_∞. Finally, the body drag coefficient was calculated as

$$C_{\mathrm{D,par}} = \frac{2 D_{\mathrm{par}}}{\rho U^2 S_b} , \qquad (14)$$

where S_b is the body frontal area of the bird (Table 1).

Results

Gliding flight characteristics

Only one of the two birds that were initially tested would glide in the tunnel. This bird only glided for brief periods the first day and not quite steadily, but the second day the bird appeared to have learned how to utilize the opportunity for gliding flight and started to glide steadily for longer periods. The bird would not glide unless the tunnel was tilted, but would glide at all tilt angles steeper than the minimum angle. The bird was able to glide steadily at speeds over a range from 7 to 11 ms^{-1}. At the lower speeds the gliding events were rarer and shorter in duration than at higher speeds. The higher speeds were clearly more suitable for the swift, although the highest speed, 11 ms^{-1}, seemed challenging for the bird in terms of maneuvering with respect to the wind tunnel walls. The typical behavior of the bird was to accelerate in flapping flight upstream into the centre of the test section, then switch to gliding flight and depending on the speed and tilt angle, it would remain stationary with respect to the test section from a couple of seconds up to approximately 10 seconds.

Wing and tail morphology

Wing span, wing area, span ratio and aspect ratio are measures of the wing morphology of a gliding bird. By measuring these variables over a range of flight and sink speeds the dynamic morphing of the bird wing can be roughly described.

The swift changed its wing morphology to a large extent between different speeds and glide angles. The span ratio, defined as the ratio between observed wing span ($b_{w,obs}$) and maximum span ($b_{w,max}$; hand held bird with manually spread wing; see Table 1), decreased linearly with speed, from approximately 0.9 at 7 ms^{-1} to 0.85 at 11 ms^{-1}, although with a large scatter (Fig. 4A). This reduction in wingspan was achieved by the bird mainly by flexing the wing at the wrist joint and thus sweeping the wing backwards. The wing area was reduced linearly with reduced span, from 0.0156 m^2 (99.0% of maximum area) at the widest span measured, 0.391 m (99.7% of maximum span) to 0.0111 m^2 (70.9% of maximum area) at the shortest span measured, 0.303 m (77.2% of maximum span; Fig 5). Figure 5 shows this relationship independent of speed.
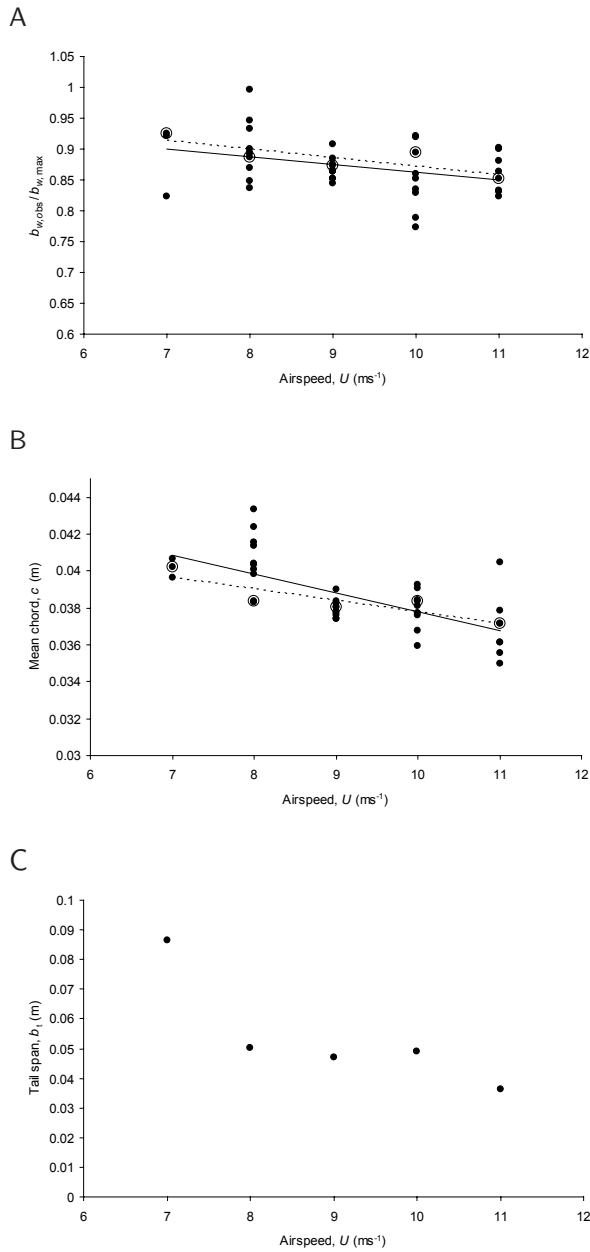
The mean chord (c) of the wing is defined as wing area/wing span. The mean chord of the swift decreased with flight speed, both regarding all speed/angle combinations and regarding minimum tilt angle for each speed (Fig. 4B). This property will have an effect on the Reynolds number.

The tail span decreased with speed from 0.09 m at 7 ms^{-1} to 0.04 at 11 ms^{-1}. The tail is spread notably more at 7 ms^{-1} than at any of the other speeds (Fig. 4C).

Flight performance

Sink speed

The sink speed (U_s) of the bird, i.e. the vertical component of the total flight speed, was calculated for the cases of minimum tilt angle of the wind tunnel for each flight speed. The sink speed showed a curvilinear relationship with speed. Fitting a second order polynomial regression equation to the data yields the

A

B

C

Figure 4. (A) Span ratio ($b_{w,obs}/b_{w,max}$) in relation to flight speed. Filled circles represent the complete data including all combinations of speed and tilt angles and open circles represent the minimum tilt angle for each speed. The solid line shows the linear regression function for the complete data ($b_{w,obs}/b_{w,max}$ = -0.0123U+0.9865; R^2= 0.13) and broken line shows the linear regression function for data points corresponding to minimum tilt angle ($b_{w,obs}/b_{w,max}$ = -0.0139U+1.0115; R^2= 0.66). (B) Mean chord (c) in relation to airspeed. Filled circles show all speed/angle combinations (c= -0.001U+0.048, R^2= 0.48) and open circles show the minimum tilt angle for each speed (c= -0.0006U+0.044, R^2= 0.75). The solid line shows the regression line fitted to the complete data set and the broken line shows the regression line fitted to the minimum tilt angles. (C) Tail span (b_t) as a function of speed. The tail is more spread at the lowest speed, 7 ms⁻¹. At all other speeds the tail is kept furled together to a large extent and at the highest speed, 11 ms⁻¹, the tail is completely furled.

relationship U_s=0.0315U^2-0.5101U+2.7588 (Fig. 6A; R^2=0.96). Minimum sink speed (U_{ms}) as estimated by the speed at the minimum of this equation was U_{ms}=8.1 ms⁻¹. If a tangent is drawn from the origin towards the curve, the speed at the intercept corresponds to the best glide speed (U_{bg}), which is estimated to U_{bg}=9.4 ms⁻¹ (Fig. 6A).

Lift and drag

Lift and drag was calculated based on the

weight of the bird and the tilt angle of the wind tunnel, i.e. the angle of descent of the glide path, according to eqs. 2 and 3. Drag was further dissolved into induced drag (D_{ind}), parasite drag (D_{par}) and profile drag (D_{pro}). Induced drag was calculated according to eq. 6, using an induced drag factor (k) of 1.1, parasite drag was estimated from the wake (see below) and profile drag was calculated according to eq. 7. Total drag showed a curvilinear relationship with speed (D=0.0016U^2-0.0302U+0.1761, R^2=0.95) with a minimum at 9.44 ms⁻¹. Induced drag decreased with speed (D_{ind}=0.002U+0.039, R^2=0.96). Profile drag showed a shallow U-shaped relationship with speed (D_{pro}=0.0013U^2-0.025U+0.1286, R^2=0.96), with a minimum at 9.6 ms⁻¹, while parasite drag increased with speed (D_{par}=0.0019U-0.0039; R^2=0.99; Fig. 6B). The speed specific maximum ratio of lift to drag (L:D) showed an inversely quadratic relationship with airspeed (L:D=-0.4849U^2+9.2059U+31.204, R^2=0.9376; Fig. 6C). The maximum of the second order polynomial regression equation was used to estimate the maximum L:D, which was 12.5. This maximum was reached at a flight speed of 9.5 ms⁻¹ (although the maximum L:D ratio measured was 12.7 at 10 ms⁻¹).
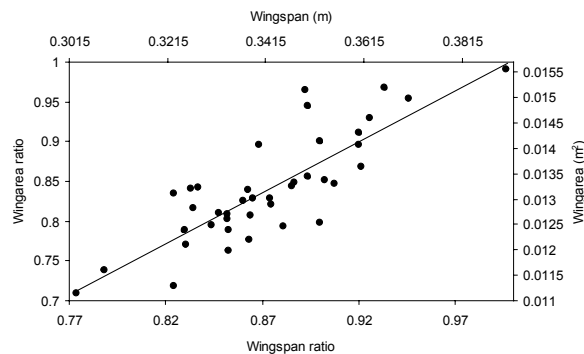
Figure 5. Wing area (S) as a function of wingspan (bw) presented in absolute measures and as ratio of maximum. There is a linear positive relationship between wing span and wing area. Regression for span ratio: $S^* = 1.28 b_w^* - 0.2785$, $R^2 = 0.68$ regression for absolute measures: $S = 0.0514 b_w - 0.0044$; $R^2 = 0.68$.

The coefficient of lift (C_L) was calculated at the minimum glide angle for each speed according to eq. 8, using the measured wing area or the sum of the wing area and tail area. The lift coefficient decreased from 0.96 at 7 ms^{-1} to 0.48 at 11 ms^{-1} ($C_L = 0.0154 U^2 - 0.4031 U + 3.0377$, $R^2 = 0.99$) with wing area as reference and from 0.81 at 7 ms^{-1} to 0.43 at 11 ms^{-1} ($C_L = 0.0101 U^2 - 0.2827 U + 2.3095$, $R^2 = 0.99$) with the sum of wing and tail area as reference (Fig. 7A). The highest C_L measured here is not necessarily the maximum attainable for the bird. The maximum tilt angle of the tunnel is 6.3° and with an even steeper tilt angle the true maximum C_L may be higher. Analogously, the minimum speed, or stall speed, may be slower than the minimum speed measured here, 7 ms^{-1}. Coefficient of total
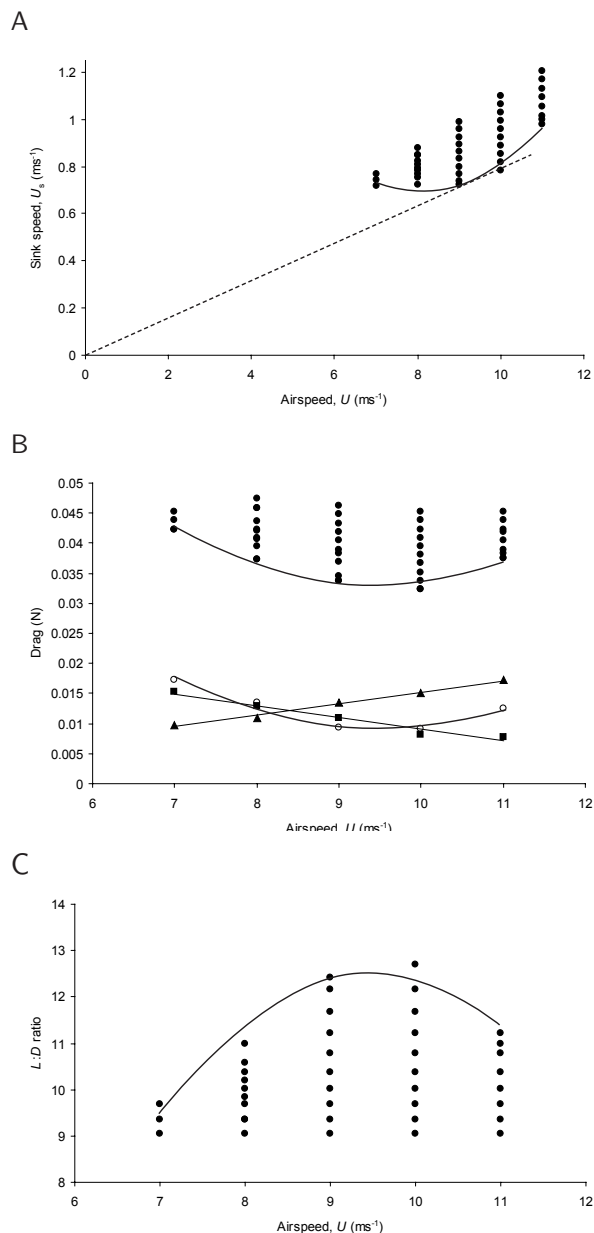

Figure 6. (A) Minimum sink speed in relation to airspeed. The relationship can be described with a second order regression polynomial: $U_s = 0.0315 U^2 - 0.5101 U + 2.7588$, $R^2 = 0.961$. The speed at the minimum of this equation corresponds to the minimum sink speed; $U_{ms} = 8.1$ ms^{-1}. If a tangent is drawn from the origin towards the curve ($U_s = 0.0795 U$), the speed at the intercept corresponds to the best glide speed, $U_{bg} = 9.4$ ms^{-1}. (B) Drag as a function of airspeed. Filled circles represent total drag for all speed and tilt angle combinations, squares represent induced drag and triangles represent profile/parasite drag. Total drag has a minimum at 9.44 ms^{-1}. Induced drag decreased with airspeed and the combined profile and parasite drag showed a U-shaped curve with a minimum at 8.54 ms^{-1}. (C) Maximum lift to drag ratio ($L:D$) as a function of airspeed. Maximum $L:D$ showed a curvilinear relationship with airspeed ($L:D = -0.4849 U^2 + 9.2059 U + 31.204$, $R^2 = 0.9376$), with a maximum of 12.5 at a flight speed of 9.5 ms^{-1}.
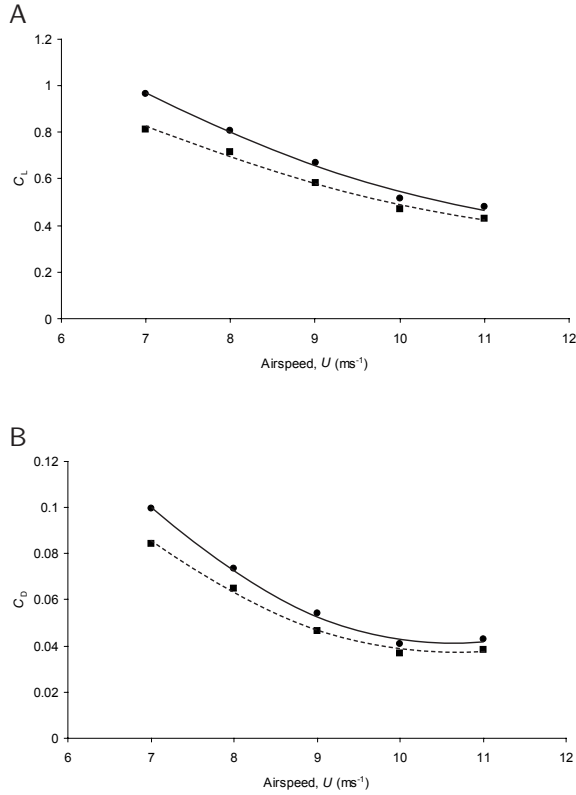
A

B

Figure 7. Coefficient of lift and drag at minimum tilt angle as a function of airspeed. Circles represent coefficients calculated using only wing area as reference area, while squares represent coefficients calculated using the combined area of the wings and tail as reference area. (A) Second order polynomial regression for coefficient based on wing area alone: $C_L = 0.0154 U_2 - 0.4031 U + 3.0377$, $R^2 = 0.99$, and for joint wing area and tail area: $C_L = 0.0101 U^2 - 0.2827 U + 2.3095$, $R^2 = 0.99$. (B) Coefficient of drag decreases with flight speed but levels out within the measured range. Second order polynomial regression for C_D based on wing area alone: $C_D = 0.0044 U^2 - 0.0946 U + 0.5449$, $R^2 = 0.99$, and for combined wing area and tail area: $C_D = 0.0035 U^2 - 0.0754 U + 0.4404$, $R^2 = 0.99$.

drag (C_D) was calculated, similar to C_L, for the minimum glide angle of each speed according to eq. 9. The coefficient of drag decreased non-linearly from 0.1 at 7 ms^{-1} to 0.043 at 11 ms^{-1} $(C_D = 0.0044 U^2 - 0.0946 U + 0.5449$, $R^2 = 0.99)$ with wing area as reference and from 0.084 at 7 ms^{-1} to 0.038 at 11 ms^{-1} $(C_D = 0.0035 U^2 - 0.0754 U + 0.4404$, $R^2 = 0.99)$ with the sum of wing and tail area as reference. Both curves flatten out between 10 ms^{-1} and 11 ms^{-1} (Fig. 7B).

Profile drag coefficient was calculated similarly to the total drag coefficient (cf. eq. 9) for all speed and tilt angle combinations. Plotting $C_{D,pro}$ against C_L gives the polar area (terminology from Tucker, 1987), which describes the relationship between $C_{D,pro}$ and C_L for the morphing swift wing (Fig. 8). Minimum $C_{D,pro}$ was 0.011 and was found at 10 ms^{-1}.

Wake topology

The wake of the gliding swift consists of two main structural parts: a pair of wingtip vortices and a pair of tail vortices. Figure 9 shows characteristic images of the vector and vorticity fields at 7 ms^{-1}, 9 ms^{-1} and 11 ms^{-1} that visualize the trailing wingtip vortex of the left wing and both tail vortices. The wingtip vortex is similar at all speeds, but the tail vortices differ. At 7 ms^{-1} the tail vortices are far apart as a consequence of the widely spread tail, while at 9 ms^{-1} and 11 ms^{-1} the tail vortices are gradually closer together. The same pattern emerges when plotting the tail span measured on the bird in flight against speed (see Fig. 4C).

Images from one high speed SDPIV sequence of 9 ms^{-1} gliding flight were compiled into a 3D wake representation by translating the time delay between the images $(\Delta t = 1/200$ s) into spatial displacement $(\Delta x = \Delta t U_\infty)$, assuming a constant
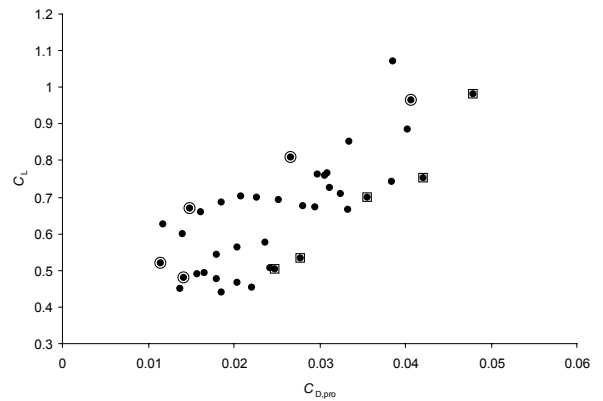

Figure 8. Polar area for the wings of the swift gliding at equilibrium for all airspeed and tilt angle combinations examined. Open circles correspond to minimum tilt angle and open squared correspond to the highest tilt angle.
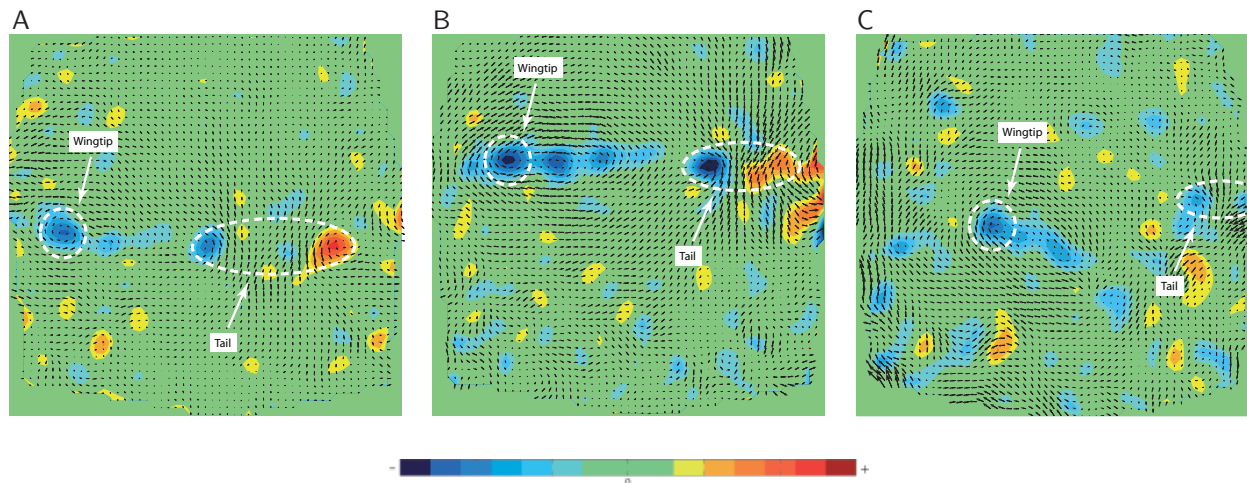
Figure 9. Example images of the vector and vorticity fields at (A) 7 ms^{-1}, (B) 9 ms^{-1} and (C) 11 ms^{-1}. The wingtip vortex is similar at all speeds, but the tail vortices differ. At 7 ms^{-1} the tail vortices are farther apart compared to the higher speeds.

convection contributed by the freestream velocity (U_∞) alone. The compiled 3D image was used to plot the vorticity iso-surface of the wake (Fig. 10). The iso-surface plot shows the normalized constant streamwise vorticity (iso-value = 80s^{-1}) trailing behind the gliding bird.

Quantitative wake measurement

Wingtip circulation, tail circulation and lift

The main features of the wake of the gliding swift are the wingtip vortices and the tail vortices (Fig. 10). Circulation (Γ) of these structures was measured for each sequence and the average was calculated (Fig. 11). The circulation of the wingtip vortices decreases in strength with increasing speed, whereas the tail vortices vary with speed without any apparent trend.
Lift was calculated according to eq. 11 for each flight speed. The model involved wingtip vortices and tail vortices as these were assumed to result from lift generation. The model is described conceptually in figure 12.

Total lift calculated from the wake-based model showed good agreement with the lift calculated based on the glide angle of the flight

path (Fig. 13A). The lift calculated with the model was 105%, 98%, 101%, 101% and 105% of the lift calculated based on the glide angle of the bird for 7, 8, 9, 10 and 11 ms^{-1}, respectively.

Body wake defect and estimate of parasite drag

The estimate of body drag was an attempt to distinguish this from the total drag of the bird. The calculated body drag, or parasite drag, increased with speed from 0.0097 N at 7 ms^{-1} to 0.0172 N at 11 ms^{-1} (Fig. 13B) In proportion to the calculated total drag based on glide angle this estimated drag of the body varies from 23% at 7 ms^{-1} to 46% at 11 ms^{-1}. The parasite drag coefficient calculated according to eq. 14 decreases from 0.30 at 7 ms^{-1} to 0.22 at 11 m^{-1} (Fig. 13C).
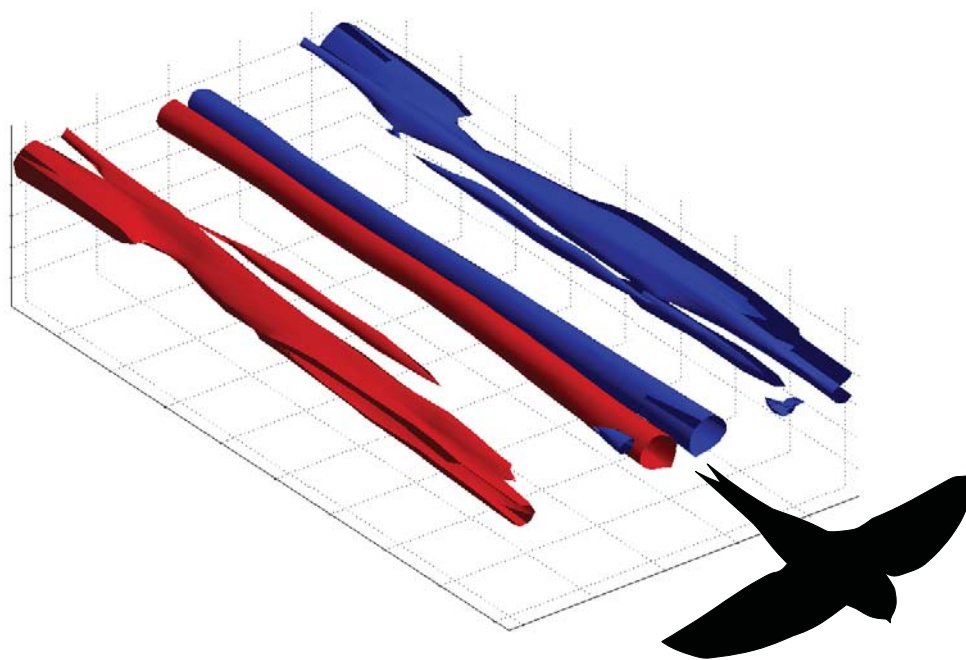
Figure 10. Vorticity iso-surface plot at airspeed of 9 ms^{-1}. The view is obliquely from above and from the front of the bird's flight path, as indicated by the bird-silhouette. The plot is based on data from one side of the bird, wing and tail, that have been mirrored in the plot to illustrate the complete wake. Tail vortices and wingtip vortices are the major structures in the wake of the gliding swift and appear clearly in this plot.

Discussion

Flight behavior

The swift turned out to be a skillful glider in the wind tunnel. This was perhaps not surprising, since these birds glide for a considerable proportion of the time also in the wild (Lentink et al., 2007; Henningsson et al. 2009). On the contrary, it was surprising that one bird
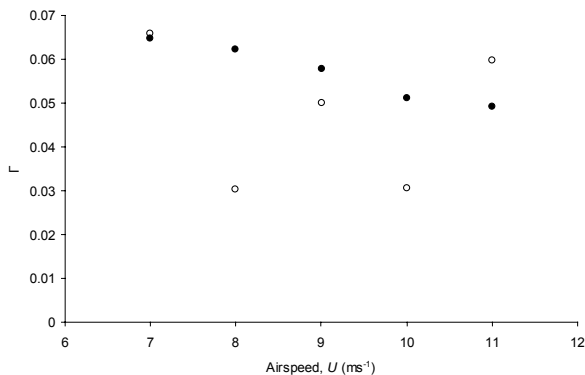

Figure 11. Circulation (Γ) as a function of airspeed. Filled circles represent wingtip circulation and open circles represent tail circulation. Wingtip circulation decreases with speed, whereas tail circulation shows no apparent relationship with speed. At several speeds the circulation of the tail is of the same order as that of the wingtip.

never started to glide properly and it took the other bird a couple of days before it began exploring the opportunity for gliding flight in the tunnel. Once the single bird had started to explore gliding flight it soon started to glide for relatively long periods. The bird would glide at any tilt angle lower or equal to the lowest possible for each speed. The stability of the glides could vary, typically the glides would be shorter at very high and at very low tilt angles. When approaching the lowest angle the glides would typically become shorter and the bird would also glide less frequently, suggesting that it was at its performance limit. The range of flight speeds that the swift would glide at was rather limited, 7-11 ms^{-1}, although, this range is similar to what has been recorded for flapping flight before in a wind tunnel (Henningsson et al. 2008) and 11 ms^{-1} is the highest speed any swift has been flying at in the tunnel so far.

Flight performance

The highest coefficients of lift (C_L) measured for the swift was 0.96 or 0.81 if excluding or including the tail area in the calculation (Fig. 7A). Lentink et al. (2007) examined the glide performance of swifts by measuring lift and

drag of preserved wings. They found C_L between 0.8 and 1.1, which is in good agreement with the results presented here for a live bird. The C_L of the swift can also be compared to that of a jackdaw (*Corvus monedula*; Rosén and Hedenström, 2001), a pigeon (*Columba livia*; Pennycuick 1968), a Harris' hawk (*Parabuteo unicinctus*; Tucker and Heine, 1990) and a laggar falcon (*Falco jugger*; Tucker and Parrot, 1970; Tucker, 1987; Table 2). Apart from the pigeon, these species are all raptors more or less adapted for soaring flight. The swifts are, in their ecology and morphology unlike most birds, they are aerial insectivores and have quite unique wing morphology, with a very long hand section and a short arm section. The maximum C_L for the swift was the same as for the pigeon, but lower than in the soaring specialists (Table 2). This could reflect diverging adaptations of the wing design between these birds, where a high C_L is required for minimum turn radius when circling in thermals and during take-off and landing. The maximum *L:D* ratio was similar in the swift as the maximum of the other species (Table 2), which is remarkable considering that the swift is the smallest species. However, the swift compensates this by having relatively long wings (high aspect ratio; Table 2) that reduces the induced drag and gives such a favorable *L:D*. The larger soaring specialists, except the laggar falcon, have separated primaries to generate a slotted wingtip. Slotted wingtips have been shown to reduce induced drag by vertical spreading of the vortices shed at the wingtip
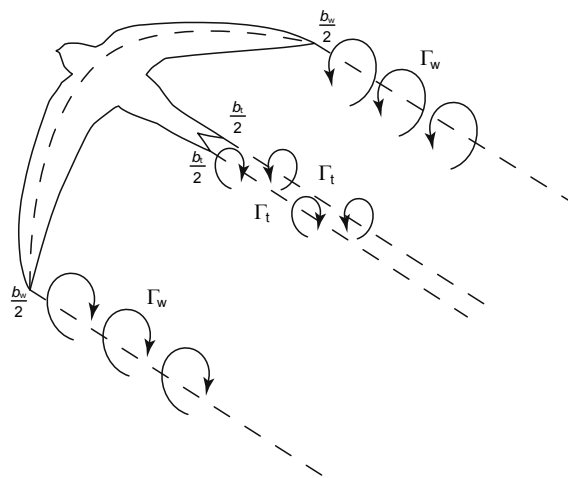

Figure 12. Illustration of the wake-based model consisting of a pair of trailing wingtip vortices and a pair of trailing tail vortices. Dashed lines behind the bird symbolizes vortex lines left behind the bird in the wake and the dashed line following the wings of the bird symbolizes the bound vortex, which is assumed to be connected to the trailing wingtip vortices.

(Tucker, 1993), and so they appear to achieve high *L:D* by minimizing drag.

The drag as calculated based on the glide angle of the bird represents the drag of the whole configuration. This includes several parts, among which the induced drag was estimated from theory. A similar approach was used by Rosén and Hedenström (2001) on the jackdaw. In that study an estimate of combined profile and parasite drag was derived by subtracting the induced drag from the total drag. If summarizing profile and parasite drag for the swift, an interesting feature is that the induced

Table 2. Data for five birds compiled from literature.

Species	Mass (g)	Wingspan (m)	Aspect ratio	U_{ms} (ms⁻¹)	U_{bg} (ms⁻¹)	Max *L:D*	C_L
Harris' hawk[1]	0.702	1.02	5.5	-	-	10.9	1.60
Jackdaw[2]	0.180	0.60	6.1	7.4	8.3	12.6	1.49
Laggar falcon[3]	0.570	1.01	7.7	-	-	10	1.60
Pigeon[4]	-	0.67	6.0	-	-	12.5	0.96
Swift[5]	0.042	0.39	9.8	8.1	9.4	12.5	0.96

[1]Tucker and Heine (1990)
[2]Rosén and Hedenström (2001)
[3]Tucker and Parrot (1970); Tucker (1987)
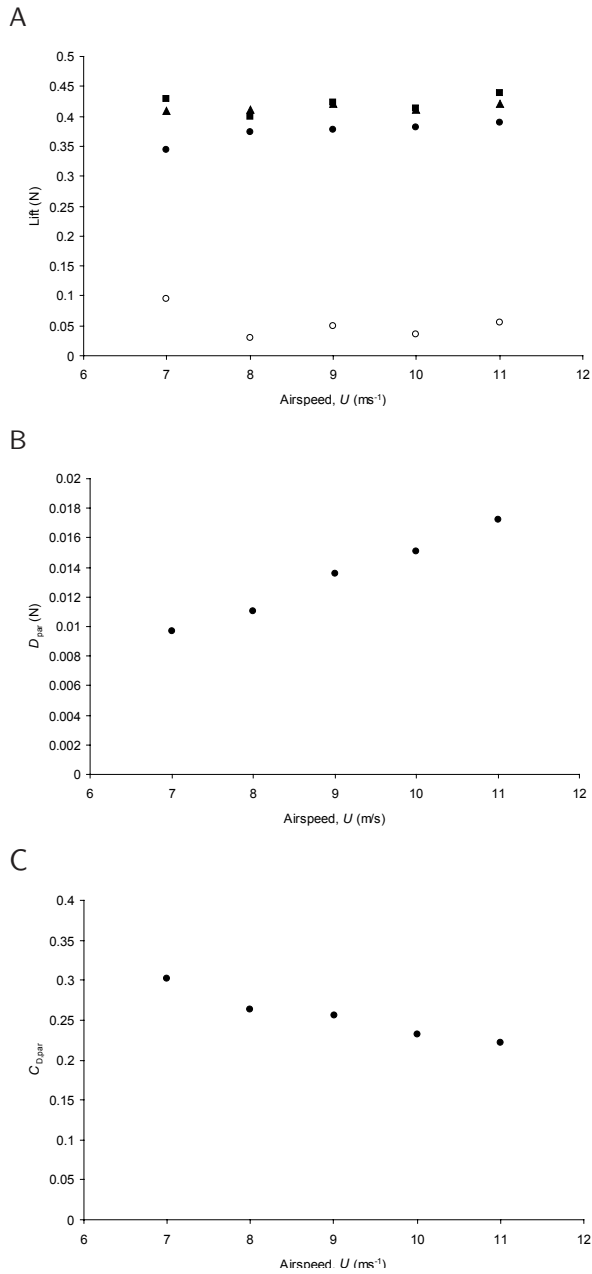[4]Pennycuick (1968)
[5]The present study

A

B

C

Figure 13. (A) Lift as a function of airspeed. Filled circles represent lift generated by the wingtip vortices and open circles represent lift generated by the tail vortices. Squares represent the sum of lift measured in the wake and triangles represent the lift calculated based on glide angle. (B) Parasite drag in relation to airspeed. Drag of the body, as a fraction of the total drag estimated based on the glide angle of the bird, increased from 23% at 7 ms^{-1} to 46% at 11 ms^{-1}. (C) Parasite drag coefficient in relation to airspeed.

drag is lower than the profile/parasite drag, whereas these components were opposite for the jackdaw. The low induced drag for the swift compared with the jackdaw can be explained if, for illustrative purposes, rearranging eq. 6 into

$$D_{ind} = \frac{2kS\left(\dfrac{W}{S}\right)^2}{\rho\pi U^2 AR}, \qquad (15)$$

where (W/S) is the wing loading and AR is the aspect ratio of the wing. The wing loading for the swift was 26 kg/m² and for the jackdaw it was 30 kg/m² (Rosén and Hedenström, 2001) The aspect ratio for the swift was 9.8 and 6 for the jackdaw. Thus, for any given speed, the numerator will be lower and denominator will be higher for the swift compared with the jackdaw, both resulting in a lower D_{ind}.

Gliding wake and forces estimated from it

The wake of the gliding swift is comparatively simple. The main features are a pair of wingtip vortices and a pair of tail vortices. Spedding (1987) studied the wake of a kestrel (*Falco tinnunculus*) in gliding flight. In that study only the wingtip vortices were apparent, while the tail vortices were not observed and therefore not included in the model developed to describe the wake. In the wake of the swift the tail vortices are prominent features, in fact, the circulation of the tail vortices is sometimes nearly as high as that of the wingtip vortices. However, despite the high circulation of the tail vortices the effective contribution to the total lift is small in comparison to the wingtip vortices, due to the small span of the tail (recall eqs. 10 and 11). The model of the wake of the gliding swift proposed here and the forces estimated showed reasonable agreement with the lift calculated based on the glide angle of the bird. This model includes wingtip vortices and tail vortices and the circulation measured in the wake is assumed to directly reflect the circulation of the lift generating bound vortex. This is assumed to

be a simplified view, since it does not take into account the circulation distribution on the wing and assumes no convection in the wake other than that of the freestream flow. The model is based on the measured wake span and not the span of the bird, which means that it takes into account the contraction of the wake (e.g. Milne-Thompson, 1966), but other than that it is assumed that the wake is unaffected as it travels downstream the bird. The fact that the model, despite its simplicity, matches the expected force to such a large extent, suggests that the wake of a gliding bird is indeed simple.

As mentioned above, the drag calculated based on glide angle represents the total drag. Since the system for flow visualization used gives also the out-of-plane (x) velocities, an attempt was made to estimate the drag of the body, parasite drag, from the drag of the whole bird based on wake defect. The results showed that the drag coefficient of the body was from 0.30 at 7 ms^{-1} to 0.22 at 11 ms^{-1}. Note that this coefficient is not directly comparable to the total coefficient of drag calculated here, since the characteristic area used for the total drag coefficient was the wing area, whereas for the body drag coefficient the body frontal area was used (Pennycuick, 2008). A comparable body drag coefficient of the swift body was estimated by Lentink et al. (2007) by measuring the drag of a stuffed wingless swift body using an aerodynamic balance. In that study the body drag coefficient was found to be on average 0.26. The range measured here includes this value and the average over all speeds was 0.26. Measuring drag on dead/ stuffed bird bodies has been proposed to result in an overestimate compared with the true drag generated by a live bird in flight (Tucker 1973, Pennycuick et al. 1988; but see Hedenström and Liechti 2001). The results of this study suggest that this is not necessarily the case under all circumstances.

Profile drag could be estimated in this study since the induced drag could be calculated and the parasite drag could be measured. This is, as mentioned, the most difficult aerodynamic component to measure (Pennycuick 1989, 2008), although, it has been done a few times before on live birds. Tucker and Heine (1990)

did a similar study like the current one on a Harris' hawk gliding in a wind tunnel. In that study profile drag was estimated, similar to this study, by subtracting induced drag and parasite drag from the measured total drag to yield the profile drag coefficient, $C_{D,pro}$. However, Tucker and Heine (1990) calculated parasite drag based on equivalent flat plate area. The same Harris' hawk was used by Pennycuick et al. (1992) to estimate the profile drag by measuring the pressure of the air behind the wing. The results from these two approaches of estimating profile drag of the same bird differed, Tucker and Heine (1990) found a range of $C_{D,pro}$ from 0.003 to 0.097, while Pennycuick et al. (1992) found a range from 0.008-0.052. In the present study of the swift the range of $C_{D,pro}$ was from 0.011 to 0.048. The lower end is higher for the swift than the lower end for the Harris' hawk, while the upper end is lower for the swift than the upper end for the Harris' hawk. The shape of the polar area of the swift is similar to that of the Harris' hawk as described by Tucker and Heine (1990), while the shape of the polar area found by Pennycuick et al. (1992) for the Harris' hawk differed. In such polar plots, the left-hand side of the polar area boundary represents the polar curve for minimum drag, whereas the right-hand side of it represents the polar curve for maximum drag. This maximum drag polar does not correspond to the maximum drag polar curve possible for the bird unless the wings stalls (Tucker and Heine, 1990). There were no signs that the wings of the swift were stalling at any occasion during the experiments, so it is likely that the right-hand boundary in the polar area not fully represent the true maximum drag polar for the swift. However, as can be seen in figure 8, $C_{D,pro}$ for the maximum tilt are all found along the right-hand boundary, suggesting that the bird is maintaining equilibrium gliding by braking with the wings, i.e. adding to the total drag. Furthermore, $C_{D,pro}$ for minimum tilt angle are all located along the left-side boundary, which is expected if the bird at these occasions adjusts its wing shape to minimize drag.

Acknowledgements

References

Hedenström, A. (1993). Migration by soaring or flapping flight in birds: the relative importance of flight cost and speed. *Phil. Trans. R. Soc. Lond. B* **342**, 353–361.

Hedenström, A. and Liechti, F. (2001) Field estimates of body drag coefficient on the basis of dives in passerine birds. *J. Exp. Biol.* **204**, 1167-1175.

Hedenström, A., van Griethuijsen, L., Rosén, M. and Spedding, G. R. (2006). Vortex wakes of birds: recent developments using digital particle image velocimetry in a wind tunnel. *Animal Biol.* **56**, 535-549.

Hedenström, A., Johansson, L. C., Wolf, M., von Busse, R., Winter, Y. and Spedding, G.R. (2007). Bat flight generates complex aerodynamic tracks. *Science* **316**, 894-897.

Hedenström, A., Muijres, F. T., von Busse, R., Johansson, L. C., Winter, Y. and Spedding, G. R. (2009) High-speed stereo DPIV measurements of wakes of two bat species flying freely in a wind tunnel. *Exp. Fluids* **46**, 923-932.

Henningsson, P., Karlsson, H., Bäckman, J., Alerstam, T. & Hedenström, A. (2009) Flight speeds of swifts (*Apus apus*): seasonal differences smaller than expected. *Proc. R. Soc. B* **276**, 2395-2401.

Hubel, T. Y., Hristov, N. I., Swartz, S. M. and Breuer, K. S. (2009) Time-resolved wake structure and kinematics of bat flight. *Exp. Fluids*, **46**, 933-943.

Idrac, M. P. (1924). Contributions à l'étude duvol des albatros. *C.R. Acad. Sci. Paris* **179**, 28–30.

Johansson, L. C., Wolf, M., von Busse, R., Winter, Y., Spedding, G. R. and Hedenström, A. (2008) The near and far wake of Pallas' long tongued bat (*Glossophaga soricina*). *J. Exp. Biol.* **211**, 2909-2918.

Lentink, D., Müller, U.K., Stamhuis, E.J., Kat, R., Gestel, W. Van, Veldhuis, L. L. M., Henningsson, P., Hedenström, A., Videler, J.J. & Leeuwen, J.L van. 2007 How swifts control their glide performance with morphing wings. *Nature* **446**, 1082-1085.

Milne-Thompson, L.M. (1966). *Theoretical Aerodynamics.* New York: Dover.

Parrott, C. G. (1970). Aerodynamics of gliding flight of a black vulture *Coragyps atratus. J. Exp. Biol.* **53**, 363–374.

Pennycuick, C. J. (1960). Gliding flight of the fulmar petrel. *J. exp. Biol.* **37**, 330-8.

Pennycuick, C. J. (1968). A wind-tunnel study of gliding flight in the pigeon *Columba livia. J. Exp. Biol.* **49**, 509-26.

Pennycuick, C. J. (1971a). Soaring behaviour and performance of some east African birds, observed from a motor-glider. *Ibis* **114**, 178–218.

Pennycuick, C. J. (1971b). Gliding flight of the white-backed vulture *Gyps africanus. J.*

Exp. Biol. **55**, 13–38.

Pennycuick, C. J. (1975) *Mechanics of flight.* In: Avian Biology (ed. D. S. Farner and J. R. King), pp 1-75. Academic Press, New York

Pennycuick, C. J. (1982). The flight of petrels and albatrosses (Procellariiformes), observed in South Georgia and its vicinity. *Phil. Trans. R. Soc. Lond. B* **300**, 75–106.

Pennycuick, C. J. (1989). *Bird Flight Performance: A Practical Calculation Manual.* Oxford: Oxford University Press.

Pennycuick, C.J. (2008) *Modelling the Flying Bird.* Elsevier.

Pennycuick, C.J, Obrecht, H. H. and Fuller, M. R. (1988) Empirical estimates of body drag of large waterfowl and raptors. *J. Exp. Biol.*, **135**, 253-264.

Pennycuick, C. J., Alerstam, T. and Hedenström, A. (1997). A new low-turbulence wind tunnel for bird flight experiments at Lund University, Sweden. *J. Exp. Biol.* **200**, 1441–1449.

Rosén, M. and Hedenström, A. (2001) Gliding flight in a jackdaw: a wind tunnel study. *J. Exp. Biol.* **204**, 1153-1166.

Rosén, M. and Hedenström, A. (2002) Soaring flight in the eleonora's falcon (*Falco Eleonorae*).*The Auk*, **119**, 835-840.

Rosén M., Spedding, G. R. and Hedenström, A. (2007). Wake structure and wingbeat kinematics of a house-martin *Delichon urbica. J. R. Soc. Interface*, 10.1098/rsif.2007.0215.

Spaar, R. and Bruderer, B. (1996) Soaring migration of steppe eagles *Aquila nepalensis* in southern Israel: flight behaviour under various wing and thermal conditions, *J. Avian Biol.*, **8**, 288-297.

Spaar, R. and Bruderer, B. (1997) Optimal flight behavior of soaring migrants: a case study of migrating steppe buzzards, *Buteo buteo vulpinus. Behav. Ecol.*, **8**, 288-297.

Spedding, G. R. (1987). The wake of a kestrel *Falco tinnunculus* in gliding flight. *J. Exp. Biol.* **127**, 45–57.

Spedding, G. R., Rosén, M. & Hedenström, A. (2003). A family of vortex wakes generated by a thrush nightingale in free flight in a wind tunnel over its entire natural range of flight speeds. *J. Exp. Biol.* **206**, 2313–2344.

Spedding, G. R., Hedenström, A. and Johansson, L. C. (2009) A note on wind-tunnel turbulence measurements with DPIV. *Exp. Fluids.* **46**, 527-537.

Tucker, V. A. (1973) Body drag, feather drag and interference drag of the mounting strut in a peregrine falcon, *Falco peregrinus. J. Exp. Biol.* **149**, 449-468.

Tucker, V. A. (1987). Gliding birds: the effect of variable wingspan. *J. Exp. Biol.* **133**, 33–58.

Tucker, V. A. (1988). Gliding birds: descending flight of the whitebacked vulture, *Gyps africanus. J. Exp. Biol.* **140**, 325–344.

Tucker, V. A. and Parrot, G. C. (1970). Aerodynamics of gliding flight in a falcon and other birds. *J. Exp. Biol.* **52**, 345–367.

Tucker, V. A. and Heine, C. (1990). Aerodynamics of gliding flight in a Harris' hawk, *Parabuteo unicinctus. J. Exp. Biol.* **149**, 469–489.

Tucker, V. A., Cade, T. J. and Tucker, A. E. (1998). Diving speeds and angles of a gyrfalcon (*Falco rusticolus*). *J. Exp. Biol.* **201**, 2061–2070.

Withers, P. C. (1981). The aerodynamic performance of the wing in red-shouldered hawk *Buteo linearis* and a possible aeroelastic role of

wing-tip slots. *Ibis* **123**, 239–247.

IV

Flight speeds of swifts (*Apus apus*): seasonal differences smaller than expected

P. Henningsson[1,*], H. Karlsson[2], J. Bäckman[2], T. Alerstam[2] and A. Hedenström[1]

[1]*Department of Theoretical Ecology, and* [2]*Department of Animal Ecology, Lund University, 223 62 Lund, Sweden*

We have studied the nocturnal flight behaviour of the common swift (*Apus apus* L.), by the use of a tracking radar. Birds were tracked from Lund University in southern Sweden during spring migration, summer roosting flights and autumn migration. Flight speeds were compared with predictions from flight mechanical and optimal migration theories. During spring, flight speeds were predicted to be higher than during both summer and autumn due to time restriction. In such cases, birds fly at a flight speed that maximizes the overall speed of migration. For summer roosting flights, speeds were predicted to be lower than during both spring and autumn since the predicted flight speed is the minimum power speed that involves the lowest energy consumption per unit time. During autumn, we expected flight speeds to be higher than during summer but lower than during spring since the expected flight speed is the maximum range speed, which involves the lowest energy consumption per unit distance. Flight speeds during spring were indeed higher than during both summer and autumn, which indicates time-selected spring migration. Speeds during autumn migration were very similar to those recorded during summer roosting flights. The general result shows that swifts change their flight speed between different flight behaviours to a smaller extent than expected. Furthermore, the difference between flight speeds during migration and roosting among swifts was found to be less pronounced than previously recorded.

Keywords: common swift; *Apus apus*; migration; roosting flight; flight behaviour; radar tracking

1. INTRODUCTION

Flight mechanical theory has been recognized as a framework for understanding optimal flight speeds among migratory birds. Most central is the so-called power curve, describing the relationship between mechanical power and flight speed of the bird (Pennycuick 1968). From the power curve, three characteristic flight speeds can be derived and two of these have been proposed to be the most ecologically relevant in the migratory behaviour of birds. The exact flight speeds and the shape of the curve are often difficult to asses because many parameters are difficult to estimate (e.g. Alerstam 2003; Hedenström 2008). However, this is often not the most important issue if the relationship between flight speeds in different ecological situations can be determined. The three speeds are the minimum power speed (V_{mp}), the maximum range speed (V_{mr}) and the flight speed associated with time minimization (V_{mt}; Alerstam & Lindström 1990; Alerstam 1991; Hedenström & Alerstam 1995), respectively. Theoretically, V_{mr} will be intermediate of V_{mp} and V_{mt} (e.g. Alerstam & Hedenström 1998; figure 1). V_{mp} is the relevant flight speed if the aim is to minimize the energy consumption per unit time, i.e. staying aloft for as long as possible on a given amount of fuel. If the aim is instead to minimize the energy consumption per unit distance, the appropriate flight speed is V_{mr}, which maximizes the distance covered on a given amount of fuel. V_{mt} is

expected in time-selected migration, likely to arise when there is something to gain from being first to occupy high-quality territories (e.g. Kokko 1999), or when matching temporally narrow peaks in food abundance is of crucial importance.

From the theory, it can also be predicted that birds adopting energy- or time-optimizing strategies should adjust their flight speed so that they increase their airspeed in headwind and reduce it in tailwind (e.g. Tucker & Schmidt-Koenig 1971; Pennycuick 1978). Liechti *et al.* (1994) showed that this also applies to the strength of a side wind component, with optimal airspeeds increasing with increasing side wind, provided that the birds maintain a constant track over ground.

To test whether birds adjust airspeed in accordance with predictions, we studied the nocturnal flight behaviour of common swifts (*Apus apus* L.) using tracking radar during spring, summer and autumn. The swift is a suitable candidate for exhibiting all of the three characteristic flight speeds. During spring migration, flight speeds are expected to be higher (closer to V_{mt}) than during autumn migration if the birds are time selected during spring. Swifts experience competition at the breeding areas both regarding available nest sites and mates (e.g. Lack 1956). A late arrival involves both the risk of not finding a nest and not finding a mate. During autumn migration, flight speeds closer to V_{mr} would be expected since the time restriction probably is less pronounced. During summer roosting flights (Weitnauer 1952, 1980; Lack 1956; Bruderer & Weitnauer 1972; Snow & Perrins 1998; Bäckman & Alerstam 2001, 2002; Tarburton & Kaiser 2001), the airspeed is predicted to be lower (V_{mp}) than
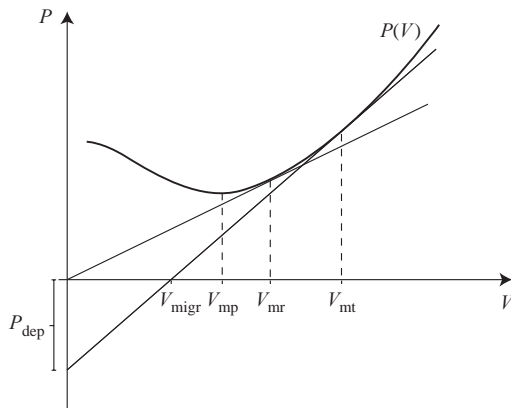
Figure 1. A conceptual power curve. It is costly to fly slowly as well as fast. In between, the curve has its minimum that corresponds to the minimum power speed (V_{mp}). If a tangent is drawn from the origin to the curve, the maximum range speed (V_{mr}) is obtained. If the fuel deposition rate (P_{dep}) for a bird at stopover sites along the migratory journey is taken into account, the optimal speed is the time minimizing speed (V_{mt}). In this case, the *y*-axis is extended downwards to include the fuel-deposition rate. V_{mt} is found by drawing a tangent from the point of the current deposition rate to the power curve. The intercept between the tangent and the *x*-axis corresponds to the overall speed of migration (V_{migr}).

during both spring and autumn migrations since the expected aim for the birds is to minimize energy spent per unit time during this behaviour.

2. MATERIAL AND METHODS

(a) *Study species*
The common swift is renowned for its extremely aerial life style. From the moment the young swift leaves the nest, it sets out on a very long journey. It will spend almost its entire lifetime in the air, day and night. The only time swifts land for a considerable time period is during breeding, although juvenile swifts are known to roost in trees on rare occasions during extreme weather (Holmgren 2004). They forage on the wing, collect nest materials on the wing, sleep on the wing and perform yearly migrations between Europe and Africa. At night, the swifts generally roost on the wing apart from during breeding (Weitnauer 1952, 1980; Lack 1956; Bruderer & Weitnauer 1972; Snow & Perrins 1998; Bäckman & Alerstam 2001, 2002; Tarburton & Kaiser 2001). In the late evening, around sunset, swifts ascend to altitudes of 1–2 km orienting themselves into headwinds during roosting in order to minimize displacement (Bäckman & Alerstam 2001).

(b) *The tracking radar*
The radar used for this study is an automatic tracking radar (X-band, 200 kW peak power, 0.25 ms pulse duration, 504 Hz pulse repeat frequency and 1.5° pencil beam width). It is situated at the roof of the Ecology Building (55°42′ N, 13°12′ E, 91.5 m above sea level) at Lund University, Sweden. The radar tracking data were recorded by a computer with custom-built software that records positions every 2nd second (analysis of the effect of sampling rate on airspeed estimates, see the electronic supplementary material). The radar echo signal can be sampled for an arbitrary duration and from this wing-beat frequency is

presented to the operator in real time, which makes the identification of the target being tracked relatively easy. The wing-beat frequency is derived using discrete Fourier transform analysis of echo peak amplitudes and data are stored both as the complete signal measurement as well as the calculated frequency estimates.

(c) *Data acquisition and processing*
(i) *Bird trackings*
Radar operation was performed during night time, between 23.00 and 05.00 (UTC 21.00–03.00 local time). All nights without rain clouds (which cause great disturbance to the radar signal) were chosen for operation. Data on roosting flight were collected during 1999 and 2007, and spring and autumn migration data were collected during 2006–2007. The sky was systematically searched between 5 and 35° in elevation and at approximately 2–10 km distance from the radar. Only strong and easily distinguished echoes judged to be single swifts were used for tracking. The same cues as used in Bäckman & Alerstam (2001) were used to identify swifts and distinguish them from other birds. (i) Swifts have lower wing-beat frequency (approx. 7–9 Hz) than most other birds encountered. (ii) The echo signature is characteristic, with distinct flapping and resting phases. (iii) Signal strength often changes abruptly as the swift banks during gliding bouts (Bruderer & Weitnauer 1972). Each bird was tracked during approximately 60 s during spring and autumn migrations and between 1 and 20 min during the summer roosting flights (longer tracking periods were possible for roosting birds because of their behaviour of orienting into the wind). The radar was normally operated with automatic tracking of azimuth, elevation and range, but range was sometimes tracked manually when the signal was weak. To avoid repeated measurement of the same individual, the direction of the radar antenna was changed drastically after the end of each tracking.

After acquisition, data were processed in three steps. First, each tracking was critically examined with custom-built software plotting azimuth, elevation and range separately. Obviously erroneous points in either of these were deleted and substituted by linear interpolation. Trackings with too much noise (due to rain clouds or interfering echoes) were also excluded. Second, means over 10 s intervals were calculated for each tracking to reduce noise (analysis of the effect of the length of these intervals on airspeed estimates, see the electronic supplementary material). Third, mean of these intervals was calculated to produce an estimate of the overall speed and direction for each tracking. Trackings with mean airspeeds lower than 5 m s^{-1} or higher than 25 m s^{-1} were considered erroneous and excluded (spring 1.7% out of total number of trackings, summer 1.6% and autumn 0.7%).

The radar echo signals were sampled and from these, the proportion of flapping and gliding phases (hereafter referred to as flap proportion) was calculated using a custom-written MATLAB program that uses threshold values of signal intensity to detect when the bird was flapping its wings and when it was gliding.

(ii) *Wind measurements*
To measure the wind, helium balloons carrying reflectors were released from the roof of the building and tracked from the lowest possible altitude (approx. 300–500 m) up to approximately 2500 m altitude. Simultaneously, wind speed and direction at the top of the building were measured using
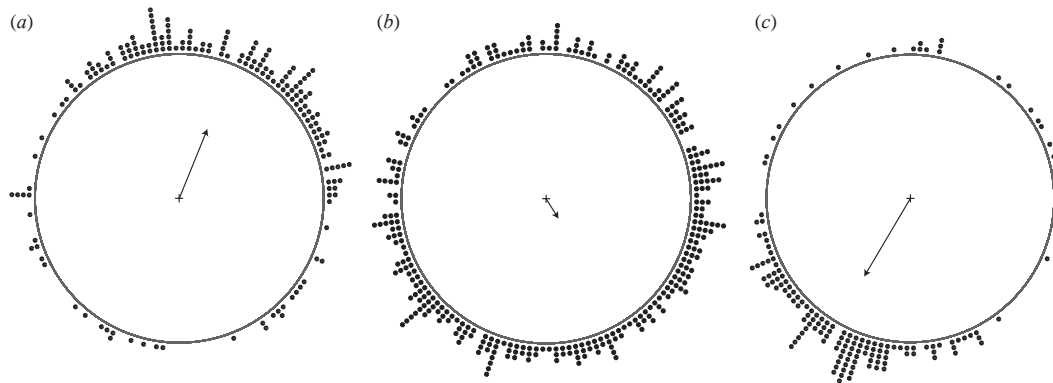
Figure 2. Track directions for the complete dataset with mean vector. Each of the stacked dots represents a tracking and each stack corresponds to the group of trackings within 2.5° intervals (in total 144 groups, 36 for each quadrant). The central vector in each subfigure corresponds to the mean vector, where length of the vector corresponds to the 'directional strength'. (*a*) spring, (*b*) summer and (*c*) autumn.

a stationary anemometer. All recorded bird trackings were within a period of maximum 2 hours before or after a wind measurement.

Each wind tracking was post-processed in three steps. First, as with bird trackings, each file was examined and erroneous points deleted. Second, means over 30 s intervals were calculated for each tracking. Third, each averaged wind tracking was used to create a complete wind profile from the ground up to maximum altitude of each tracking with a resolution of 1 m. This was done by interpolating between the interval means. This complete wind profile was used to calculate air speed and heading of each bird tracking using wind data for the exact altitude on which the bird was flying. In order to quantify the change in wind over time, we compared the difference in calculated wind speed and wind direction between the wind profile closest in time to the tracking (the one used in the real calculation) with that calculated using the subsequent wind profile. The average difference was 2.0 m s^{-1} in speed and 12.8° in direction.

(iii) Equivalent air speed
In order to make it possible to compare flight speeds between different trackings, airspeed was normalized by flight altitude to produce equivalent air speed (V_{eq}). V_{eq} corresponds to the air speed that represents the same dynamic pressure at sea level as the air speed at the bird's flight altitude. V_{eq} was calculated according to the description in the electronic supplementary material.

(d) Statistical analysis
A statistical model of the complete dataset including all three seasons; spring, summer and autumn, was derived using SPSS v. 15.0 (SPSS Inc., Chicago, IL, USA). This general linear model had V_{eq} as the dependent variable, season as fixed factor and side wind component (V_s), tailwind/head-wind component (V_t) and vertical speed (V_z) as covariates. These are all variables that are expected to influence V_{eq}. V_s was calculated as the perpendicular velocity component from the recorded wind with respect to the heading direction of the bird. V_t was calculated as the velocity component from the wind parallel to the heading direction of the bird. V_{eq} was shown by Shapiro–Wilk test to be non-normally distributed in the spring and summer data ($p < 0.001$; $p < 0.001$), and

therefore the complete dataset was log transformed prior to the statistical test. After this operation, spring and autumn data were normally distributed ($p = 0.59$; $p = 0.12$), but summer data were not ($p < 0.001$). We found the comparison between spring and autumn to be the most crucial and chose to perform analysis on the log-transformed data. The effect of season on V_{eq} was analysed by examining the residuals when season was excluded from the model. Levene's test for equality of variance was performed on the residuals, which showed that the variance was significantly different between the three subsets. One-way ANOVA with *post hoc* test Tamhane (designed for unequal variances) was performed on the residuals to test the difference in V_{eq} between the three seasons.

3. RESULTS
This study is based on a total of 637 trackings, of which 176 are from spring migration (May), 311 from summer roosting flights (July) and 150 from autumn migration (August). Mean directions of tracks during the three seasons are presented in figure 2, and mean values and standard deviation for variables are presented in table 1. Mean V_{eq} during spring was 10.6 m s^{-1}, during summer 9.0 m s^{-1} and during autumn 9.2 m s^{-1}. Ground speed during spring was 11.5 m s^{-1}, during summer 6.4 and 8.8 m s^{-1} during autumn. Mean vertical speed in all three cases was close to zero. Flap proportion of birds during spring was 55 per cent, during summer 66 per cent and during autumn 62 per cent. Mean track direction during spring was towards NNE (22.1°; table 1) and during autumn towards SSW (210.6°; table 1), which is expected for birds entering and leaving Sweden at the southwest corner of the country. The spring and autumn data show relatively strong mean vectors ($r = 0.51$ and 0.63, respectively; table 1), implying low scatter, with a slightly higher scatter during spring compared with autumn. Rayleigh's test gave $p < 0.001$, $Z = 46.6$ and $p < 0.001$, $Z = 58.7$ for spring and autumn, respectively. During summer roosting flights, the track directions were highly scattered ($r = 0.17$), while the mean vector was still significant according to Rayleigh's test ($p < 0.001$, $Z = 8.8$) due to large sample size.

Table 1. Mean values and mean directions with standard deviation for the complete dataset. (Rows with track, heading and wind show *r*-values whereas remaining rows show s.d.)

	spring ($N=176$)		summer ($N=311$)		autumn ($N=150$)	
variable	mean	s.d./*r*-value	mean	s.d./*r*-value	mean	s.d./*r*-value
ground speed (m s^{-1})	11.5	7.0	6.4	3.9	8.8	4.9
equivalent air speed (m s^{-1})	10.6	3.9	9.0	2.1	9.2	1.5
vertical speed (m s^{-1})	0.04	0.4	0.00	0.5	0.07	0.5
altitude (m)	980	345	1335	610	1374	474
track (°)	22	0.51	149	0.17	211	0.63
heading (°)	334	0.56	237	0.53	178	0.66
wind (°)[a]	271	0.54	246	0.43	110	0.25
wind speed (m s^{-1})	9.4	4.6	8.9	4.6	7.6	2.8

[a] Wind refers to the direction from where the wind is coming.

Table 2. (*a*) The statistical model of the complete dataset containing all three seasons. Dependent variable is V_{eq}. ** indicate significance to the level of $p<0.01$. $R^2=0.105$ (Adj. $R^2=0.098$). (*b*) Parameter estimates of the complete model using log-transformed V_{eq}. Season 1, 2 and 3 corresponds to spring, summer and autumn, respectively.

(*a*) parameter	d.f.	S.S.	F	*p*-value
season	2	0.388	21.713	0.000**
vertical speed	1	0.001	0.102	0.750
side wind	1	0.131	14.669	0.000**
tailwind	1	0.082	9.177	0.003**
error	631	5.638		

			95% confidence interval	
(*b*) parameter	B	s.e.	lower bound	upper bound
(season=1)	0.049	0.011	0.028	0.070
(season=2)	−0.013	0.010	−0.032	0.007
(season=3)	0.932	0.009	0.913	0.950
vertical speed (V_z)	0.003	0.008	−0.014	0.019
side wind (V_s)	0.004	0.001	0.002	0.006
tailwind (V_t)	−0.002	0.001	−0.003	−0.001

(a) *Statistical model*

The model that was constructed for analysing the variation in V_{eq} between the three seasons and description of each parameter is presented in table 2. The model includes four parameters expected to influence V_{eq} based on theory: V_z, V_s, V_t and season. Season had a highly significant effect on V_{eq} ($p<0.001$), while V_z did not influence V_{eq} significantly ($p=0.750$). Both wind components (V_s and V_t) were significant factors ($p<0.001$ and $p<0.005$, respectively). The effect of V_s was to increase V_{eq} while the effect of V_t was to decrease V_{eq}.

(b) *Effect of season on flight speed*

There was a significant difference in V_{eq} between spring and summer ($p<0.001$) and spring and autumn ($p<0.001$), but not between summer and autumn ($p=0.777$; figure 3). The mean flight speed during spring migration (10.6 m s^{-1}) was higher than during autumn migration (9.1 m s^{-1}), and it was the lowest during the summer roosting flights (9.0 m s^{-1}). The standard deviation in V_{eq} during spring

(s.d. $=3.04$ m s^{-1}) was also higher than during autumn (s.d. $=1.50$ m s^{-1}), while during summer it was intermediate (s.d. $=2.14$ m s^{-1}). Shapiro–Wilk test of normality shows that the spring and summer data deviate from normality ($p<0.001$; $p<0.001$). For the spring data, this is due to a tail of high-speed flyers that skews the distribution towards the right (figure 4*a*). In summer, a similar pattern as during spring was found, but there were fewer high-speed flyers than in spring (figure 4*b*).

4. DISCUSSION

(a) *Speed differences among seasons*

The main focus of this study was the difference in flight speeds during three different phases of the life of birds: spring migration, autumn migration and the special case of summer roosting flight among swifts. The choice of the swift as study species was because it was possible to reliably identify to species based on the very characteristic echo signature. The swift is expected to fly at a lower speed during roosting flight than during migration. Furthermore, the swift is predicted to fly at a higher speed during spring migration than during autumn migration, if it is of importance to arrive early at the breeding site in spring.

The prediction that swifts fly at a higher speed during migration than during roosting was supported by our observation when comparing summer and spring, but not when comparing summer and autumn.

The prediction that swifts fly faster during spring migration compared with autumn migration was in agreement with the results.

Bruderer & Weitnauer (1972) studied the spring migration and summer roosting flights of swifts. In that study, the mean air speed was found to be 11.1 m s^{-1} during migration and 6.4 m s^{-1} during summer roosting flights, a finding that has been generally quoted in support of adaptive speed adjustment according to flight mechanical theory. In this study, we find a less pronounced difference in flight speed between spring and summer. The difference in results between the two studies can, at least partly, be attributed to a difference in methodology; (i) spring migration was studied during night in this study and during day by Bruderer and Weitnauer, (ii) positions were logged every second in this study compared with every 20th second in the study by Bruderer and Weitnauer. Mean flight speeds during spring in the two studies are similar (10.6 compared to 11.1), suggesting
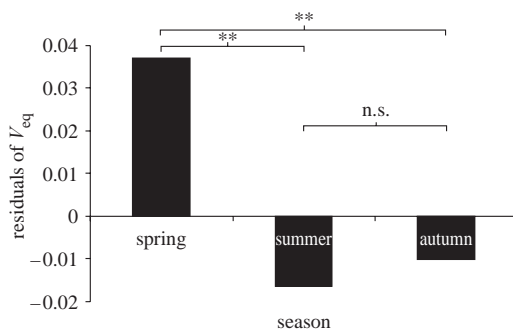
Figure 3. Residuals of log-transformed V_{eq} when season was excluded from the model. [**] indicates significant difference ($p < 0.001$). This was found by performing one-way ANOVA with Tamhane *post hoc* test on the residuals of V_{eq} between seasons when excluding season from the model.
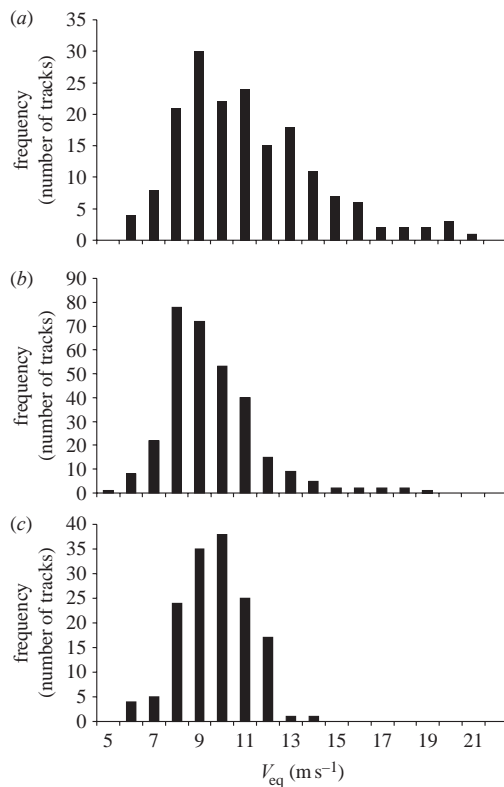

Figure 4. Distribution of V_{eq} during (*a*) spring, (*b*) summer and (*c*) autumn.

that flight speeds are similar between night and day. During roosting flight, the birds typically fly along a very irregular path at very low ground speed, constantly orienting themselves towards the wind (Bäckman & Alerstam 2002). This circuitous track in combination with a lower position recording rate may have resulted in an underestimate of the length of the true flight path and thereby also the actual flight speed (Bruderer & Weitnauer 1972). On migration, the flight path is straight and the

speed estimate is therefore accurately estimated also by recording one position every 20th second. The effect of sampling rate on speed estimates of summer roosting birds has been investigated and is presented in the electronic supplementary material.

Another example of adaptive speed adjustments in birds is the skylark that has been found to adjust flight speed when comparing display flight (V_{mp}) and migration ($\geq V_{mr}$; Hedenström & Alerstam 1996).

(b) Time-selected migration and sprint migration

The prediction that swifts during spring migration have a higher flight speed than during autumn migration states that this is due to time selection in spring, meaning that birds arriving earlier to the breeding area should have a better chance of finding a mate and a nest and therefore also have higher breeding success (e.g. Kokko 1999). This advantage could introduce a tendency towards increased flight speeds in order to perform a faster migration to breeding area (flying at V_{mt}).

Between spring and autumn, the variance in V_{eq} was different. During spring, the variance of V_{eq} was much larger (by a factor of almost four) than during autumn. This larger variance appears to be mostly due to a 'tail' of high-speed flyers in spring (figure 4*a*). This subgroup was examined more closely by taking a subsample of the spring data containing all birds flying at $V_{eq} \geq 13$ m s^{-1} (19% of the spring tracks). The group showed no abnormalities in V_z, V_s, V_t or altitude, implying that these individuals were not flying under any special wind situations or performed steep dives. Swifts are known to be able to fly at high speeds; records of up to 28 m s^{-1} exist (Oehme 1968; Bruderer & Weitnauer 1972). We can only speculate about the reason for the fast flying individuals in the spring data: it can be heavier individuals that fly faster; it can be strong individuals that simply have the opportunity to fly faster; or it can be individuals that are close to their goal and can afford a sprint towards the final destination (Alerstam 2006). Also, the individuals during spring potentially consist of two groups, breeders and non-breeders, as swifts migrate to breeding areas also during the years before reaching sexual maturity. These non-breeders reside in proximity to breeding colonies searching for potential mates and nest sites (e.g. Lack 1956; Tarburton & Kaiser 2001), and may not be under such strong time restriction and therefore fly at lower speeds (V_{mr}) than individuals that are migrating to breed. If this is the case, the flight speed of the adult breeding swifts during spring migration may be underestimated by the population mean.

(c) Migration strategy

The prediction that flight speeds are higher in time-selected spring migration (V_{mt}) was developed based on the assumption that the birds perform stopovers to forage (Alerstam & Lindström 1990; Hedenström & Alerstam 1995). During these stopovers, the birds will have a certain net food intake rate that will determine the optimal flight speed towards the next stopover site in order to minimize time spent on migration. One could argue that the swifts are atypical in that respect, because they fly continuously and may potentially also forage on migration without doing regular stopovers. This strategy has been shown to occur among birds that have the

possibility to forage on migration without making stopovers (e.g. Strandberg & Alerstam 2007). If this is the case, the optimal flight speed would depend on other factors, such as the benefit of offsetting energy consumption during migration flight and the cost of reduced effective travel speed (Alerstam *et al.* 1993; Hedenström & Alerstam 1995; Strandberg & Alerstam 2007) and would consequently be unknown from the basis of the current data. It may well be that a fly-and-forage behaviour is used by swifts, but in that case it would be most likely to occur during diurnal flights. We studied the nocturnal flights and during night it is unlikely that the birds forage. Bruderer & Weitnauer (1972) found that diurnal spring migrating swifts had an airspeed of $11.1 \, \mathrm{m \, s^{-1}}$, which is similar to that of nocturnal spring migration in this study ($10.6 \, \mathrm{m \, s^{-1}}$). This suggests that there is no major difference between diurnal and nocturnal migratory flight speeds.

During autumn migration, we predicted that the optimal flight speed would be V_{mr}, while on roosting flights, the predicted optimal flight speed was V_{mp} (i.e. lower than during autumn), but the results show that there was no significant difference between summer and autumn flight speeds. Again, as with spring migration, one could propose that the swift perform a fly-and-forage strategy during autumn migration, but as during spring, this is likely to occur during diurnal flight only, and would not affect the flight speeds we investigate in this study. There are indications that swifts do not perform fly-and-forage migration during daytime either. Hedenström & Alerstam (1998) presented an estimate of the speed of migration of $150 \, \mathrm{km \, d^{-1}}$ or $1.7 \, \mathrm{m \, s^{-1}}$ for swifts. The mean ground speed during autumn migration in this study was $8.8 \, \mathrm{m \, s^{-1}}$ or $32 \, \mathrm{km \, h^{-1}}$. This means that, in order to advance $150 \, \mathrm{km \, d^{-1}}$, the birds need to fly for $4.7 \, \mathrm{h \, d^{-1}}$, which is easily covered during the nocturnal flight hours and would then mean that the advancement on migration during daytime is small. A simple check of the time budget thus suggests that the swifts do not perform fly-and-forage migration during autumn, but rather feed during daytime with little progress and consequently are expected to fly at V_{mr} during night.

(d) Specialized flight performance in the swift?

If swifts perform stopovers, it would be unlike most other birds that actually interrupt their flight for foraging. Swifts fly while foraging and would possibly have a higher cost compared with a passerine foraging in a forest patch. In that case the net intake rate is lower for the swift than for the passerine. As an example, the fuel deposition rate for the barn swallow (*Hirundo rustica*), which is also an aerial forager, has been found to be relatively low (Lindström 2003). On the other hand, a study of the flapping flight aerodynamics of a swift in a wind tunnel showed that the aerodynamic efficiency (meaning effective L : D) of the swift is higher than any other bird studied so far (Henningsson *et al.* 2008). This would imply that the power required to fly would hypothetically fall below that of a similarly sized passerine, if energetic efficiency is inferred from the aerodynamic efficiency, even though the conversion factor (output work/input work) is unknown. A conceptual comparison is presented in figure 5. With more efficient flight (lower over all mechanical power), the difference between V_{mp} and V_{mr} is decreased.
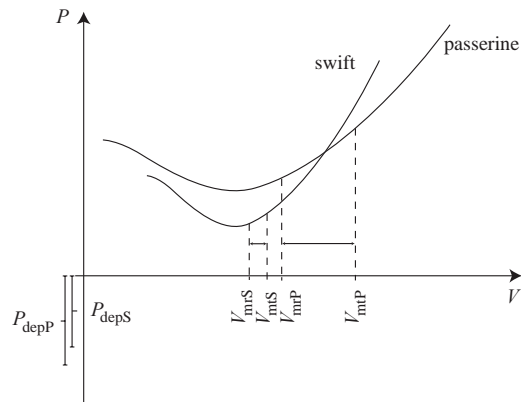
Figure 5. A conceptual comparison between swift and passerine power curves. If the overall power of flight and the net intake rate during stopover for the swift is lower than for the passerine, the same pattern as seen in this study emerges; the difference between V_{mt}, V_{mr} and V_{mp} is smaller for the lower curve than for the upper curve. 'S' and 'P' in the subscript denote 'swift' and 'passerine', respectively.

Furthermore, one could speculate that swifts are optimized for flight at a certain flight speed (Lentink *et al.* 2007; Henningsson *et al.* 2008), although Oehme (1968) showed that they are capable of flying at higher speeds than found in this study. This would follow the reasoning by Thomas & Hedenström (1998), where they discuss how this would affect the shape of the power curve and the characteristic flight speeds. If a bird is specialized in flying at a certain speed, performance would decrease rapidly if operating away from the optimum, i.e. the power curve would rise more steeply both below and above this desired flight speed. As a consequence, V_{mp}, V_{mr} and V_{mt} would then be close to each other (figure 5) and difficult to distinguish by observations. This may possibly be part of the explanation to the small difference between summer and autumn flight speeds that was found in this study. A similar pattern was found in a wind tunnel study of the aerodynamic gliding performance of swift wings. The speed involving the highest maximum duration (the gliding flight equivalence to V_{mp} in flapping flight) and the speed resulting in the highest maximum glide ratio (the gliding flight equivalence to V_{mr} in flapping flight) were found to be similar; 7.7 and $8.1 \, \mathrm{m \, s^{-1}}$, respectively (Lentink *et al.* 2007). Pure gliding flight is not directly comparable with the flap-gliding flight that the swifts perform during typical flight, but the fact that the swifts in this study were shown to glide for approximately 40 per cent of the flight time justifies such a comparison. Observed flight speeds were approximately $9 \, \mathrm{m \, s^{-1}}$ during summer roosting flights and autumn migration and $10.6 \, \mathrm{m \, s^{-1}}$ during spring migration, which show that even during gliding bouts, the speed would be close to the aerodynamic glide optimum (Lentink *et al.* 2007). It is even possible that the birds adjust their speed slightly during both gliding and flapping phases to avoid constant acceleration/deceleration or ascent/descent, resulting in a mean flight speed that is a compromise between the optimal flapping speed and the optimal gliding speed.

The possibility that the shape of the power curve differs between more or less efficient flyers and between species with different flight modes (cf. Tobalske *et al*. 2003; Alerstam *et al*. 2007) in ways that may restrict or widen the difference between significant flight speeds represents a fascinating subject for further research.

REFERENCES

Alerstam, T. 1991 Bird flight and optimal migration. *Trends Ecol. Evol.* **6**, 210–215. (doi:10.1016/0169-5347(91)90024-R)

Alerstam, T. 2003 Bird migration speed. In *Avian migration* (eds P. Berthold, E. Gwinner & E. Sonnenschein), pp. 253–267. Heidelberg, Germany: Springer.

Alerstam, T. 2006 Strategies for the transition to breeding in time-selected migration. *Ardea* **94**, 347–357.

Alerstam, T. & Hedenström, A. 1998 The development of bird migration theory. *J. Avian Biol.* **29**, 343–369. (doi:10.2307/3677155)

Alerstam, T. & Lindström, Å. 1990 Optimal bird migration: the relative importance of time, energy, and safety. In *Bird migration* (ed. E. Gwinner), pp. 331–351. Heiderlberg, Germany: Springer.

Alerstam, T., Gudmundsson, G. & Larsson, B. 1993 Flight tracks and speeds of Antarctic and Atlantic seabirds: radar and optical measurements. *Phil. Trans. R. Soc. Lond. B* **340**, 55–67. (doi:10.1098/rstb.1993.0048)

Alerstam, T., Rosén, M., Bäckman, J., Ericson, P. G. P. & Hellgren, O. 2007 Flight speeds among bird species: allometric and phylogenetic effects. *PLoS Biol.* **5**, 1656–1662. (doi:10.1371/journal.pbio.0050197)

Bäckman, J. & Alerstam, T. 2001 Confronting the winds: orientation and flight behaviour of the roosting swift, *Apus apus. Proc. R. Soc. Lond. B* **268**, 1081–1087. (doi:10.1098/rspb.2001.1622)

Bäckman, J. & Alerstam, T. 2002 Harmonic oscillatory orientation relative to the wind in nocturnal roosting flights of the swift *Apus apus. J. Exp. Biol.* **205**, 905–910.

Bruderer, B. & Weitnauer, E. 1972 Radarbeobachtungen über Zug und Nachtflüge des Mauerseglers (*Apus apus*). *Rev. Suisse Zool.* **79**, 1190–1200.

Hedenström, A. 2008 Adaptations to migration in birds: behavioural strategies, morphology and scaling effects. *Phil. Trans. R. Soc. B* **363**, 287–299. (doi:10.1098/rstb.2007.2140)

Hedenström, A. & Alerstam, T. 1995 Optimal flight speed of birds. *Phil. Trans. R. Soc. Lond. B* **348**, 471–487. (doi:10.1098/rstb.1995.0082)

Hedenström, A. & Alerstam, T. 1996 Skylark optimal flight speeds for flying nowhere and somewhere. *Behav. Ecol.* **7**, 121–126. (doi:10.1093/beheco/7.2.121)

Hedenström, A. & Alerstam, T. 1998 How fast can birds migrate? *J. Avian Biol.* **29**, 424–432. (doi:10.2307/3677161)

Henningsson, P., Spedding, G. R. & Hedenström, A. 2008 Vortex wake and flight kinematics of a swift in cruising flight in a wind tunnel. *J. Exp. Biol.* **211**, 717–730. (doi:10.1242/jeb.012146)

Holmgren, J. 2004 Roosting in tree foliage by common swifts *Apus apus. Ibis* **146**, 404–416. (doi:10.1111/j.1474-919X.2004.00274.x)

Kokko, H. 1999 Competition for early arrival in migratory birds. *J. Anim. Ecol.* **68**, 940–950. (doi:10.1046/j.1365-2656.1999.00343.x)

Lack, D. 1956 *Swifts in a tower*. London, UK: Methuen.

Lentink, D. *et al*. 2007 How swifts control their glide performance with morphing wings. *Nature* **446**, 1082–1085. (doi:10.1038/nature05733)

Liechti, F., Hedenström, A. & Alerstam, T. 1994 Effect of sidewinds on optimal flight speed of birds. *J. Theor. Biol.* **170**, 219–225. (doi:10.1006/jtbi.1994.1181)

Lindström, Å. 2003 Fuel deposition rates in migrating birds: causes, constraints and consequences. In *Bird migration* (eds P. Berthold, E. Gwinner & E. Sonnenschein), pp. 307–320. Heidelberg, Germany: Springer.

Oehme, H. 1968 Der Flug des Mauersegler (*Apus apus*). *Biol. Zentralblatt* **87**, 287–311.

Pennycuick, C. J. 1968 Power requirements for horizontal flight in the pigeon *Columbia livia. J. Exp. Biol.* **49**, 527–555.

Pennycuick, C. J. 1978 Fifteen testable predictions about bird flight. *Oikos* **30**, 165–176. (doi:10.2307/3543476)

Snow, D. W. & Perrins, C. M. 1998 *The birds of the Western Palearctic, concise*. Oxford, UK: Oxford University Press.

Strandberg, R. & Alerstam, T. 2007 The strategy of fly-and-forage migration, illustrated for the osprey (*Pandion haliaetus*). *Behav. Ecol. Sociobiol.* **61**, 1865–1875. (doi:10.1007/s00265-007-0426-y)

Tarburton, M. K. & Kaiser, E. 2001 Do fledgling and pre-breeding common swifts *Apus apus* take part in aerial roosting? An answer from a radiotracking experiment. *Ibis* **143**, 255–263. (doi:10.1111/j.1474-919X.2001.tb04481.x)

Thomas, A. L. R. & Hedenström, A. 1998 The optimal flight speeds of flying animals. *J. Avian Biol.* **29**, 469–477. (doi:10.2307/3677166)

Tobalske, B. W., Hedrick, T. L., Dial, K. P. & Biewener, A. A. 2003 Comparative power curves in bird flight. *Nature* **421**, 363–366. (doi:10.1038/nature01284)

Tucker, V. A. & Schmidt-Koenig, K. 1971 Flight speeds of birds in relation to energetics and wind direction. *The Auk* **88**, 97–107.

Weitnauer, E. 1952 Uebernachtet der Mauersegler, *Apus apus* (L.), in der luft? *Orn. Beob.* **49**, 37–44.

Weitnauer, E. 1980 *Mein Vogel—Aus dem Leben des Mauersegler Apus apus*. Liestal, Switzerland: Basellandschaft licher Natur- und Vogelschutzverband.

SUPPLEMENTARY MATERIAL: Calculation of equivalent air speed (V_{eq})

Airspeed of each bird tracking was normalized by flight altitude to produce equivalent air speed (V_{eq}), following the method of Pennycuick (1989) according to

$$V_{eq} = V_a * \sqrt{\frac{\rho_T}{\rho_0}} \,,$$
(1)

where V_a is the true airspeed, ρ_T is the actual air density at the current flight altitude and ρ_0 is the standard air density at sea level, 1.226 kg/m^3. Actual air density (ρ_T) was estimated as

$$\rho_T = \rho_0 * \left(\frac{P_T}{P_0} \right),$$
(2)

assuming a temperature of 15° C, where P_T is the pressure at the flight altitude and P_0 is the standard atmospheric pressure, 1013.25 hPa. The pressure at the flight altitude (P_T) was estimated as

$$P_T = P_0 \left(1 - \left[\frac{0.0065 * h}{273 + T} \right] \right)^{4.256},$$
(3)

where h is the flight altitude of the bird and T is the temperature (here assumed to be 15° C; Pennycuick 1989).

References

Pennycuick, C. J. 1989 *Bird flight performance – A practical calculation manual*. Oxford University Press, Oxford, UK.

SUPPLEMENTARY MATERIAL: Analysis of effect on airspeed estimate by length of intervals for calculated means

1. OBJECTIVE

The average airspeed in the present study was calculated based on 10 second intervals. Means of these 10 second intervals were calculated and the final mean airspeed for each complete tracking was calculated as the mean of these 10 seconds interval means. The speed estimate will potentially be affected by the length of the intervals and therefore we investigated the magnitude of this effect.

2. ANALYSIS

To study the effect of the chosen length of the mean intervals on speed estimates we processed data using different length of these intervals: 4, 8, 12, 16, 20, 24, 28, 32 seconds. We performed the analysis on a sub sample of summer roosting birds (n=89), since these tracks were less straight than those of migrating birds which is when speed estimates are expected to be sensitive to sampling rate.

3. RESULT

The analysis shows that using longer intervals to calculate the means result in a larger difference in estimated airspeed compared with the shortest interval (Fig. 1). The change in difference is non-linear, with largest change among the shorter intervals. Shorter intervals will pick up more of the noise of the radar, while longer intervals will possibly be too coarse to satisfactorily represent the true flight path. The large change between eight and four second interval presumably reflects the influence of noise on the estimates. This analysis can only give us an indication of what the correct length is and we believe that the chosen interval of 10 seconds is appropriate, since it may be a balance between the risk of influence from noise and under sampling of the true flight path.
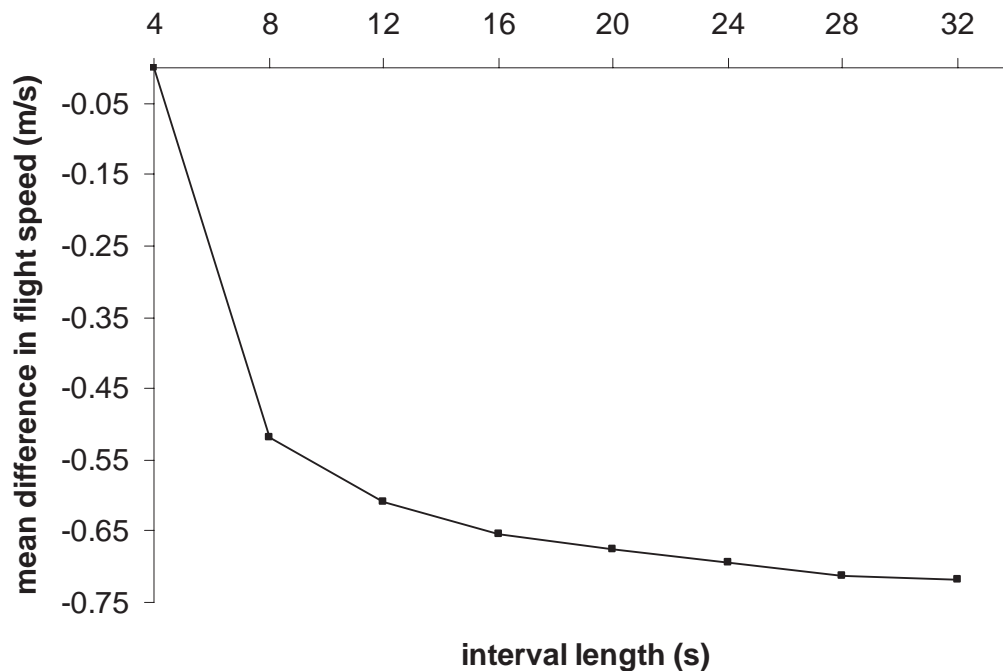

Figure 1. The average difference in speed estimate for different length of intervals for calculating means. Values show the difference compared with the four second interval.

SUPPLEMENTARY MATERIAL: Analysis of effect on speed estimate by sampling rate

1. OBJECTIVE

Speed estimates are likely to be affected by the sampling rate used during tracking. In the present study positions were recorded every 2nd second. We performed an analysis of the effect of sampling rate on speed estimate. Furthermore, we have treated a subset of roosting trackings according to Bruderer & Weitnauer (1972) to explicitly investigate the effect of the differences in method on speed estimates between that study and the present one.

2. ANALYSIS

To investigate the effect of sampling rate on the speed estimate we reduced the effective sampling rate of a subset of roosting trackings (n=17) stepwise to contain positions every 4th, 6th, 8th, 10th, 16th and 30th second. Each of these sets of files was then processed as the original full resolution files and the ground speeds of these were compared with the original result. To study the effect of difference in method between the present study and that by Bruderer & Weitnauer (1972) we used the files reduced to a sampling rate of every 30th second (the sampling rate used by Bruderer & Weitnauer (1972)) and calculated mean flight speed by averaging over the speeds between each of the points without any intermediate steps.

3. RESULT

The analysis shows that increasing the time between recorded positions (lowering the sampling rate) gives a speed underestimate. Figure 2 shows the mean difference in calculated ground speed for each sampling rate compared with the original full resolution files (containing positions every 2nd second). The replicated Bruderer & Weitnauer method showed that the difference in speed estimate against the full resolution files was on average - 0.15 m/s.
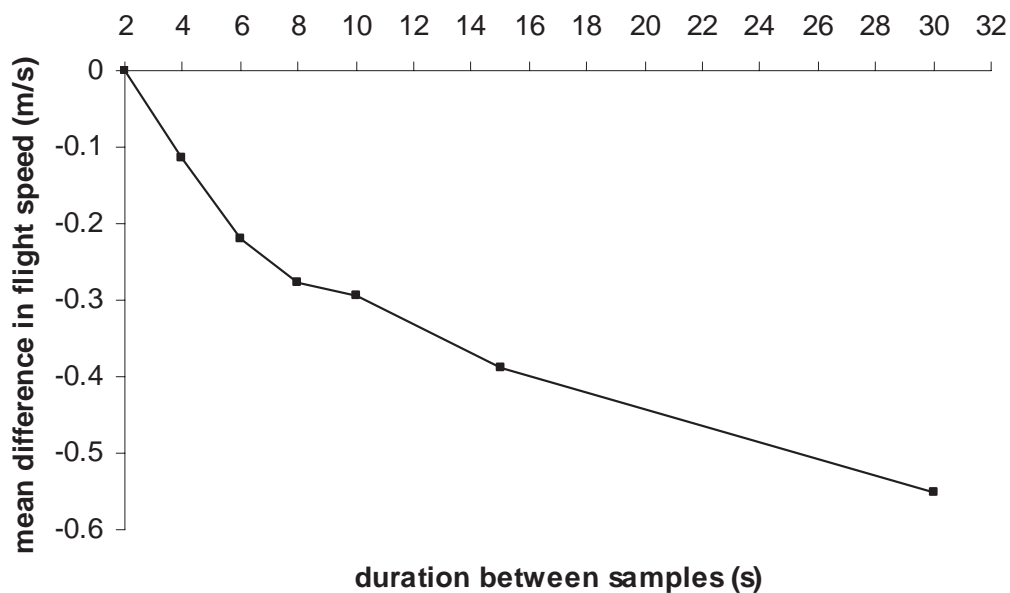

Figure 2. Mean difference in calculated speed for different sampling rate compared with the original full resolution file containing positions every 2nd second.

SUPPLEMENTARY MATERIAL: Display of wind directions for different wind speeds during the three seasons; spring, summer and autumn

Figure 4. Plots of wind directions of different wind speed intervals for the three seasons. Each of the stacked dots represents a tracking and each stack corresponds to the group of trackings within a 2.5 degree intervals. The central vector in each sub-figure corresponds to the mean vector, where length of the vector corresponds to the 'directional strength'. The direction is expressed as from where the wind is coming. In 5-10 m/s winds of summer and autumn the winds were found to be bimodal (r2-vector larger than r).

How swift are swifts *Apus apus*?

Per Henningsson, L. Christoffer Johansson and Anders Hedenström

Department of Theoretical Ecology, Ecology Building, Lund University, SE-223 62 Lund, Sweden

Swifts are renowned for their fast flight manner which has fascinated people in all times. However, previous studies of swifts in flight during migration and roosting flights have shown that the birds operate over a narrow range of flight speeds compared with most other birds studied. In this study we have focused on the special flight behavior often called 'screaming parties'. During these flights the birds appear to reach very high speeds and therefore we used a stereo high-speed camera setup to measure the flight speeds of the birds during this behavior with high accuracy. The birds were found to fly at much higher speeds during 'screaming parties' than during migration or roosting, on average twice as fast, 20.9 ms-1 ($\pm$ 5.1 ms^{-1}) in horizontal speed. The highest record was 31.1 ms^{-1} which is the highest measured yet for a swift in self powered flight. Furthermore, the birds were performing steep climbing flights, on average 4.0 ms^{-1} ($\pm$ 2.8 ms^{-1}) in vertical velocity. A clear trade-off between horizontal speed and vertical speed was found, suggesting that the birds are operating at their maximum.

Introduction

Swifts are considered as fast flyers and as an example, the white-throated needletail *Hirundapus caudacutus* has been reported as possibly the fastest bird in the world in flapping self-powered flight reaching speeds up to 47 ms^{-1} (del Hoyo et al. 1999), although details on the method used in the study is not available. Studies of speeds of stooping falcons report even higher speeds of above 50 ms^{-1} (Peter and Kestenholz 1998, Tucker et al. 1998), but this flight converts potential energy into aerodynamic work. Alerstam et al (2006; supplementary material) presented a compiled record of flight speeds of continuous flapping flight in 138 species of birds and among the fastest were the common pochard *Aythya ferina*, long-tailed

duck *Clangula hyemalis* and common scooter *Melanitta nigra* flying at 22-24 ms^{-1}.

All swifts in the family Apodidae (which includes the needletails) have long and slender wings with a short arm section and a long hand section. Measurements of lift and drag force on wings of common swifts *Apus apus* (hereafter referred to as swifts) revealed that by sweeping the wings the birds can extend the performance envelope beyond that of a fixed wing of the same configuration. Furthermore, the body has a streamlined design with low drag (Lentink et al. 2007). This combination of wing and body design is potentially suitable both for fast flight and for energy efficient flight (Lentink et al. 2007, Henningsson et al. 2008).

Measurements of flight speeds among swifts during migration and during roosting flights

show that the mean flight speed is around 10 ms^{-1} and that the chosen flight speeds are within a relatively narrow range (Bruderer and Weitnauer 1972, Bäckman and Alerstam 2001, Henningsson et al. 2009) suggesting that swifts are in some way restricted in terms of favorable flight speeds (Henningsson et al. 2009). Yet, the swift has been shown to be able to fly at considerably higher speeds in horizontal flight, up to 28 ms^{-1}, at least for shorter periods (Oehme 1968, Bruderer and Weitnauer 1972). At breeding sites swifts exhibit a special behavior involving fast flight in flocks, often at low altitude and especially close to a breeding colony. The phenomenon is often referred to as 'screaming parties' based on the vocalizations the birds emit during these flights. Both breeders and non-breeders take part in these events that presumably is some sort of social behavior, but the function of this behavior is not well understood (Lack 1956). During such 'screaming flights' the birds often appear to reach very high speeds, which was the reason for measuring the speeds during these flights. Since previous studies suggest that swifts, during migratory and roosting flight, are restricted to a narrow range of flight speeds, it is of special interest to examine the capability of these birds in terms of flight speed. Here we determine the flight speed of swifts in the field with high accuracy using high-speed filming.

Materials and methods

The high-speed stereo camera system

We used two high-speed cameras (Basler pilot GigE vision camera piA640-210 gm, 648×488 pixel resolution progressive scan CCD, max. 210 fps, Basler AG, Ahrensburg, DE-SH, Germany) mounted on a steel beam to film the birds in the field. The beam was, in turn, mounted on a tripod in the centre between the cameras. The distance between the two cameras was 1400 mm and their relative angle difference relative to the beam was 7.0°. The single tripod setup allowed the whole rig to be turned around the centre (azimuth) and also to be rotated in vertical direction (elevation) without changing the mutual positions of the cameras. The two cameras operated separately and were only synchronized with each other at triggering. The data from the two cameras were streamed continuously to a laptop via two separate gigabit Ethernet connections and recorded by software also controlling frame rate and exposure time of the two cameras (Streampix 4, Norpix, Inc., Montreal, CA-QC, Canada). For this study the frame rate was set to 200 Hz. Since the frame grabbing of the cameras were unsynchronized, time-stamps were used during analysis to verify that the images in each frame pair was obtained at the same time (within ± 0.0005 s). The setup is essentially the same as that used by e.g. Buchanan and Evans (2000) with the difference that we used high-speed cameras.

The cameras were directed towards a swift colony located in the gable of a house and birds were filmed when passing through the field of view. Birds were prior to each filming observed before entering the measurement volume and they approached the colony in level flapping flight, in most cases from the same direction, and then flew closely past it in an upward directed flight path either flapping or gliding.

Camera calibration

The stereo setup was calibrated using images of a reference object consisting of nine poles put into the ground in a 3×3 grid covering an area of approximately 2×2 meters. Each pole had a length of 2 m and markers on 0.5, 1, 1.5 and 2 m height, in total 36 markers on the nine poles uniformly distributed within a volume of 2×2×2 m. The distance between the camera rig and the centre of the calibration volume was 8 meters, which corresponded to the estimated average distance to the filmed birds. The coordinates [x, y and z] of each of the reference points within the calibration volume were carefully measured in the field. The image coordinates of the reference markers in the two camera views were digitized manually using a custom written Matlab software. The real world coordinates

of the reference markers were then used to calculate camera coefficients for transforming two-dimensional image coordinates from the two camera views into three-dimensional real world coordinates by direct linear transform (DLT), using freely available Matlab (The MathWorks, Inc., USA) routines (courtesy of Christopher Reinschmidt, http://isbweb.org/software/movanal.html). The quality of the calibration was tested by measuring reference lengths (length of the tiles on the roof) and reference angles (the slope of the roof) from the films and comparing the results with the real world measures. A reference length of 361 mm was from the films calculated to 369 mm (8 mm difference) and a reference angle of 45° was from the films calculated to 44.8°. Total error can thus be estimated as 8/361 mm (2%; spatial) + 0.0005/0.005 s (10%; temporal, maximum) = 12 %.

Analysis of flight trajectories

The position of the beak was digitized manually in each frame of the two views using the above mentioned Matlab software. Standard error (SE) in the positions were calculated based on the residuals between the expected position based on the DLT coefficients and the positions manually pinpointed in the two camera views. These error estimates were used to calculate standard error of the mean (SEM). The average standard error over all positions in all sequences was 0.02 m and the average length of the sequences was 19 frames which corresponds to the number of estimates. SEM for positions of the raw data can then be calculated as:

$$\varepsilon(x, y, z) = \left(\frac{0.02}{\sqrt{19}} \right) = \pm 0.0046 \text{ m}$$

and for speed estimates

$$\varepsilon(V) = \left(\frac{0.0046}{0.005} \right) = \pm 0.92 \text{ ms}^{-1},$$

where 0.005 corresponds to Δt (1/200 Hz) and for acceleration estimates

$$\varepsilon(a) = \left(\frac{0.92}{0.005} \right) = \pm 184 \text{ ms}^{-2}.$$

Using the DLT camera coefficients the position of the beak in three-dimensional real-world coordinates was estimated. Cubic smoothing splines (Matlab CSAPS; smoothing parameter set to 1 and data points weighted by the inverse of the error for each point in the sequence calculated in the digitization program as described above) were applied to the coordinates of the trajectory of the beak in each sequence. The smoothing spline reduces the error in the position estimates due to digitization error.

The first derivatives of the splines were used to calculate the mean velocities for each sequence; horizontal velocity (V_{h}) and vertical velocity (V_{z}). Since the expected error of an acceleration estimate was high (± 184 ms^{-1}), acceleration was not used for further analysis. Individuals that were performing notably extreme maneuvers, such as rolls or turns, were excluded from further analysis since this behavior strongly reduces their flight speeds.

For sequences with birds in flapping flight (continuous) the number of frames of the maximum numbers of complete wingbeats within each sequence of continuous flapping was counted. The number of wingbeats was then divided by the total duration of these wingbeats to determine the wingbeat frequency.

Wind speed estimation

A day, 29 June 2008, with clear skies and calm winds was chosen as experiment day in order to minimize effects of weather and winds on the flight behavior of the birds. A simple estimate of the potential maximum wind were made by imaging a string hanging freely in the wind from a pole ca 10 meters from where the birds were flying and digitally measuring the angle of the string against the vertical plane when exposed to different winds. The same string with the same length was later on calibrated in the Lund University wind tunnel (about the wind tunnel, Pennycuick et al. 1997) by recording the angle at different speeds.

Results

Flight speed

This study is based on flight trajectories of 25 sequences of swifts in low altitude diurnal display flight ('screaming parties') filmed during one day at the end of June, 2008. Average length of the trajectories was 1.95 m and the paths were straight as the birds flew past the colony. Position raw data, before applying smoothing splines, are presented in figure 1. Around the swift colony, where the experiments were performed, many swifts reside, both breeding and non-breeding birds. Yet, the risk of repeated sampling can not be ruled out. Maximum potential wind speed during measurements was estimated to 2.6 ms^{-1}. This estimate corresponds to the maximum wind speed in gusts of wind, which were carefully avoided; cameras where only triggered if winds were low. Furthermore, wind direction was from the side of the flight trajectories of the birds. Since this suggests minimum effect of wind, no correction for wind was made on the data. Still, the wind estimate indicates the level of potential error in flight speed estimate due to wind. On average the birds flew with a horizontal speed (V_h) of 20.9 ms^{-1} ($\pm$5.1 ms^{-1}, n = 25), ranging from 11.9 ms^{-1} to 31.1 ms^{-1} (Fig. 2a). All except one of the birds performed climbing flight as
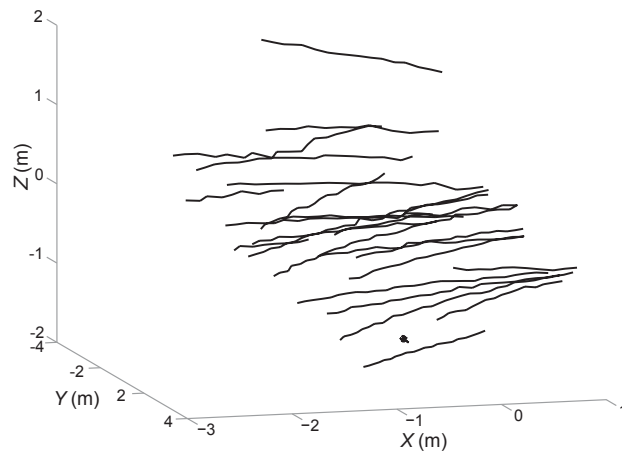

Figure 1. Raw, unsmoothed, data of the 25 flight trajectories of the swifts as viewed obliquely from in front of their flight paths. Most birds performed climbing flight over the roof of the house as they flew past the colony.
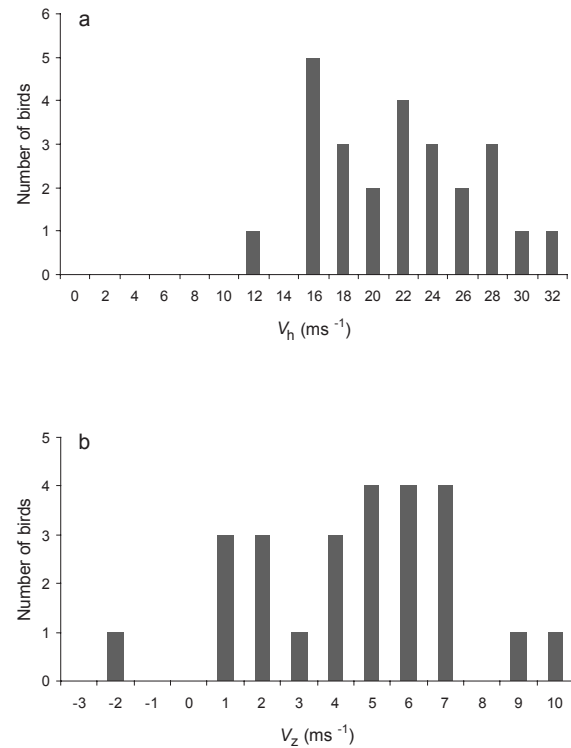

Figure 2. a) Distribution of horizontal velocity (V_h); average 20.9 ms^{-1} and standard deviation 5.1 ms^{-1}. b) Distribution of vertical velocity (V_z); average 4.0 ms^{-1} and standard deviation 2.8 ms^{-1}.

they flew close past the colony. Mean vertical speed (V_z, positive V_z corresponds to climbing flight) was 4.0 ms^{-1} ($\pm$2.8 ms^{-1}, n = 25) and it ranged between -2.7 ms^{-1} and 9.6 ms^{-1} (Fig. 2b).

Reduced major axis regression between horizontal speed and vertical speed showed a significant negative relationship (b=-1.798, P<0.001); an increase in vertical speed (steeper climbing flight) resulted in a decrease in horizontal speed (Fig. 3).

Wingbeat frequency

Mean wingbeat frequency of the birds in flapping flight was 10.4 Hz ($\pm$ 0.9 Hz, n = 15) and it ranged from 9.1 Hz to 12.5 Hz. Reduced major axis regression between wingbeat frequency and horizontal speed showed a significant relationship (b = 0.193, P<0.05; Fig. 4) as did regression
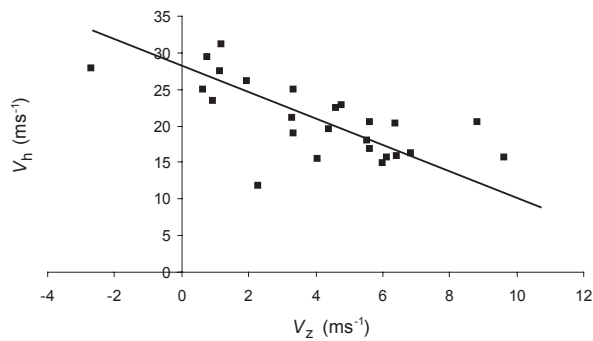
Figure 3. Horizontal velocity (V_h) plotted against vertical velocity (V_z). Reduced major axis regression shows a significant negative relationship between horizontal speed and vertical speed. The regression equation is: $V_h = -1.798 V_z + 28.14$ ($b = -1.798$, $R^2 = 0.445$, P<0.001).

between wingbeat frequency and vertical speed ($b = -0.3128$, P<0.05) although the R^2-value (= 0.003) was extremely low for the latter showing that almost none of the variation in the data is explained.

Discussion

Flight speed

The main focus of this study was the flight speeds of swifts during the special flight behavior referred to as 'screaming flight'. During these flights the birds appear to push themselves to perform at their maximum, perhaps as some sort of display involving demonstration of flight strength towards other individuals. The results show that the birds do fly at high speeds during 'screaming parties', on average 20.9 ms⁻¹, which is roughly twice as fast as the average speed recorded on for example spring migration (Bruderer and Weitnauer 1972, Henningsson et al. 2009). The maximum speed recorded in this study was 31.1 m/s, which is the highest yet recorded for a swift in self-powered flight (non-diving, cf. Oehme 1968, Bruderer and Weitnauer 1972). Mean vertical speed of the birds in this study was 4.0 ms⁻¹ and the maximum was 9.6 ms⁻¹, which are also very high. Sustained vertical speed (defined as at least 4 min of

uniform rate of continuous ascent) in swifts has been measured using tracking radar to be on average 1.34 ms⁻¹ (Hedenström and Alerstam 1992). This implies that the birds in this study are flying at both vertical speeds and horizontal speeds well outside their assumed possible range of sustainable flight speeds. The extreme flight speeds and climb rates suggest that the swifts use anaerobic muscle work during these flights, when power output can be increased during short bursts of sprint performance up to about twice the power output of aerobic muscle work (e.g. Weis-Fogh and Alexander 1977). When testing the relation between horizontal speed and vertical speed a clear significant negative relationship was found; higher vertical speed resulted in lower horizontal speed. This also suggests that the birds are operating at a performance maximum, or a constant fraction thereof, since there is a trade-off between these two speeds. A bird operating below its maximum would not need to allocate velocities between vertical and horizontal direction but would be able to maintain the same horizontal speed while increasing vertical speed. The power available for horizontal flight, P_h and power available for vertical flight, P_z, together corresponds to the maximum power possible for the bird, P_{max}, i.e., $P_{max} = P_h + P_z$. Flying with horizontal speed at V_{mp} (minimum-power speed, see e.g. Pennycuick 1989, Pennycuick 2008) involves the lowest power and therefore the highest margin
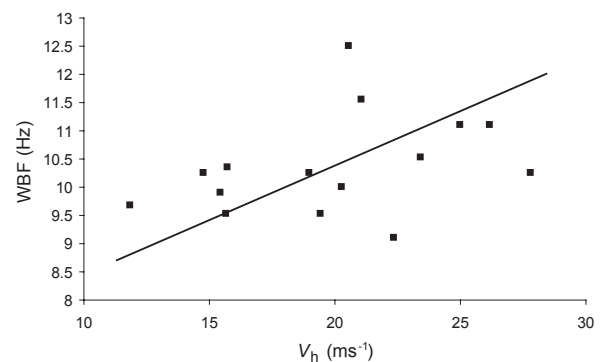

Figure 4. Wingbeat frequency (WBF) plotted against horizontal velocity (V_h). Reduced major axis regression shows a significant relationship. The regression equation is: WBF $= 0.193 V_h + 6.535$ ($b = 0.193$, $R^2 = 0.123$, P<0.05).

to P_{max} and thereby the highest potential P_z and consequently the highest V_z (since $V_z = P_z/mg$), where g is the acceleration due to gravity and m is the mass of the bird. On the other side of the spectrum P_{max} can be completely allocated to power for horizontal speed that would then give $V_{h, max}$ (and $V_z = 0$). The birds in this study are found to fly somewhere in between these extremes, as can be seen in the negative correlation between V_z and V_h in Fig 3. From reduced major axis regression (excluding cases with $V_z <0$), theoretical $V_{h,max}$ can be derived by seeking the intercept of the function with the y-axis (V_h when V_z is zero), giving $V_{h,max}$ of 29.2 ms^{-1} for the current data. Notice that the highest speed recorded, 31.1 ms^{-1}, is not far off this value.

Wingbeat frequency

The wingbeat frequency of swifts in high-speed 'screaming flight' was found to be higher than previously recorded for migratory and roosting swifts. Bruderer and Weitnauer (1972) recorded a mean wingbeat frequency during diurnal migration flights of 8 Hz, Oehme (1968) recorded 7 Hz during diurnal foraging flights and Bäckman and Alerstam (2001, 2002) recorded 7.6 Hz in nocturnal roosting flights. In this study the frequency ranged between 9.1 Hz and 12.5 Hz with a mean of 10.4 Hz which is significantly higher than previous records (95% confidence interval: 9.9 to 10.9 Hz). There was a significant positive correlation between wingbeat frequency and horizontal speed. Although statistically significant, the R^2-value ($= 0.12$) however indicates that the relationship is weak (Fig. 4). This relationship would suggest that increasing the wingbeat frequency is partly how high flight speeds are achieved. On the other hand, one may argue that since the relationship between wingbeat frequency and flight speed is weak, the higher wingbeat frequency relative to other studies does not appear to contribute significantly to increased speed. In that case some other kinematic parameter(s) must be responsible for the high speeds, such as e.g.

increased stroke amplitude (cf. Henningsson et al. 2008), changed angle of attack or changed wing sweep. Swept wings have been suggested to be favorable for swifts in high speed flight (Lentink et al. 2007) and have also been proposed to generate a leading edge vortex (LEV, Videler et al. 2004), which boosts lift but also increase drag. A study of the flappet lark *Mirafra rufocinnamomea* showed that the birds doubled their wingbeat frequency from 11 Hz during cruising flight to 24 Hz during display flights and it was suggested that this behavior is a sexually selected feat. The increase in wingbeat frequency of the flappet larks did not appear to have any aerodynamic function but was solely associated with display (Norberg 1991). Although the increase in wingbeat frequency of the swifts from cruising flight to 'screaming flight' was less dramatic it is possible that it has a similar function of advertising viability by performance of flight capacity.

Acknowledgements

References

Alerstam, T. 1987. Radar observations of the stoop of the peregrine falcon *Falco peregrinus* and the goshawk *Accipiter gentilis*. - Ibis **129**, 267-273.

Bruderer, B. and Weitnauer, E. 1972. Radarbeobachtungen über Zug und Nachtflüge des Mauerseglers (*Apus apus*). - Rev. Suisse Zool. **79**, 1190-1200.

Buchanan, K. L. and Evans, M. R. 2000. The effect of tail streamer length on aerodynamic performance in the barn swallow. - Behav. Ecol. **11**, 228-238.

Bäckman, J. and Alerstam, T. 2001. Confronting the winds: orientation and flight behaviour of the roosting swift, *Apus apus.* - Proc. R. Soc. B **268**, 1081-1087.

Bäckman, J. and Alerstam, T. 2002. Harmonic oscillatory orientation relative to the wind in nocturnal roosting flights of the swift *Apus apus.* - J. Exp. Biol. **205**, 905-910.

del Hoyo, J., Elliott, A. and Sargatal, J. eds 1999. Handbook of the birds of the world. Vol 5. Barn-owls to Hummingbirds. - Lynx Edicions, Barcelona.

Henningsson, P., Karlsson, H., Bäckman, J., Alerstam, T. and Hedenström, A. 2009. Flight speeds for different seasons: the case of the swift. - Proc. R. Soc. B. **276**, 2395-2401.

Henningsson, P., Spedding, G. R. and Hedenström, A. 2008. Vortex wake and flight kinematics of a swift in cruising flight in a wind tunnel. - J. Exp. Biol. **211**, 717-730.

Lack, D. 1956. Swifts in a tower. – Methuen, London.

Lentink, D., Müller, U.K., Stamhuis, E.J., de Kat, R., van Gestel, W., Veldhuis, L.L.M., Henningsson, P., Hedenström, A., Videler, J.J. and van Leeuwen, J.L. 2007. How swifts control their glide performance with morphing wings. - Nature **446**, 1082-1085.

Norberg, R. Å. 1991 The flappet lark *Mirafra rufocinnamomea* doubles its wingbeat rate to 24 Hz in wing-clap display flight: A sexually selected feat. - J. Exp. Biol. **159**, 515-523.

Oehme, H. 1968. Der Flug des Mauersegler (*Apus apus*). - Biol. Zentralblatt **87**, 287-311.

Pennycuick, C. J. 1989. Bird Flight Performance: A Practical Calculation Manual. - Oxford University Press, Oxford.

Pennycuick, C. J. 2008. Modelling the Flying Bird. Academic Press - Elsevier, Amsterdam, Boston, Heidelberg, London, New York, Oxford, San Diego, San Francisco, Singapore, Sydney, Tokyo.

Pennycuick, C. J., Alerstam, T. and Hedenström, A. 1997. A new low-turbulence wind tunnel for bird flight experiments at Lund University, Sweden. - J. Exp. Biol. **200**, 1441-1449.

Peter, D. and Kestenholz, M. 1998. Sturzflüge von Wanderfalke Falco peregrinus und Wüstenfalke F. pelegrinoides. - Orn. Beob. **95**, 107-112.

Tucker, V.A., Cade, T.J. and Tucker, A.E. 1998. Diving speeds and angles of a gyrfalcon (*Falco rusticolus*). - J. Exp. Biol. **201**, 2061-2070.

Weis-Fogh, T. and Alexander, R. McN. 1977. The sustained power output from striated muscle. - In: T.J. Pedley (ed.) Scale Effects in Animal Locomotion. London Academic Press, London, pp. 511-525.

Videler, J. J., Stamhuis, E. J. and Povel, G. D. E. 2004. Leading-Edge Vortex Lifts Swifts. - Science **306**, 1960-1962.

Videler, J. J. 2005. Avian Flight. - Oxford University Press, Oxford.

VI

Compensation for wind drift by migrating swifts

Håkan Karlsson[1], Per Henningsson[2,] Johan Bäckman[1], Anders Hedenström[2] and Thomas Alerstam[1]

[1] *Department of Animal Ecology, Ecology Building, Lund University, SE-223 62 Lund, Sweden*
[2] *Department of Theoretical Ecology, Ecology Building, Lund University, SE-223 62 Lund, Sweden*

We have investigated the orientation in relation to wind by common swifts *Apus apus* during nocturnal spring and autumn migration. Swifts are highly adapted to a life in the air, showing wind-dependent orientation during nocturnal roosting flights, and may be expected to be more efficient in their wind drift/compensation behaviour than nocturnal passerine migrants which are usually subjected to full or partial wind drift. A tracking radar in Lund in southern Sweden was used to record the orientation of common swifts (identified by their characteristic radar echo signature) on nocturnal migration flights and to measure wind conditions at the altitudes where the birds were flying. Comparing track and heading directions under easterly and westerly winds revealed that the swifts shifted their headings distinctly into the wind with the result that track directions were similar (not significantly different) under the different wind conditions. Since this pattern of complete compensation for drift from crosswinds occurred during both spring and autumn migration there were no indications of differences between age classes. In addition, we found a distinct effect of sidewinds on equivalent airspeeds, with swifts increasing their airspeed with increasing sidewind components. Such a response has been theoretically predicted as part of an optimal behaviour for counteracting wind drift but has hereto not been empirically demonstrated. Our results suggest that important differences may exist between species in their capacities to orient in relation to the wind and that the swift may be particularly efficient in adjusting heading direction and airspeed to obtain complete compensation for wind drift during high-altitude nocturnal migratory flights.

Introduction

Moving through the air without the ability to hide from the wind involves the risk of being geographically displaced. Migratory birds spend much time in the air while covering vast geographical distances, and wind has the potential to greatly influence navigation as well as flight cost and timing.

Numerous studies have investigated how migrating birds orient in relation to the wind – to what extent they are drifted by crosswinds or compensate for the wind drift. The general picture emerging from these studies is that birds show highly variable and complex orientation responses ranging from full or partial drift to complete compensation or even overcompensation (cf. reviews by Alerstam 1976, Richardson

1991, Liechti 2006). The explanations for this variability in orientation response to wind are not well understood, but it has been suggested that drift/compensation behaviour may differ between species, ages and between flight conditions (e.g. altitude, visibility, light) that may affect the birds' sensing of the effect of wind. Furthermore, it has been predicted that birds may reduce travel time and energy costs by adopting strategies of adaptive drift, allowing themselves to be drifted to variable degree depending on the wind pattern and distance to the destination (Alerstam 1979, Liechti 1975).

For nocturnal passerine bird migration, full or partial wind drift seems to be the most common pattern (e.g. Cochran & Kjos 1985, Liechti 1993, Zehnder et al. 2001, Bäckman & Alerstam 2003, Karlsson et al. in prep.) Nocturnal high-altitude migration of insects like moths is strongly affected by wind with the moths often orienting close to the downwind direction (or changing their orientation partly towards their preferred migratory directions), indicating that also moths have mechanisms of sensing and responding to the wind in darkness (Chapman et al. 2008, Reynolds et al. 2009). There are only a few cases, under special circumstances of very low flight altitudes close to a river or along a coastline where nocturnal bird migrants have been reported to show a large degree of compensation for wind drift (Bingman et al. 1982, Åkesson 1993).

In this study we have investigated the nocturnal drift/compensation behaviour of a specific species, the common swift, in order to find out if interspecific differences in this behaviour may exist among nocturnal bird migrants. Because of its adaptations to a life in the air we expect that the swift may be more efficient than nocturnally migrating passerines to orient in relation to the wind.

During the annual cycle and while travelling between temperate breeding grounds and wintering quarters in tropical Africa, the common swifts typically only land during breeding and while tending to the nest (although occasional roosting in trees or masts occurs; cf. Holmgren 2004). Flight altitudes during nocturnal spring and autumn migration usually range between 500 and 2000 m above sea level, with mean altitudes at 1000-1400 m asl (Henningsson et al. 2009).

Earlier studies have revealed some fascinating facts about the flight behaviour of the swift. Bäckman & Alerstam (2001, 2002) have shown that the birds orient into the wind during their nocturnal roosting flights. Heading into the wind minimizes the risk of being carried away large distances by the wind. This behaviour indicates that the birds must have some way of determining wind direction and potentially also the strength of the wind. Being such accomplished fliers with a well-developed sensitivity to the wind, these birds should be well equipped to deal with unwanted deviations from the intended flight path due to wind drift also during migration.

It is possible to identify swifts tracked by radar from their highly characteristic radar echo signature (Bruderer & Weitnauer 1972, Bäckman & Alerstam 2001, Henningsson et al. 2009). By studying a specific species, something that is not commonly feasible in radar studies, we can minimize the risk of bias due to pseudodrift that may arise as a consequence of differential departures under different wind conditions of species and/or populations with different preferred migratory mean directions (Evans 1966, Nisbet & Drury 1967, Alerstam 1978).

We predicted that common swifts show a high degree of compensation for wind drift and that the degree of compensation is highest during spring when the birds are considerably closer to the destination areas (Alerstam 1979) and when the sample consists of birds that have successfully achieved at least one migratory journey. Young and inexperienced birds, which make up part of the sample during autumn migration, may be less prone or able than adult birds to compensate for wind drift, possibly because they migrate by a comparatively simple "clock-and-compass" system (Berthold 2001) not allowing correction for geographical displacement to the same extent as the more complex navigation system used by experienced birds (see Perdeck 1958, Åkesson 2003, Thorup et al. 2003, 2007).

Apart from adjusting heading directions to compensate for wind drift, flight speeds could also be adjusted. Liechti et al. (1994) and

Liechti (1995) described how flight speeds, in an effective response to drift, should be increased as the crosswind component increases. However, as Liechti (2006) summarized theory and results relating to the issues of behavioural responses to different wind conditions he pointed out that no empirical study has yet confirmed increased airspeeds as a result of increasing cross-winds (see also Hedenström et al. 2002).

Methods

The tracking radar (PV882, 200 kW peak power, 0.25 μs pulse duration, 504 Hz pulse repetition frequency (PRF), 1.5° pencil beam width, X-band) used to sample the flight behaviour of migrating swifts was located on the roof of the Ecology Building (91.5 m above sea-level; 55° 42' 50''N, 13° 12' 27''E) in Lund, southernmost Sweden. The radar was operated in manual mode (the operator scans for suitable targets) until an echo of a bird was found, after which the radar was switched into automatic tracking mode.

Data from the radar (elevation, azimuth and distance) were recorded by custom-built software and sent from the radar to the computer every 2nd second. Analysing the radar echo signal (using DFT; Discrete Fourier Transform analysis; for more information on the procedure see e.g. Bäckman & Alerstam 2003) allowed us to derive wing-beat pattern and frequency for each target.

Data were collected on nocturnally migrating swifts during night-time (22:00-05:00 local time in spring; 21:00-02:00 local time in autumn) in spring (7th May-1st June) 2006-2007 and autumn (4th-11th August) 2005-2006. We used the same characteristics of the radar echo signature as criteria for identification that have earlier been described by Bäckman & Alerstam (2001) and Henningsson et al. (2009). Swifts show pronounced wingbeat frequencies around 7 Hz, and the pattern of flapping- and gliding phases is characteristic and easily recognizable. Furthermore, the swift frequently and abruptly banks, causing the strength of the radar signal

to be temporarily much reduced (Bruderer and Weitnauer 1972).

When searching for echoes the sky was scanned in a systematic manner and each tracking lasted for approximately 60 seconds, after which the antenna was directed into another sector of the sky in order to avoid repeated samples of the same individual.

During the night, helium filled balloons were released and tracked by the radar in order to measure the speed and direction of the wind along an altitudinal gradient from approximately 300 to 2500 metres altitude.

The processing of data began with a thorough examination of every recorded data-point and obvious errors, e.g. if the radar momentarily lost the target, were removed. If the deletion was in the middle of a tracking the data-point(s) were substituted by a linear interpolation. By combining bird flight data with wind data (at a maximum of 2 hrs from the tracking of the bird, else the bird was not included in the analysis), heading directions and airspeeds were calculated. Overall mean directions (track, heading and wind) and speeds (ground-, air- and wind speeds as well as vertical speed) were calculated for each target as described by Henningsson et al. 2009. Birds showing airspeeds lower than 5 m/s or greater than 25 m/s were not included since these airspeeds were not considered as representative for migrating swifts. Airspeeds were recalculated into equivalent airspeeds (Pennycuick 2008) in order to remove the effect of flight altitude on flight speeds and to facilitate comparisons with our earlier study concerning flight speeds of swifts (Henningsson et al. 2009).

Circular statistics were used to calculate mean directions and mean vector lengths (r; where r=1 corresponds to no scatter while r=0 represents a uniform scatter among individual directions (Batschelet 1981).

A General Linear Model analysis (GLM) was performed in the statistical software SPSS (version 17.0) in order to address the question of the influence of sidewind on flight speeds. The model was performed on [10]log-transformed equivalent airspeeds as dependent variable and included season as fixed factor and vertical speed, tailwind component, sidewind component

(calculated as the component of the wind vector that was perpendicular to the heading direction) and potential interactions between season and sidewind component as covariates.

Results

Flight directions during spring and autumn

Spring migration was represented by 176 trackings and autumn migration by 150 trackings of migrating swifts. Mean flight directions and mean vector lengths (r) are presented in Figure 1 and Table 1. The results indicate migration along a NNE-SSW axis of track directions. Scatter (r) is similar between track and heading, both in spring and autumn, with heading directions being slightly more concentrated than track directions.

Effect of crosswind on directions

The sample was divided into two groups depending on wind directions, westerly (W) and easterly (E) winds respectively. As can be seen from Figure 2 and Table 1, track directions were very similar between the two wind categories, whereas heading directions were clearly adjusted towards the wind direction.

In autumn the mean track direction (198°) under W winds was slightly more to the south
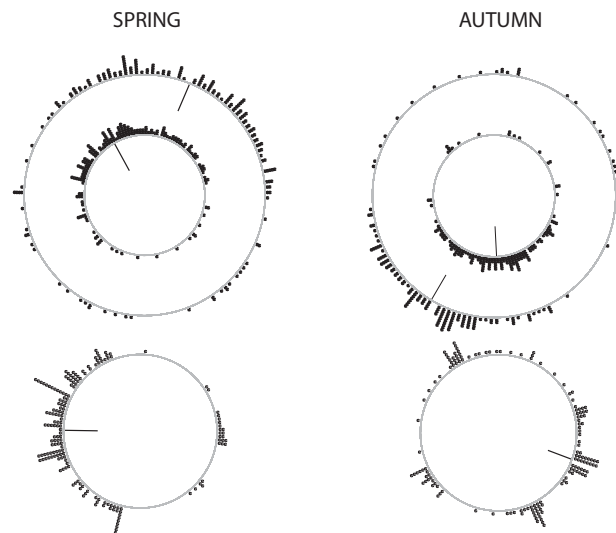

SPRING · AUTUMN

Figure 1. Upper row: Flight directions with mean directions. Outer circles represents track directions and inner circles represents heading directions. Lower row: Wind directions with mean directions. Note that wind directions are defined as directions from which the wind is blowing. Each dot represents the mean flight and wind direction of an individual swift tracked by radar on nocturnal migration. Data on mean direction and mean vector lengths are given in Table 1.

than the mean track direction (220°) under E winds, but this difference was not statistically significant (Mann-Whitney p=0.11, U=2074). In contrast, mean heading directions were clearly and significantly different (Mann-Whitney p<0.001, U=596) between W and E winds (222° and 158°, respectively; Table 1). The estimated magnitude of drift as calculated

Table 1. Mean flight directions (track- and heading directions) and mean vector lengths (r) for migratory swifts recorded by tracking radar during spring and autumn in southern Sweden. Data for the total seasonal sample are presented (cf Fig 1) as well as for seasonal samples divided into westerly and easterly winds (Fig 2; categories west and east respectively). N = number of individuals tracked. Also mean directions and mean vector lengths of wind data are given for each sample.

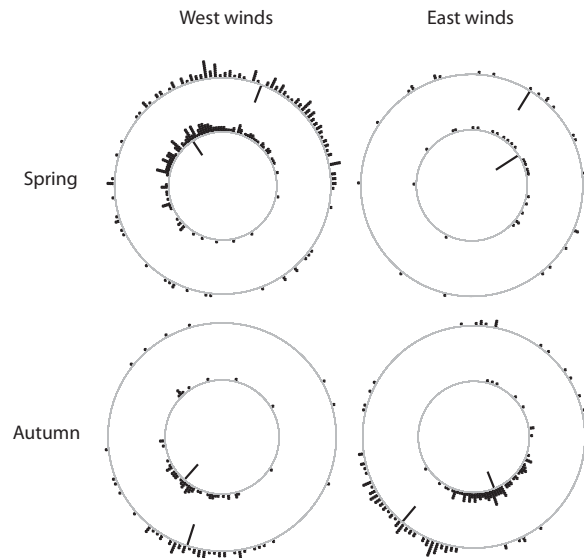| Season	Category	N	Track	r	Heading	r	Wind	r
Spring	All	176	22°	0.51	334°	0.56	271°	0.54
Spring	West	151	21°	0.54	326°	0.65	271°	0.78
Spring	East	25	32°	0.38	57°	0.55	94°	0.89
Autumn	All	150	211°	0.63	178°	0.66	110°	0.25
Autumn	West	55	198°	0.74	222°	0.67	291°	0.66
Autumn	East	95	220°	0.58	158°	0.80	111°	0.78

West winds   East winds

Spring

Autumn

Figure 2. Flight directions (outer circles: track; inner circles: heading) for swifts flying in west- and east winds respectively during spring and autumn. Mean directions are indicated as bars. Data on mean directions and mean vector lengths are given in Table 1.

from these mean directions is 0.26 (eq. 4 in Green & Alerstam 2002) on a scale where 0 is complete compensation and 1 is full drift. Thus we cannot exclude that there was an element of partial drift, although this possible small drift

effect is not statistically significant.

In spring, the difference between mean track directions under E versus W winds was even smaller than in autumn and again not statistically significant (Mann-Whitney p=0.73, U=1805). Furthermore, the mean track direction was shifted into the wind rather than away from it as expected with wind drift. It should be noted that the sample size for the E-wind category is small with only 25 trackings, but still there was a significant directionality (mean vector length significantly larger than 0) for the samples of both track and heading directions (p<0.05, Rayleigh test; all categories in Table 1 were significant according to the Rayleigh test). The mean heading directions were again clearly and significantly different in W and E winds (326° versus 57°, Table 1; Mann-Whitney p<0.001, U=690). The estimated magnitude of drift in spring was -0.14 (negative values indicate overcompensation; cf. Green & Alerstam 2002), but this was not significantly different from complete compensation (drift = 0). Thus, results from both seasons indicate that swifts change their headings into the wind in such a way that complete (or close to complete) compensation for wind drift is achieved.

Table 2. Results from the General Linear Model (GLM) are presented for log-transformed equivalent airspeeds. (a) Parameters included in the model. (b) Parameter estimates for all parameters included in the model.

(a)	Parameter	d.f	S.S.	F	p-value
	Vertical speed	1	0.002	0.162	0.688
	Sidewind	1	0.121	12.309	0.001
	Tailwind	1	0.018	1.825	0.178
	Season	1	0.181	18.417	0.000
	Error	321	3.158		

(b)	Parameter	B	s.e.	95% confidence interval	
				lower bound	upper bound
	Intercept	0.931	0.011	0.910	0.952
	Vertical speed	-0.005	0.013	-0.030	0.020
	Sidewind	0.005	0.001	0.002	0.008
	Tailwind	-0.001	0.001	-0.003	0.001
	Spring	0.048	0.011	0.026	0.070
	Autumn	0.000			

Effect of crosswind on flight speeds

The results from a GLM analysis of the effect of crosswinds (sidewind component) on equivalent airspeeds are presented in Table 2. There was a significant effect of sidewinds on flight speeds (p<0.01) and this effect was similar both in spring and autumn with no significant interaction between season and sidewind. The results indicated an increase in airspeed by a factor of 1.012 (=$10^{0.005}$; Table 2) for every 1 m/s increase in the sidewind component. As an example, this corresponds to an increase in airspeed by approximately 10% with a sidewind component of 8 m/s compared to no sidewind. We also investigated the relationship between equivalent airspeed and sidewind component when sidewind component was calculated relative to the track direction (substituting the sidewind parameter in the GLM). The result when sidewinds were calculated based on track directions was very similar (p<0.001, parameter estimate (B) 0.009, 95% confidence interval: 0.005-0.012) to that presented in Table 2, where sidewinds were calculated based on heading directions.

Discussion

Flight directions during spring and autumn

Ringing recoveries of young swifts during autumn indicate a primarily southerly mean migratory direction towards wintering grounds (Fransson et al. 2008). These results are, however, based on a very limited number of recoveries. Our results indicate migratory (track) directions through southern Sweden primarily towards SSW. Heading directions are directed more towards south (Figure 1, Table 1). Gatter (2000) found, when studying swifts during passage in southwest Germany, indications of a shift in mean migratory direction during the autumn migration season from southwesterly track directions during early autumn migration to directions pointing more due south towards the end of autumn migration.

The main sampling period of our data (first half of August) corresponds to the part of the autumn migratory season when Gatter found a mean track direction pointing to SW (Gatter 2000).

Both track and heading directions were slightly more concentrated in autumn than in spring. A high proportion of the birds taking part of autumn migration are presumably young birds, without prior migratory experience. Lack of experience have been hypothesized to lead to a larger amount of scatter among these birds than among adult birds (e.g. Bäckman & Alerstam 2003), but we found no clear evidence of this in the present study.

Effect of crosswind on directions

When we divided the data-set into birds travelling in west- and east winds, respectively (Figure 2, Table 1), we found a pronounced response in heading directions to compensate for wind drift. Track directions remained more or less the same irrespective of the wind, strongly indicating, and in line with our prediction, a dominating component of compensation.

When analysing wind drift phenomena there is a risk of falsely interpreting diverging mean directions of different contingents of individuals, migrating under different wind condition, as being the result of wind drift. In this study, we have been able to reduce the risk of such pseudodrift correlations by investigating the response in flight directions within a single species, without apparent subpopulations (in Scandinavia) with distinctly different breeding- or wintering grounds.

Contrary to our prediction, our results do not indicate any substantial differences between spring and autumn in the swifts' compensatory behaviour. Thus, we see no evidence of young birds exhibiting a different behaviour than adults. The assumed high proportion of young birds during autumn migration makes it likely that we would have been able to recognize such differences if they existed.

Very few studies have reported full compensation

among nocturnal migrants. Bingman et al (1982) and Åkesson (1993) both report nearly full compensation among passerine birds that were migrating at low altitudes close to distinct landmarks or leading lines, such as a river (Bingman et al 1982) or along a coastline (Åkesson 1993). Since full or partial drift seem to be more common among nocturnal passerine migrants (e.g. Cochran &Kjos 1985, Liechti 1993, Zehnder et al 2001, Bäckman & Alerstam 2003, Karlsson et al. in prep.) the results in this study show that swifts may be especially well equipped to compensate for wind drift during migration.

Effect of crosswind on flight speeds

The results show that swifts increase their airspeed by a factor of 1.012 (95% confidence interval 1.005-1.019) for every 1 m/s increase in crosswinds. To the best of our knowledge this study is the first case of empirical confirmation of this theoretical prediction (cf. Hedenström et al. 2002, Liechti 2006). Since we investigated sidewind- and tail/headwind components separately (cf. Liechti et al. 1994, Shamoun-Baranes et al. 2007) it is somewhat surprising that we did not find a significant effect of the tail-/headwind parameter on equivalent airspeed (cf. Henningsson et al. 2009). Adjustments in airspeeds resulting from different wind conditions could be a response either to minimize flight costs or to avoid drift. We suggest that the compensatory speed adjustment we have observed in this study is primarily associated with compensation for wind drift. However, there is no way to completely distinguish the two phenomena.

The response with respect to sidewind in equivalent airspeeds is present both among spring and autumn migrants. Thus, there are no indications that this response in flight speed would be restricted to adults. Should inexperienced juveniles have exhibited inferior compensation skills, this most likely would have resulted in differences between spring and autumn response to sidewind components.

Since adjustments of the same order, concerning both heading directions and flight speeds, are evident in both spring and autumn, we find nothing that supports the prediction that the magnitude of compensation would differ depending on the distance remaining to the final destination (Alerstam 1979, Liechti 1995).

Our results suggest that important differences may exist between species in their capacities to orient in relation to the wind and that the swift may be particularly efficient in adjusting heading direction and airspeed to obtain complete compensation for wind drift during high-altitude nocturnal migratory flights. Is this ability the result of an aerial lifestyle, where nocturnal roosting flights, as well as not landing when faced with severe weather conditions, greatly favours individuals with precise skills for navigation and for sensing the wind?

Acknowledgements

References

Åkesson, S. 1993. Coastal migration and wind drift compensation in nocturnal passerine migrants. Ornis Scandinavica, **24**, 87-94.

Åkesson, S. 2003. Avian long-distance navigation: experiments with migratory birds. In *Avian Migration* (Ed. by P. Berthold, E. Gwinner and E. Sonnenschein), pp. 471-492. Berlin, Heidelberg: Springer-Verlag.

Alerstam, T. 1976. Bird migration in relation to wind and topography. PhD-thesis. Lund: Department of Animal Ecology, Lund University (51pp)

Alerstam, T. 1978. A graphical illustration of pseudodrift. Oikos, **30**, 409-412.

Alerstam, A. 1979. Wind as selective agent in bird migration. Ornis Scandinavica, **10**, 76-93.

Bäckman, J. & Alerstam, T. 2001. Confronting the winds: orientation and flight behaviour of the roosting swift, *Apus apus*. Proceedings of the Royal Society of London, Series B, **268**, 1081-1087.

Bäckman, J. & Alerstam, T. 2002. Harmonic oscillatory orientation relative to the wind in nocturnal roosting flights of the swift *Apus apus*. Journal of Experimental Biology, **205**, 905-910.

Bäckman, J. & Alerstam, T. 2003. Orientation scatter of free-flying nocturnal passerine migrants: components and causes. Animal Behaviour, **65**, 987-996.

Berthold, P. 2001. Bird migration, A general survey (2nd Ed). Oxford University Press.

Bingman, V.P., Able, K.P. & Kerlinger, P. 1982. Wind drift, compensation, and the use of landmarks by nocturnal bird migrants. Animal Behaviour, **30**, 49-53.

Bruderer, B. & Weitnauer, E. 1972. Radarbeobachtungen über Zug und Nachtflüge des Mauerseglers (*Apus apus*). Revue suisse de zoologie, **79**, 1190-1200.

Chapman, J.W., Reynolds, D.R., Mouritsen, H., Hill, J.K., Riley, J.R., Sivell, D., Smith, A.D. & Woiwod, I.P. 2008. Wind selection and drift compensation optimize migratory pathways in a high-flying moth. Current Biology, **18**, 514-518.

Cochran, W.W. &Kjos, C.G. 1985. Wind drift and migration of thrushes: a telemetry study. Illinois Natual. History Survey Bulletin, **33,** 297-330.

Evans, P.R. 1966. An approach to the analysis of visible migration and a comparison with radar observations. Ardea, **54**, 14-44.

Fransson, T., Österblom, H. & Hall-Karlsson, S. 2008. *Svensk ringmärkningsatlas, Vol. 2.* Naturhistoriska Riksmuseet, Stockholm. *With English summary*

Gatter, W. 2000. *Vogelzug und Vogelbestände in Mitteleuropa.* Aula-Verlag, Germany.

Hedenström, A., Alerstam, T., Green, M. &Gudmundsson, G.A. 2002. Adaptive variation of airspeed in relation to wind, altitude and climb rate by migrating birds in the Arctic. Behavioral Ecology and Sociobiology, **52**, 308-317.

Henningsson, P., Karlsson, H., Bäckman, J., Alerstam, T. & Hedenström, A. 2009. Flight speeds of swifts (*Apus apus*): seasonal differences smaller than expected. Proceedings of the Royal Society of London, Series B, **276**, 2395-2401.

Holmgren, J. 2004. Roosting in tree foliage by Common Swifts *Apus apus*. Ibis, **146**, 404-416.

Liechti. F. 1993. Nächtlicher Vogelzug im Herbst über süddeutschland: Winddrift und Kompensation. Journal für Ornithology, **134**, 373-404.

Liechti, F. 1995. Modelling optimal heading and airspeed of migrating birds in relation to energy expenditure and wind influence. Journal of Avian Biology, **26**, 330-336.

Liechti, F. 2006. Birds: blowin' by the wind? Journal für Ornithology, **147**, 202-211.

Liechti, F., Hedenström, A. & Alerstam, T. 1994. Effects of sidewinds on optimal flight speeds of birds. Journal of Theoretical Biology, **170**, 219-225.

Nisbet, I.C.T. & Drury, W.H. Jr. 1967. Orientation of spring migrants studied by radar. Bird-Banding, **38**, 173-186.

Pennycuick, C.J. 2008. *Modelling the flying bird.* London, Academic Press (Elsevier).

Perdeck, A.C. 1958. Two types of orientation in migrating *Sturnus vulgaris* and *Fringilla coelebs* as revealed by displacement experiments.

Ardea, **46**, 1-37.

Reynolds, A.M., Reynolds, D.R., Smith, A.D. & Chapman, J.W. 2009. A single wind-mediated mechansism explains high-altitude "non-goal" oriented headings and layering of nocturanlly migrating insects. **Proc. R. Soc. B** doi: 10.1098/rspb.2009.1221

Richardson, W.J. 1991. Wind and orientation of migrating birds: a review. In: *Orientation in Birds* (Ed. by Berthold, P.), pp 226-249. BirkhäuserVerlag, Basel.

Shamoun-Baranes, J., Loon, E. von., Liechti, F. & Bouten, W. 2007. Analyzing the effect of wind on flight: pitfalls and solutions. Journal of Experimental Biology, **210**, 82-90.

Thorup, K., Alerstam, T., Hake, M. &Kjellén, N. 2003. Bird orientation: compensation for wind drift in migrating raptors is age dependent. Proceedings of the Royal Society of London, Series B, **270** (suppl.), S8-S11.

Thorup, K., Bisson, I-A., Bowlin, M., Holland, R.A., Wingfield, J.C., Ramenofsky, M. &Wikelski, M. 2007. Evidence for a navigational map stretching across the continental U.S. In a migratory songbird. Proceedings of the National Academy of Sciences, **104**, 18115-18119.

Zehnder, S., Åkesson, S., Liechti, F. & Bruderer, B. 2001. Nocturnal fall bird migration at Falsterbo, south Sweden. Journal of Avian Biology, **32**, 239-248.

The following is a list of Doctoral theses (Lund University,Sweden) from the Department of Animal Ecology (nos. 1-78, from no. 79 and onwards denoted by (A)) and Theoretical Ecology (T). (E) refers to Doctoral theses from the Department of Chemical Ecology/Ecotoxicology during the years 1988-1995.

1. CHARLOTTE HOLMQVIST. Problem on marine-glacial relicts on account on the genus *Mysis*. 6 May 1959.
2. HANS KAURI. Die Rassenbildung bei europäischen Rana-Arten und die Gültigkeit der Klimaregeln. 9 May 1959.
3. PER DALENIUS. Studies on the Oribatei (Acari) of the Torneträsk territory in Swedish Lapland. 14 May 1963.
4. INGEMAR AHLÉN. Studies on the history of distribution, taxonomy and ecology of the Red Deer in Scandinavia. 21 May 1965.
5. STAFFAN ULFSTRAND. Bentic animal communities of river Vindelälven in Swedish Lapland. 8 May 1968.
6. SAM ERLINGE. Food habits, home range and territoriality of the otter *Lutra lutra* L. 6 May 1969.
7. GUNNAR MARKGREN. Reproduction of moose in Sweden. 17 May 1969.
8. ARNE BERGENGREN. On genetics, evolution and history of the heath-hare, a distinct population of the arctic hare, *Lepus timidus* L. 17 October 1969.
9. HåKAN HALLANDER. Habitats and habitat selection in the wolf spiders *Pardosa chelata* (O.F. Müller) and *P. pullata* (Clerck). 20 March 1970.
10. ULF SCHELLER. The Pauropoda of Ceylon. 29 May 1970.
11. LEIF NILSSON. Non-breeding ecology of diving ducks in southernmost Sweden. 2 December 1970.
12. RUNE GERELL. Distributional history, food habits, diel behaviour, territoriality, and population fluctuations of the mink *Mustela vison* Schreber in Sweden. 30 March 1971.
13. INGRID HANSSON. Skull nematodes in mustelids. 3 June 1971.
14. STURE ABRAHAMSSON. Population ecology and relation to environmental factors of *Astacus astacus* Linné and *Pacifastacus leniusculus* Dana. 3 June 1971.
15. LENNART HANSSON. Food conditions and population dynamics of Scandinavian granivorous and herbivorous rodents. 26 November 1971.
16. SVEN-AXEL BENGTSON. Ecological segregation, reproduction and fluctuations in the size of duck populations in Iceland. 21 April 1972.
17. STEN ANDREASSON. Distribution, habitat selection, food and diel activity of Swedish freshwater sculpins (*Cottus* L.). 5 May 1972.
18. KERSTIN SVAHN. Coccidian blood parasites in Lacertids. 17 May 1972.
19. RUTGER ROSENBERG. Macrofaunal recovery in a Swedish fjord following the closure of a sulphite pulp mill. 13 April 1973.
20. SVEN ALMQVIST. Habitat selection and spatial distribution of spiders in coastal sand dunes. 25 May 1973.
21. TORSTEN MALMBERG. Population fluctuations and pesticide influence in the rook *Corvus frugilegus* L., in Scania, Sweden 1955-1970. 25 May 1973.
22. ANDERS SÖDERGREN. Transport, distribution, and degradation of organochlorine residues in limnic ecosystems (defended at the Dept of Limnology). 23 May 1973.
23. BERITH PERSSON. Effects of organochlorine residues on the whitethroat *Sylvia communis* Lath. 7 December 1973.
24. PLUTARCO CALA. The ecology of the ide *Idus idus* (L.) in the river Kävlingeån, South Sweden. 23 May 1975.
25. ÅKE GRANMO. Effects of surface active agents on marine mussels and fish. 26 May 1975.
26. BO W SVENSSON. Population ecology of adult *Potamophylax cingulatus* (Steph.) and other Trichoptera at a South Swedish stream. 15 October 1975.
27. STEN NORDSTRÖM. Associations, activity, and growth in lumbricids in southern Sweden. 6 April

1976.

28. STEN RUNDGREN. Environment and lumbricid populations in southern Sweden. 8 April 1976.
29. CHRISTIAN OTTO. Energetics, dynamics and habitat adaptation in a larval population of *Potamophylax cingulatus* (Steph.) (Trichoptera). 9 April 1976.
30. JAN LÖFQVIST. The alarm-defence system in formicine ants. 21 May 1976.
31. LARS HAGERMAN. Respiration, activity and salt balance in the shrimp *Crangon vulgaris* (Fabr.). 22 October 1976.
32. THOMAS ALERSTAM. Bird migration in relation to wind and topography. 29 October 1976.
33. LARS M NILSSON. Energetics and population dynamics of *Gammarus pulex* L. Amphipoda. 20 December 1977.
34. ANDERS NILSSON. Ticks and their small mammal hosts. 24 May 1978.
35. SÖREN SVENSSON. Fågelinventeringar - metoder och tillämpningar. (Bird censuses - methods and applications.) 23 May 1979.
36. BO FRYLESTAM. Population ecology of the European hare in southern Sweden. 1 June 1979.
37. SVEN G NILSSON. Biologiska samhällen i heterogena miljöer: En studie på fastland och öar. (Biological communities in heterogeneous habitats: A study on the mainland and islands.) 12 October 1979.
38. BJÖRN SVENSSON. The association between *Epoicocladius flavens* (Chironomidae) and *Ephemera danica* (Ephemeroptera). 26 October 1979.
39. GÖRAN HÖGSTEDT. The effect of territory quality, amount of food and interspecific competition on reproductive output and adult survival in the magpie *Pica pica*; an experimental study. 29 February 1980.
40. JON LOMAN. Social organization and reproductive ecology in a population of the hooded crow *Corvus cornix*. 9 April 1980.
41. GÖRGEN GÖRANSSON. Dynamics, reproduction and social organization in pheasant *Phasianus colchicus* populations in South Scandinavia. 26 September 1980.
42. TORSTEN DAHLGREN. The effects of population density and food quality on reproductive output in the female guppy, *Poecilia reticulata* (Peters). 27 February 1981.
43. AUGUSTINE KORLI KORHEINA. Environments and co-existence of *Idotea* species in the southern Baltic. 15 May 1981.
44. INGVAR NILSSON. Ecological aspects on birds of prey, especially long-eared owl and tawny owl. 9 October 1981.
45. TORBJÖRN von SCHANTZ. Evolution of group living, and the importance of food and social organization in population regulation; a study on the red fox (*Vulpes vulpes*). 23 October 1981.
46. OLOF LIBERG. Predation and social behaviour in a population of domestic cat. An evolutionary perspective. 11 December 1981.
47. BJÖRN MALMQVIST. The feeding, breeding and population ecology of the brook lamprey (*Lampetra planeri*). 12 March 1982.
48. INGVAR WÄREBORN. Environments and molluscs in a non-calcareous forest area in southern Sweden. 19 March 1982.
49. MAGNUS SYLVÉN. Reproduction and survival in common buzzards (*Buteo buteo*) illustrated by the seasonal allocation of energy expenses. 26 March 1982.
50. LARS-ERIC PERSSON. Structures and changes in soft bottom communities in the southern Baltic. 23 April 1982.
51. GÖRAN BENGTSSON. Ecological significance of amino acids and metal ions, a microanalytical approach. 24 May 1982.
52. JAN HERRMANN. Food, reproduction and population ecology of *Dendrocoelum lacteum* (Turbellaria) in South Sweden. 10 December 1982.
53. BO EBENMAN. Competition and differences in niches and morphology between individuals, sexes and age classes in animal populations, with special reference to passerine birds. 8 April 1983.
54. HANS KÄLLANDER. Aspects of the breeding biology, migratory movements, winter survival, and

population fluctuations in the great tit *Parus major* and the blue tit *P. caeruleus*. 29 April 1983.

55. JOHNNY KARLSSON. Breeding of the starling (*Sturnus vulgaris*). 6 May 1983.

56. CARITA BRINCK. Scent marking in mustelids and bank voles, analyses of chemical compounds and their behavioural significance. 17 May 1983.

57. PER SJÖSTRÖM. Hunting, spacing and antipredatory behaviour in nymphs of *Dinocras cephalotes* (Plecoptera). 1 June 1983.

58. INGE HOFFMEYER. Interspecific behavioural niche separation in wood mice (*Apodemus flavicollis* and *A. sylvaticus*) and scent marking relative to social dominance in bank voles (*Clethrionomys glareolus*). 9 December 1983.

59. CHRISTER LÖFSTEDT. Sex pheromone communication in the turnip moth *Agrotis segetum*. 30 November 1984.

60. HANS KRISTIANSSON. Ecology of a hedgehog *Erinaceus europaeus* population in southern Sweden. 7 December 1984.

61. CHRISTER BRÖNMARK. Freshwater molluscs: Distribution patterns, predation and interactions with macrophytes. 19 April 1985.

62. FREDRIK SCHLYTER. Aggregation pheromone system in the spruce bark beetle *Ips typographus*. 26 April 1985.

63. LARS LUNDQVIST. Life tactics and distribution of small ectoparasites (Anoplura, Siphonaptera and Acari) in northernmost Fennoscandia. 10 May 1985.

64. PEHR H ENCKELL. Island life: Agency of Man upon dispersal, distribution, and genetic variation in Faroese populations of terrestrial invertebrates. 3 June 1985.

65. SIGFRID LUNDBERG. Five theoretical excursions into evolutionary ecology: on coevolution, pheromone communication, clutch size and bird migration. 7 November 1985.

66. MIKAEL SANDELL. Ecology and behaviour of the stoat *Mustela erminea* and a theory on delayed implantation. 8 November 1985.

67. THOMAS JONASSON. Resistance to frit fly attack in oat seedlings, and ecological approach to a plant breeding problem. 13 November 1985.

68. ANDERS TUNLID. Chemical signatures in studies of bacterial communities. Highly sensitive and selective analyses by gas chromatography and mass spectrometry. 3 October 1986.

69. BOEL JEPPSSON. Behavioural ecology of the water vole, *Arvicola terrestris*, and its implication to theories of microtine ecology. 27 May 1987.

70. TORSTEN GUNNARSSON. Soil arthropods and their food: choice, use and consequences. 2 June 1987.

71. THOMAS MADSEN. Natural and sexual selection in grass snakes, *Natrix natrix*, and adders, *Vipera berus*. 4 September 1987.

72. JENS DAHLGREN. Partridge activity, growth rate and survival: Dependence on insect abundance. 4 December 1987.

73. SCOTT GILBERT. Factors limiting growth of sympatric *Peromyscus* and *Clethrionomys* populations in northern Canada. 11 December 1987.

74. OLLE ANDERBRANT. Reproduction and competition in the spruce bark beetle *Ips typographus*. 8 April 1988.

75. EINAR B OLAFSSON. Dynamics in deposit-feeding and suspension-feeding populations of the bivalve *Macoma baltica*; an experimental study. 29 April 1988.

76. JAN-ÅKE NILSSON. Causes and consequences of dispersal in marsh tits, time as a fitness factor in establishment. 11 May 1988.

77. PAUL ERIC JÖNSSON. Ecology of the southern Dunlin *Calidris alpina schinzii*. 13 May 1988.

78. HENRIK G SMITH. Reproductive costs and offspring quality: the evolution of clutch size in tits (*Parus*). 20 May 1988.

79. BILL HANSSON. (A) Reproductive isolation by sex pheromones in some moth species. An electrophysiological approach. 14 October 1988.

80. ANDERS THURÉN. (E) Phthalate esters in the environment: analytical methods, occurrence, distribu-

tion and biological effects. 4 November 1988.

81. KARIN LUNDBERG. (A) Social organization and survival of the pipistrelle bat (*Pipistrellus pipistrellus*), and a comparison of advertisement behaviour in three polygynous bat species. 10 February 1989.
82. HAKON PERSSON. (A) Food selection, movements and energy budgets of staging and wintering geese on South Swedish farmland. 6 December 1989.
83. PETER SUNDIN. (E) Plant root exudates in interactions between plants and soil micro-organisms. A gnotobiotic approach. 16 March 1990.
84. ROLAND SANDBERG. (A) Celestial and magnetic orientation of migrating birds: Field experiments with nocturnal passerine migrants at different sites and latitudes. 28 September 1990.
85. ÅKE LINDSTRÖM. (A) Stopover ecology of migrating birds. 12 October 1990.
86. JENS RYDELL. (A) Ecology of the northern bat *Eptesicus nilssoni* during pregnancy and lactation. 26 October 1990.
87. HÅKAN WITTZELL. (T) Natural and sexual selection in the pheasant *Phasianus colchicus*. 27 September 1991.
88. MATS GRAHN. (A) Intra- and intersexual selection in the pheasant *Phasianus colchicus*. 27 May 1992.
89. ANN ERLANDSSON. (A) Life on the water surface: behaviour and evolution in semiaquatic insects. 25 September 1992.
90. GUDMUNDUR A GUDMUNDSSON. (A) Flight and migration strategies of birds at polar latitudes. 2 October 1992.
91. IO SKOGSMYR. (T) Pollination biology, venereal diseases and allocation conflicts in plants. 9 October 1992.
92. ANDERS VALEUR. (E) Utilization of chromatography and mass spectrometry for the estimation of microbial dynamics. 16 October 1992.
93. LENA TRANVIK . (A) To sustain in a stressed environment: a study of soil Collembola. 27 November 1992.
94. KATARINA HEDLUND. (A) Animal-microbial interactions: The fungivorous Collembola.
12 February 1993.
95. HANS EK. (E) Nitrogen acquisition, transport and metabolism in intact ectomycorrhizal associations studied by 15N stable isotope techniques.14 May 1993.
96. STAFFAN BENSCH. (A) Costs, benefits and strategies for females in a polygynous mating system: a study on the great reed warbler. 24 September 1993.
97. NOÉL HOLMGREN. (T) Patch selection, conflicting activities and patterns of migration in birds.15 October 1993.
98. ROLAND LINDQUIST. (E) Dispersal of bacteria in ground water - mechanisms, kinetics and consequences for facilitated transport. 3 December 1993.
99. JOHAN NELSON. (A) Determinants of spacing behaviour, reproductive success and mating system in male field voles, *Microtus agrestis*. 20 May 1994.
100. MARIA SJÖGREN. (A) Dispersal in and ecto-mycorrhizal grazing by soil invertebrates. 30 September 1994.
101. DENNIS HASSELQUIST. (A) Male attractiveness, mating tactics and realized fitness in the polygynous great reed warbler. 14 October 1994.
102. DORETE BLOCH. (A) Pilot whales in the North Atlantic. Age, growth and social structure in Faroese grinds of long-finned pilot whale, *Globicephala melas*. 16 December 1994.
103. MAGNUS AUGNER. (T) Plant-plant interactions and the evolution of defences against herbivores. 10 February 1995.
104. ALMUT GERHARDT. (E). Effects of metals on stream invertebrates. 17 February 1995.
105. MARIANO CUADRADO. (A) Site fidelity and territorial behaviour of some migratory passerine species overwintering in the Mediterranean area. 31 March 1995.
106. ANDERS HEDENSTRÖM. (T) Ecology of Avian Flight. 7 April 1995.

107. OLOF REGNELL. (E) Methyl mercury in lakes: factors affecting its production and partitioning between water and sediment. 21 April 1995.

108. JUNWEI ZHU. (A) Diversity and conservatism in moth sex pheromone systems. 4 May 1995.

109. PETER ANDERSON. (A) Behavioural and physiological aspects of oviposition deterrence in moths. 12 May 1995.

110. JEP AGRELL. (A) Female social behaviour, reproduction and population dynamics in a non-cyclic population of the field vole (*Microtus agrestis*).19 May1995.

111. SUSANNE ÅKESSON. (A) Avian Migratory Orientation: Geographic, Temporal and Geomagnetic Effects. 22 September 1995.

112. ADRIAN L. R. THOMAS. (A) On the Tails of Birds. 29 September 1995.

113. WENQI WU.(A) Mechanisms of specificity in moth pheromone production and response. 8 December 1995.

114. PER WOIN.(E) Xenobiotics in Aquatic Ecosystems: Effects at different levels of organisation. 15 December 1995.

115. K. INGEMAR JÖNSSON. (T) Costs and tactics in the evolution of reproductive effort. 12 April 1996.

116. MATS G.E. SVENSSON. (A) Pheromone-mediated mating system in a moth species. 30 October 1996.

117. PATRIC NILSSON. (T) On the Ecology and Evolution of Seed and Bud Dormancy. 9 May 1997.

118. ULF OTTOSSON. (A) Parent-offspring relations in birds: conflicts and trade-offs. 16 May 1997.

119. ERIK SVENSSON. (A) Costs, benefits and constraints in the evolution of avian reproductive tactics: a study on the blue tit. 6 June 1997.

120. MARIA SANDELL. (A). Female reproductive strategies and sexual conflicts in a polygynous mating system. 6 March 1998.

121. ULF WIKTANDER. (A) Reproduction and survival in the lesser spotted woodpecker. Effects of life history, mating system and age. 3 April 1998.

122. OLA OLSSON. (A) Through the eyes of a woodpecker: understanding habitat selection, territory quality and reproductive decisions from individual behaviour. 17 April 1998.

123. PETER VALEUR. (A) Male moth behaviour and perception in the pheromone plums. 24 April 1998.

124. LARS PETTERSSON. (A) Phenotypic plasticity and the evolution of an inducible morphological defence in crucian carp. 19 March 1999.

125. JOHANNES JÄREMO. (T) Plant inducible responses to damage: evolution and ecological implications. 23 April 1999.

126. ÅSA LANGEFORS. (A) Genetic variation in Mhc class IIB in Atlantic Salmon: Evolutionary and Ecological Perspectives. 10 September 1999.

127. NILS KJELLÉN. (A) Differential migration in raptors. 12 November 1999.

128. ANDERS NILSSON. (A) Pikeivory: behavioural mechanisms in northern pike piscivory. 14 January2000.

129. JÖRGEN RIPA. (T) Population and community dynamics in variable environments. 21 January 2000.

130. BJÖRN LARDNER. (A) Phenotypic plasticity and local adaptation in tadpoles. 28 April 2000.

131. IRENE PERSSON. (A) Parental and embryonic behaviours in precocial birds. 19 May 2000.

132. ROGER HÄRDLING. (T) Evolutionary resolutions of conflicts with mates and offspring. 6 October 2000.

133. ÅSA LANKINEN. (T) Pollen competition as a target for sexual selection in plants. 17 November 2000.

134. THOMAS OHLSSON. (A) Development and maintenance of quality indicators in pheasants. 15 December 2000.

135. ANDERS KVIST. (A) Fuelling and flying: adaptations to endurance exercise in migrating birds. 20 April 2001.

136. ANNA-KARIN AUGUSTSSON. (A). On enchytraeids and naidids: Life-history traits and response to environmental stress. 23 May 2001.

137. MARIO PINEDA. (T). Evolution in Multicellular Mitotic Lineages. 31 August 2001.
138. LIV WENNERBERG. (A). Genetic variation and migration of waders. 9 November 2001
139. NICLAS JONZÉN. (T). Inference and management of populations in variable environments. 14 December 2001.
140. DAGMAR GORMSEN. (A). Colonization processes of soil fauna and mycorrhizal fungi. 21 December 2001.
141. PETER FRODIN. (T). Species interactions and community structure. 15 Mars 2002.
142. JOHAN BÄCKMAN (A). Bird Orientation: External Cues and Ecological Factors. 26 April 2002.
143. MÅNS BRUUN. (A). On starlings and farming: population decline, foraging strategies, cost of reproduction and breeding success. 7 June 2002.
144. JAKOB LOHM. (A). MHC and genomic diversity in Atlantic salmon (*Salmo salar* L.) 11 October 2002.
145. LARS RÅBERG. (A). Costs in ecology and evolution of the vertebrate immune system. 18 October 2002.
146. HELENE BRACHT JÖRGENSEN. (A). Food selection and fitness optimisation in insects. 13 December 2002.
147. MARTIN GREEN. (A). Flight strategies in migrating birds: when and how to fly. 31 January 2003.
148. BENGT HANSSON (A). Dispersal, inbreeding and fitness in natural populations. 21 February 2003.
149. MIKAEL ROSÉN. (A). Birds in the flow: Flight mechanics, wake dynamics and flight performance. 11 April 2003.
150. JONAS HEDIN. (A). Metapopulation ecology of Osmoderma eremita - dispersal, habitat quality and habitat history. 23 May 2003.
151 HELENA WESTERDAHL. (A). Avian MHC: variation and selection in the wild. 10 October 2003.
152. KEN LUNDBORG. (T). Food hoarding: Memory and social conditions - an evolutionary approach. 16 January 2004.
153. RICHARD OTTVALL (A). Population ecology and management of waders breeding on coastal meadows. 19 February 2004.
154. RACHEL MUHEIM (A). Magnetic Orientation in Migratory Birds. 20 February 2004.
155. MARIA HANSSON (A). Evolution and ecology of AhR genes in Atlantic salmon (*Salmo salar* L.). 23 April 2004.
156. MARTIN STJERNMAN (A). Causes and consequences of blood parasite infections in birds. 29 October 2004.
157. MARTIN GRANBOM (A). Growth conditions and individual quality in starlings. 19 November 2004.
158. ANNA GÅRDMARK (T). Species interactions govern evolutionary and ecological effects of population harvesting. 27 May 2005.
159. JONAS WALDENSTRÖM (A). Epidemiology and population structure of Campylobacter jejuni and related organisms in wild birds. 2 December 2005.
160. HELEN IVARSSON (T). Strategy Games: on survival and reproduction. 9 December 2005.
161. SEBASTIAN TROÈNG (A). Migration of sea turtles from Caribbean Costa Rica: Implications for management. 14 December 2005.
162. EMMA SERNLAND (T). Optimal strategies and information in foraging theory. 16 December 2005.
163. MIKAEL ÅKESSON (A). Quantitative genetics and genome structure in a wild population: the use of a great reed warbler pedigree. 29 September 2006.
164. LENA MÅNSSON (T). Understanding weather effects on, in and from large herbivore population dynamics. 13 October 2006.
165. ERIK ÖCKINGER (A). Butterfly diversity and dispersal in fragmented grasslands. 17 November 2006.
166. JESSICA K. ABBOTT (A). Ontogeny and population biology of a sex-limited colour polymorphism. 23 November 2006.
167. OLOF HELLGREN (A). Avian malaria and related blood parasites: molecular diversity, ecology and

evolution. 15 December 2006.

168. ANNA NILSSON (A).The problem of partial migration - the case of the blue tit. 19 January 2007.

169. PATRIK KARLSSON NYED (T). Food webs, models and species extinctions in a stochastic environment. 16 February 2007.

170. MARKUS FRANZÉN (A). Insect Diversity in Changing Landscapes. 16 May 2007.

171. MAJ RUNDLÖF (A). Biodiversity in agricultural landscapes: landscape and scale-dependent effects of organic farming. 15 June 2007.

172. OSKAR BRATTSTRÖM (A). Ecology of red admiral migration. 21 September 2007.

173. MICHAEL TOBLER (A). Maternal programming: costs, benefits and constraints of maternal hormone transfer. 5 October 2007.

174. FREDRIK HAAS (T). Hybrid zones and speciation - insights from the European Crow hybrid zone. 25 January 2008.

175. JACOB JOHANSSON (T). Evolving ecological communities in changing environment. 1 February 2008.

176. THOMAS GOSDEN (A). The Preservation of Favoured Morphs in the Struggle Between Sexes. 29 May 2008.

177. ROINE STRANDBERG (A). Migration strategies of raptors – spatio-temporal adaptions and constraints in travelling and foraging. 24 September 2008.

178. SARA S. HENNINGSSON (A). On the role of migration for the distribution of arctic birds – a circumpolar perspective. 25 September 2008.

179. JONAS KNAPE (T). Population dynamics and demography – inference from stochastic models. 6 February 2009.

180. NICLAS NORRSTRÖM (T). Artificial neural networks in models of specialization and sympatic speciation. 20 February 2009.

181. JOHAN NILSSON (A). Causes and consequences of individual variation in energy turnover rates. 17 April 2009.

182. MARTA WOLF (T). Catching the Invisible: Aerodynamic Track and Kinematics of Bat and Bird Flight. 14 May 2009.

183. JULIANA DÄNHARDT (A). On the importance of farmland as stopover habitat for migrating birds. 15 May 2009.

184. SARA NAURIN (A). Avian GEnome Evolution – Gene Expression, Gene Divergence and Sexual Dimorphism. 23 October 2009.

185. JENNIE NILSSON (T). On the origin of polymorphism – consequences of competition and predation in heterogeneous environments. 13 November 2009.

186. FABRICE EROUKHMANOFF (A). The interplay between selection and constraints on phenotypic evolution and adaptive divergence. 20 November 2009.

187. SANNA HARRIS (A). Behaviour under predation risk – antipredator strategies, behavioural syndromes and sex-specific responses in aquatic prey. 15 January 2010.

188. PER HENNINGSSON (T). Always on the wing – Fluid dynamics, flight performance and flight behavior of common swifts. 29 Januari 2010.